Yeni Nesil Poli(N-isopropylacrylamid) ve Poli(akrilikasit) Temelli kompozit Elektrotların Hazırlanması ve Süperkapasitör Uygulamaları

Danıa Alovn

YÜKSEK LİSANS TEZİ

Kimya Mühendisliği Anabilim Dalı

Temmuz 2023

Preparation of New Generation Poly(N-isopropylacrylamide) and Poly(acrylicacid) Based Composite Electrodes and Supercapacitor Applications

Danıa Alovn

MASTER OF SCIENCE THESIS

Department of Chemical Engineering

July 2023

Preparation of New Generation Poly(N-isopropylacrylamide) and Poly(acrylicacid) Based Composite Electrodes and Supercapacitor Applications

A thesis submitted to the Eskisehir Osmangazi University Graduate School of Natural and Applied Sciences in partial fulfillment of the requirements fort the degree of Master of Science in Discipline of Chemical Technologies
of the Department of Chemical Engineering
by

Danıa Alovn

Supervisor: Prof. Dr. Hilal DEMİR KIVRAK

Co-Supervisor: Res. Asst. Dr. Sibel YAZAR AYDOĞAN

This thesis supported by Scientific Research Projects Commission (BAP) (Project No: 2689)

July 2023

APPROVAL OF THE THESIS

The thesis titled "Preparation of New Generation Poly(N-isopropylacrylamide) and Poly(acrylicacid) Based Composite Electrodes and Supercapacitor Applications" and submitted by Danıa Alovn has been accepted as satisfactory in partial fulfillment of the requirements for the degree of Master of Science in Department of Chemical Engineering.

Supervisor **:** Prof. Dr. Hilal DEMİR KIVRAK

Co-Supervisor **:** Res. Asst. Dr. Sibel YAZAR AYDOĞAN

Examining Committee Members:

Member : Prof. Dr. Hilal DEMİR KIVRAK

Member : Asst. Prof. ŞEFİKA KAYA

Member : Asst. Prof. Melih Beşir ARVAS

Graduation of ……..was approved by the Graduate School Board Decision on …… with the decision number of ……...

Director of the Institute

ETHICAL STATEMENT

I hereby declare that this thesis study titled “Preparation of New Generation Poly(N-isopropylacrylamide) and Poly(acrylicacid) Based Composite Electrodes and Supercapacitor Applications” has been prepared in accordance with the thesis writing rules of Eskişehir Osmangazi University Graduate School of Natural and Applied Sciences under academic consultancy of my supervisor Prof. Dr. Hilal DEMİR KIVRAK. I hereby declare that the work presented in this thesis is original. I also declare that, I have respected scientific ethical principles and rules in all stages of my thesis study, all information and data presented in this thesis have been obtained within the scope of scientific and academic ethical principles and rules, all materials used in this thesis which are not original to this work have been fully cited and referenced, and all knowledge, documents and results have been presented in accordance with scientific ethical principles and rules. 21/07/2023

Danıa ALOVN

ÖZET

Süperkapasitörler, yüksek güç yoğunlukları, hızlı şarj-deşarj hızları, çevre dostu olmaları ve uzun çevrim ömürleri nedeniyle enerji depolama sorununa önemli bir çözüm olarak büyük ilgi görmüştür. Süperkapasitörlerin verimliliği büyük ölçüde elektrot malzemelerinin özelliklerine göre belirlenmektedir.

Poli(N-izopropilakrilamid) (PNIPAM) ve poli(akrilikasit) (PAAc) polimerleri radikal polimerizasyon yöntemi ile sentezlendi. Polimerler monomer, çapraz bağlayıcı (MBA), hızlandırıcı (TEMED) ve radikal başlatıcı (APS) kullanılarak elde edildi. Daha sonra, - karbon nanotüp (KNT) ve tek metalli M(Pd, Pt, Ru, Co, Mo, Fe, Ga, Bi, Ni)/KNT katalizörleri ile polimerler kompozit (M/KNT-g-PAAc) olarak sentezlendi. Polimerler ve metal katkılandırılmış polimerler Fourier Dönüşümlü Kızılötesi Spektroskopisi (FT-IR), Mikro Raman Spektrometresi (RAMAN) ve Taramalı elektron mikroskopları ve elementel haritalama (SEM-EDX), X ışını kırınımı (XRD) yöntemleri ile analiz edilmiştir.

Bu tezde karbon keçe temelli elektrot malzemesi üzerine iyonik iletkenliği yüksek polimerler ve M(Pd, Pt, Ru, Co, Mo, Fe, Ga, Bi, Ni)/KNT kompozitlerin kaplanması ile yüksek kapasitans sergileyen yeni nesil elektrotlar geliştirildi. Elektrotların kapasitif performansları 1.0 M H_2SO_4 sulu elektrolit ortamında çevrimsel voltametri (CV), galvanostatik şarj deşarj (GCD) ve elektrokimyasal empedans spektroskopisi (EIS) teknikleri ile incelendi.

Sonuç olarak, süperkapasitör elektrot olarak işlev gören PAAc-g-(Ru/CNT) ve PAAc-g-(Ni/CNT), en yüksek spesifik kapasiteler sergilemiştir. PAAc-g-(Ru/CNT), 5 mV s^{-1} hızında 1294.5 F g^{-1} spesifik kapasiteye sahiptir ve PAAc-g-(Ni/CNT), 2.0 mA cm^{-2} akım yoğunluğunda 680.0 F g^{-1} spesifik kapasiteye sahiptir. Ayrıca, bu elektrotlar sırasıyla 1000 çevrim sonrasında %97.7 ve %94.1 yüksek kapasite koruması göstererek genişletilmiş döngü ömrü ve güçlü elektrokimyasal kararlılık sergilemiştir.

Bu sonuçlar, enerji depolama alanındaki ilerlemeye önemli bir katkı sağlamakta ve daha verimli ve sürdürülebilir enerji depolama cihazlarının geliştirilmesi için uygulanabilir

çözümler sunmaktadır. Bu tez, iyon iletken polimerlerin bir elektrot malzemesi olarak kullanıldığı enerji depolama ve enerji dönüşüm cihazları için uygun metal/karbon kompozitlerine yeni yaklaşımlar sunmuştur. Ayrıca, yüksek performanslı süperkapasitörler için yeni kompozitlerin oluşturulması konusunda önemli görüşler sunmuştur.

Anahtar Kelimeler: Süperkapasitör, Karbon nanotüp, Poli(N-izopropilakrilamid), Poli(akrilikasit).

SUMMARY

Supercapacitors have gained notable attention as a crucial solution to the energy storage challenge because of their impressive power density, rapid charge-discharge rate, eco-friendliness, and long cycle life. The efficiency of supercapacitors is largely determined by the characteristics of their electrode materials. Poly(N-isopropylacrylamide) (PNIPAM) and poly(acrylic acid) (PAAc) polymers were synthesized by radical polymerization method. The polymers were obtained after sequential mixing using polymers monomer, crosslinker (MBA), accelerator (TEMED) and radical initiator (APS). Afterward, polymers were synthesized as composite (M/CNT-g-PAAc) with Carbon nanotube (CNT) and mono-metal M(Pd, Pt, Ru, Co, Mo, Fe, Ga, Bi, Ni)/CNT catalysts. Polymers and metal-doped polymers were analyzed by Fourier Transform Infrared Spectroscopy (FT-IR), Micro Raman Spectrometer (RAMAN) and Scanning electron microscopes and elemental mapping (SEM-EDX), X-ray diffraction (XRD) methods. In this thesis, new generation electrodes with high capacitance were developed by coating carbon felt-based electrode material with high ionic conductivity polymers and M(Pd, Pt, Ru, Co, Mo, Fe, Ga, Bi, Ni)/CNT composites. The capacitive performances of the electrodes were examined by cyclic voltammetry (CV), galvanostatic charge-discharge (GCD) and electrochemical impedance spectroscopy (EIS) techniques in 1.0 M H_2SO_4 aqueous electrolyte. The resulting PAAc-g-(Ru/CNT) and PAAc-g-(Ni/CNT), which function as supercapacitor electrodes, exhibit a high specific capacitances of 1294.5 F g^{-1} at 5.0 mV s^{-1} and 680.0 F g^{-1} at 2.0 mA cm^{-2}, respectively. Additionally, these electrodes demonstrate a high capacitance retention of up to 97.7% and 94.1% after 1000 cycles, respectively, showcasing their extended cycle life and strong electrochemical stability. These results contribute to the advancement of the field of energy storage and provide practical solutions for developing energy storage devices with higher efficiency and sustainability. This thesis provided new approaches for metal/carbon composites suitable to energy storage and suitable to energy storage and energy conversion devices with ionic conducting polymers as an electrode material, as well as insights into the creation of new composites for high-performance supercapacitors.

Keywords: Supercapacitor, Carbon nanotube, Poly(N-isopropylacrylamide), Poly(acrylicacid).

ACKNOWLEDGMENT

I would like to extend my sincerest gratitude to the Almighty Allah. I am profoundly thankful to express my deepest appreciation and heartfelt thanks to my dear parents. Their constant support, both emotionally and financially, has been the foundation of my accomplishments in successfully completing my Master of Science thesis in Chemical Engineering. Their boundless love, encouragement, and selflessness have fueled my unwavering determination to achieve this significant milestone in my academic journey.

I would also like to extend my sincerest thanks to my esteemed supervisors, Prof. Dr. Hilal DEMİR KIVRAK and Res. Asst. Dr. Sibel YAZAR AYDOĞAN. Their guidance, expertise, and invaluable insights have shaped the outcome of this thesis. Their unwavering commitment to excellence and their dedication to mentoring and supporting me throughout this journey have been truly inspiring.

Additionally, I am deeply grateful to the Research Projects Commission (BAP) for granting me the opportunity and financial support to conduct my research studies on supercapacitors at Eskişehir Osmangazi University and Istanbul Cerrahpaşa University. Their belief in the significance of my research and their investment in my academic pursuits have been invaluable.

LIST OF CONTENTS

Page

LIST OF CONTENTS

Page

LIST OF FIGURES

Figure **Page**

LIST OF FIGURES

Figure **Page**

LIST OF FIGURES

Figure **Page**

LIST OF TABLES

Table **Page**

LIST OF TABLES

Table **Page**

LIST OF ABBREVIATIONS AND SYMBOLS

Symbols	**Descriptions**
ε_r	Electrolyte's relative permittivity
ε_0	Vacuum permittivity
d	Effective thickness of the double layer
A	Surface area of the electrode
C	Double-layer capacitance
a_0	Effective size of the ion
r	Pore radius
Cs	Specific capacitance
Q	Charge stored
V	Voltage
I	Current
$\oint_{V1}^{V2} I \ dV$	Integrated field from the CV measurement
ΔV	Working potential window
M	Amount of active substance in the electrode
v	Scan rate
Δt	Discharge time

Abbreviations	**Descriptions**
PNIPAM	Poly(N-isopropylacrylamide)
PAAc	Poly(acrylicacid)
CNT	Carbon nanotube
XRD	X-ray diffraction
SEM	Scanning electron microscopy
FTIR	Fourier Transform Infrared Spectroscopy

LIST OF ABBREVIATIONS AND SYMBOLS

Abbreviations	**Descriptions**
FTIR	Fourier Transform Infrared Spectroscopy
CV	Cyclic voltammetry
GCD	Galvanostatic charge discharge
EIS	Electrochemical impedance spectroscopy

1. INTRODUCTION AND PURPOSE

Energy has been a critical and essential requirement for humans since ancient times, enabling the progress of society. Traditional energy sources like coal, petroleum, wood, and natural gas have served this purpose, but they are rapidly depletion due to the increasing pace of industrialization and urbanization. Additionally, they have proven to be harmful to the environment, making them incompatible and unsustainable options for the future. On the other hand, renewable energy resources, encompassing hydropower, wind, geothermal, and marine energy, are becoming increasingly important due to their environmental friendliness, abundance, and accessibility. However, These energy sources exhibit intermittent characteristics, rendering them unable to be harnessed continuously for extended durations. (Choudhary et al., 2020). In recent times, energy sources and the environment have become significant global issues. Clean and renewable energy is becoming more crucial for the future, and research in this area has been steadily increasing (J. Li et al., 2016).

The urgent need to find alternative, renewable and environmentally friendly energy sources, due to the steady growth of the worldwide economy, heavy consumption of fossil fuels and rising environmental pollution, has driven the advancement of storage and conversion technologies. Additionally, the popularity of low-emission electric vehicles and the significant need for portable electronic devices, power tools, and electric vehicles has sparked significant research interests in creating high-performance devices to meet these needs (C. Wang et al., 2018). The growing concerns over the energy needs and the impact of greenhouse gases on the environment have led to increased investment in the development of new energy storages. Among the various options, batteries and supercapacitors are considered as the most viable for practical applications (Zhang et al., 2019).

To respond to the increasing global needs and address pressing economic challenges, the advancement and utilization of energy storage devices has become increasingly crucial. With various technologies available, such as rechargeable batteries, fuel cells, and supercapacitors, it is important to differentiate these devices based on their key characteristics, such as energy density, efficiency, voltage window, and current density. These differences can be visualized through the Ragone plot, as shown in Figure 1.1 (S. Sharma & Chand, 2023).

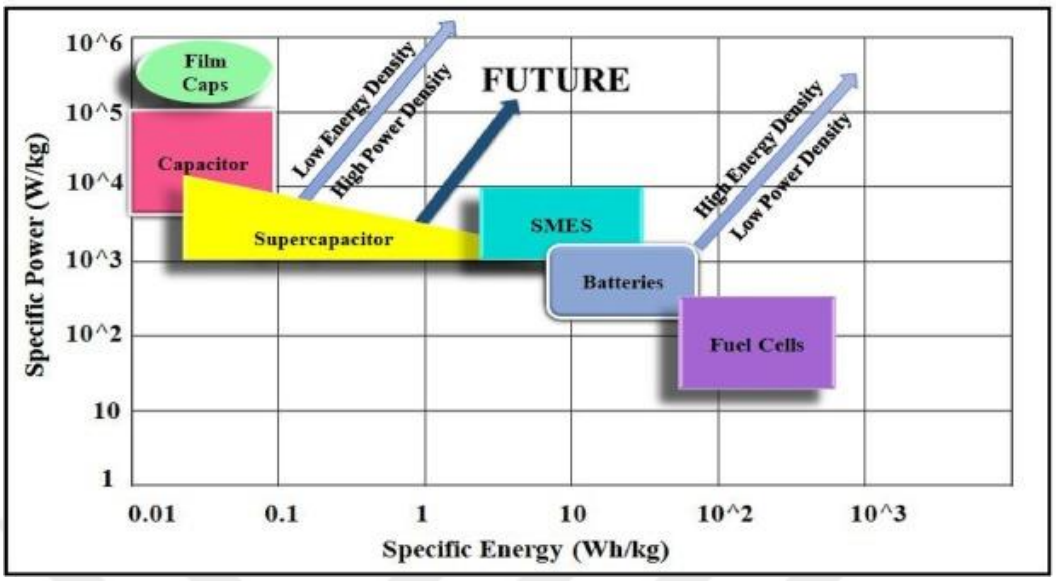

Figure 1.1 Ragone plot of distinct energy storage devices (S. Sharma & Chand, 2023).

Supercapacitors, representing a novel generation of electrochemical energy storage devices, have a charge storage mechanism and operating principle similar to that of rechargeable batteries rather than electrostatic capacitors. Due to their exceptional performance characteristics, Supercapacitors have surfaced as a highly promising and viable solution to meet the electrical energy storage demands, with their performance falling somewhere between that of rechargeable batteries and regular electrostatic capacitors. Compared to electrostatic capacitors and rechargeable batteries, supercapacitors are distinguished by their notably elevated energy and power densities. They are now being used both independently and in conjunction with other energy storage systems, like electrochemical batteries, and are being considered as a potential alternative to widely used rechargeable batteries, particularly lithium-ion batteries (Olabi et al., 2022).

Supercapacitors, in particular, have garnered attention for their exceptional properties, including extended cycle life, swift charge-discharge rate, and high energy density, making them superior to conventional batteries in many applications (Zhang et al., 2019). Supercapacitors have become a subject of extensive research owing to their exceptional prowess in energy storage capabilities, which make them highly suitable for various applications, such as the advancement of low-power electronics, such as wearables and portable devices, as well as high-power military applications. The performance of

supercapacitors (SCs) can be evaluated based on the electrochemical properties, which are determined by the combination of electrode materials and electrolytes used (Raza et al., 2018).

Supercapacitors can be categorized into two types depending on their energy storage mechanisms: pseudocapacitors and electrical double-layer capacitors (EDLCs). Pseudocapacitors demonstrate a substantial specific capacitance attributed to the occurrence of reversible redox reactions within the material. These reactions are responsible for the pseudocapacitive behavior. Common materials used in pseudocapacitors include metal based, and conducting polymer based. Unlike pseudocapacitors, EDLCs have a unique mechanism for storing and releasing energy, which is limited to the surface or interface of the electrodes. Carbon-based materials, including carbon aerogels and activated carbon, are often utilized in EDLCs for their exceptional durability during long-term use and their capability to handle high charge and discharge rates (X. Wang et al., 2022).

Apart from the materials frequently used in supercapacitor applications, poly(acrylic acid) (PAAc), is an appealing choice as a material because of its biodegradable characteristics, improved handling and processing, and robust mechanical properties. Additionally, PAAc is environmentally friendly and can form a stable complex with metals (Kam et al., 2014). Research has indicated that it exhibits favorable adhesion properties and sustains electrochemical stability throughout multiple charging/discharging cycles (Patil et al., 2013). In this field, a spin coating technique, which is both simple and affordable, was utilized to synthesize hybrid thin films of CuO and PAAc for use in supercapacitor technology (Shaikh, Pawar, Moholkar, et al., 2011). In another study, a composite film composed of Carbon nanotubes (CNTs) and polyacrylic acid (PAAc) was created using electrophoretic deposition in an aqueous PAAc containing carbon nanotubes. This material was then utilized as the electrode in the capacitive deionization (CDI) process. PAAc acts as a cation-exchange polymer and a matrix to hold the CNTs (Nie et al., 2012).

Poly(N-isopropyl acrylamide) (PNIPAM) is a thermoresponsive polymer characterized by a distinct thermoresponsive property. When dissolved in an aqueous solution, PNIPAM demonstrates a lower critical solution temperature (LCST) in the range of approximately 31–33 °C, resulting in partial dehydration and phase separation of the

dissolved polymer. Over an extensive period, the phase transition behavior of PNIPAM has been a subject of great interest among researchers, leading to a progressive comprehension of this phenomenon through a multitude of scholarly publications (Munk et al., 2013). PNIPAM, with its ability to undergo hydrophilic interactions and exhibit bioadhesiveness, holds promise as a polymer that experiences a transition in response to temperature changes, specifically at its LCST of 32 °C. While the monomer of PNIPAM may possess cytotoxicity, the polymer itself has shown no toxicity towards various cell types, making it a valuable tool for investigating bioadhesion mechanisms. These unique characteristics have positioned PNIPAM as a highly researched and studied polymer in academic literature, both in the form of grafting and coating onto material surfaces (Conzatti et al., 2017).

In their research, Patil et al. (2013) utilized a straightforward and cost-effective dip coating method to fabricate composite electrodes composed of polyacrylic acid (PAA), polypyrrole (PPY), and silver (Ag) for supercapacitor applications. The electrodes supercapacitive behavior was evaluated using cyclic voltammetry and charge-discharge tests in a three-electrode system with a 0.1 M H_2SO_4 electrolyte. The PAA/PPY/Ag composite electrodes demonstrated a remarkable specific capacitance of 226 F g^{-1} at a scan rate of 10 mV s^{-1}, along with an impressive energy density of 17.45 Wh kg^{-1} at a current density of 0.5 mA cm^{-2}.The PPY/PAA/Ag composite electrode showcases superior specific capacitance even after 2000 cycles, indicating its promising potential for supercapacitor applications, with a reported long cycle retention of 63% of its capacitance.

In a study conducted by Haiyang Wang et al. (2020), an innovative hierarchical macroporous carbon material possessing well-defined meso-microporous structures, known as HPCs, was developed through the composite of carboxylated coal-tar pitches (CCP) with poly(acrylic acid). As a consequence of the carbonizing process, a distinct molded hierarchical porous structure was formed. Thermal analysis was conducted to examine the influences of pore parameters, these developments resulted in notable accomplishments in terms of impressive capacity utilization, rapid rate capability, and exceptional long-term cycling stability. The HPC-CCP/PAA composite exhibited the largest BET surface area measuring 1294.6 m^2 g^{-1} and a a considerable total pore volume of 1.34 cm^3 g^{-1}, indicating a rapid exchange of electrolyte ions and exceptional capacitive performance. Specifically, In a two-electrode system, the material exhibited a capacitance of 292 F g^{-1} at 1.0 A g^{-1}.

Furthermore, HPCs demonstrated remarkable electrochemical stability, retaining a capacitance rate as high as 94.2% after 10,000 cycles.

In a different study, conducted by A. K. Sharma et al., the researchers investigated a composite material composed of poly(3,4-ethylenedioxythiophene) (PEDOT) and poly(N-isopropylacrylamide) (PNIPAm) nanofibers for potential applications in tissue engineering. The nanofibers were fabricated using electrospinning, and their chemical structure was analyzed using FTIR. Cyclic voltammetry was applied as the experimental technique to evaluate the conducting behavior of the composite material, revealing distinct oxidation and reduction peaks that indicated favorable redox activity. The resulting voltammogram exhibited a rectangular shape and demonstrated a significant flow of current through the electrode. The specific capacitance, extracted from the cyclic voltammogram at a scan rate of 2 mVs^{-1}, measured to be 248 Fg^{-1}. The enhanced current flow and specific capacitance were attributed to improved electrolyte penetration within the composite electrode, effectively reducing resistance. Furthermore, the PEDOT-PNIPAm composite nanofibers exhibited exceptional cell growth and a high percentage of live cells (approximately 98%), highlighting their potential as scaffolds for tissue engineering applications.

In a different study, Elashnikov et al. (2021) proposed a novel concept of a advanced externally controlled supercapacitor utilizing a temperature-responsive hydrogel doped with polypyrrole nanotubes (PPyNTs). The strategic manipulation of PPyNTs within the PNIPAm hydrogel could be achieved reversibly through light illumination or temperature elevation, enabling the tailored formation or disintegration of the nanotube conductive network on-demand. The specific capacitance derived from cyclic voltammogram (CV) curves in this work was 360 F g^{-1} at a scan rate of 100 mV s^{-1}, the supercapacitor demonstrated a retention rate of 92% after 200 cycles.

The purpose of this thesis is to develop novel high ionic conductivity polymers and their composites for supercapacitor applications. The thesis focuses on synthesizing and characterizing Poly(N-isopropylacrylamide) (PNIPAM) and poly(acrylic acid) (PAAc) polymers, as well as their composites with carbon nanotubes (CNT) and metal-doped catalysts. The goal is to enhance the capacitive properties of carbon felt-based electrodes by coating them with these polymers and composites. The thesis investigates the surface

morphology, roughness, and capacitive performance of the electrodes using several analysis techniques such as X-ray diffraction (XRD), Scanning electron microscopy (SEM-EDX), Fourier Transform Infrared Spectroscopy (FT-IR), micro Raman spectroscopy, Cyclic voltammetry (CV), Galvanostatic charge-discharge (GCD), and Electrochemical impedance spectroscopy (EIS).

2. LITERATURE REVIEW

2.1. Supercapacitor

Efficient energy storage is becoming increasingly important in meeting global economic demands, and supercapacitors are garnering increasing attention as a promising and potential candidate to fulfill this purpose. With their remarkable properties, including high power density, excellent crystallinity, substantial porosity, extended lifespan, remarkable chemical and thermal stability, diverse framework options, and a notable specific surface area, supercapacitors have the potential to provide a reliable and efficient solution for energy storage applications (S. Sharma & Chand, 2023).

Supercapacitors, commonly referred to as ultracapacitors or electrochemical capacitors, have gained significant interest owing to their capability to deliver pulse power, extended lifespan, straightforward design, and rapid charge and discharge capabilities in recent years (Patil et al., 2014). In recent years, supercapacitors have garnered significant interest from the scientific community as they offer several advantages over batteries, such as higher efficiency and the ability to handle fast charging cycles without showing a sharp decrease in efficiency. While batteries have a short lifespan, they serve as an intermediary between supercapacitors and fuel cells on the Ragone plot, as illustrated in Figure 1.1 The high capacitance value exhibited by supercapacitors is attributed to the utilization of electrical double layer capacitance and pseudocapacitance, which replace the solid dielectric material used in conventional capacitors. The performance of supercapacitors is influenced by various factors, such as the thermal stability and ionic conductivity of the materials utilized for the electrodes and electrolytes (S. Sharma & Chand, 2023).

The ultrahigh capacitance of electrochemical supercapacitors (SCs) stems from the electric double layer (EDL) theory, which explains the electrochemical charge storage at the boundary between a conductor and electrolyte. Hermann von Helmholtz was the pioneer in introducing this theory, where he noted the occurrence of charge separation at interfaces and conjectured the presence of counter ions or charge on electrode surfaces. According to his suggestion, this phenomenon results in the establishment of an electric double layer (EDL) comprising two layers with opposite polarity, separated by a molecular order distance. The

EDL serves as a molecular dielectric, effectively storing charge through electrostatic mechanisms. Subsequent development of the theory was undertaken by Gouy, Chapman, Grahame, and Stern, whose contributions furthered our understanding of the phenomenon. Moreover, increasing the surface area of the electrode material at the interface has been found to considerably enhance the capacitance of the system (Bhojane, 2022).

Supercapacitors have gained widespread popularity as electrochemical energy storage devices owing to their exceptional performance and efficient energy storage mechanisms. Recent progress in electrode materials at the nanoscale, along with the important role of electrolytes, has significantly enhanced the performance of supercapacitors. The utilization of porous carbon materials with subnanometer pores has resulted in remarkably high capacitances, while oxide materials employ surface redox reactions to store charge, leading to the pseudocapacitive effect. A fundamental comprehension of the underlying physical mechanisms that govern charge storage in these materials is essential for advancing the technology of supercapacitors (Salanne et al., 2016).

Supercapacitors, especially electric double layer capacitors (EDLCs), are known for their virtually limitless cycle life, as they utilize interfacial surface charge storage without any modification in chemical or phase state of active materials during charge-discharge cycles. However, cycle life may vary in other types of supercapacitors, like Pseudocapacitors (PCs) and hybrid supercapacitors (HSCs), because of the Faraday reaction of the active materials occurs during both the charging and discharging processes. Despite this limitation, supercapacitors still offer a significantly longer cycle life than traditional batteries, making them a promising option for energy storage applications. Moreover, supercapacitors have demonstrated exceptional capacity retention of up to 99%, maintaining their high capacitive performance over extended usage. Furthermore, supercapacitors have additional benefits such as safety and environmental friendliness. Unlike rechargeable batteries, supercapacitors do not require large amounts of electrolytes, making them safe to use and easy to recycle (Olabi et al., 2022).

Supercapacitors can be classified into two categories in terms of the charge storage mechanism. The first category comprises Electrical Double Layer Capacitors (EDLCs), where capacitance arises from the electrostatic interaction of charges occurring at the

electrode-electrolyte boundary. The second is Pseudocapacitors, in which the pseudocapacitance results from oxidation/reduction reactions taking place at the electrode/electrolyte interface (Patil et al., 2013). As opposed to this, pseudocapacitors use a sequence of quick and reversible redox reactions or Faradic charge transfer that take place at the surface of electro-active materials. Compared to EDLC, pseudocapacitors typically have a higher capacitance and energy density. The materials that are commonly used in pseudocapacitors are metal oxides, nitrides, sulfides, and conducting polymers (Huang et al., 2016).

The evaluation of supercapacitor (SC) performance requires consideration of three crucial parameters: specific capacitance (Csp), operating potential window (V), and equivalent series resistance (ESR). These parameters play a pivotal role in defining the energy and power density characteristics of the supercapacitor device. The electrode material is critical for supercapacitor performance, impacting Csp, V, and ESR, as well as commercial viability, cyclability, and compactness. As a result, current research is focused on developing innovative electrode materials to enhance the entire electrochemical performance of SCs. The objective of conducting advanced and cutting-edge research is to accomplish significant energy density and power density, rapid charging and discharging, exceptional cyclability, minimal auto-discharge, safety, and cost-effectiveness in supercapacitors. The meticulous selection of electrode materials and electrolytes is of paramount importance as they significantly influence and impact the charge storage performance. An optimal electrode material is expected to demonstrate a substantial surface area and diverse pore-size variability while also demonstrating exceptional electrical conductivity and durability. Moreover, the material's density should be sufficiently high to enable significant volumetric capacitance and energy storage. Also, electrolytes are a crucial component of the overall supercapacitor (SC) system and have a significant impact on various parameters. The use of appropriate electrolytes is essential to achieve high-performance SCs with characteristics such as broad potential windows, favorable electrochemical stability, compact solvated ionic radius, insignificant resistivity, diminished viscosity, non-toxicity, cost-effectiveness and purity. Within an electrochemical energy storage (EES) system, the transformation of chemical energy into electrical energy takes place through electrochemical reactions involving the electrode materials and the electrolytic ions. The electrolyte is of paramount importance as a crucial element within the electrochemical energy storage system,

profoundly influencing the charge storage mechanism, encompassing the creation of a double layer or reversible redox behavior. The properties of the electrolyte in electrochemical energy storage systems are predominantly influenced by various factors, including the nature and size of ions, ion concentration and solvent properties, interactions between ions and solvents, interactions between electrodes and electrolytes, and the operational potential window. These properties govern the comprehensive electrochemical attributes of the electrochemical energy storage (EES) system, encompassing aspects such as the electrical double-layer (EDL) and pseudocapacitance behavior, as well as the energy and power density, and operational lifespan. Table 2.1 displays the ionic conductivities of several aqueous electrolytes utilized in various electrochemical tests (Bhojane, 2022).

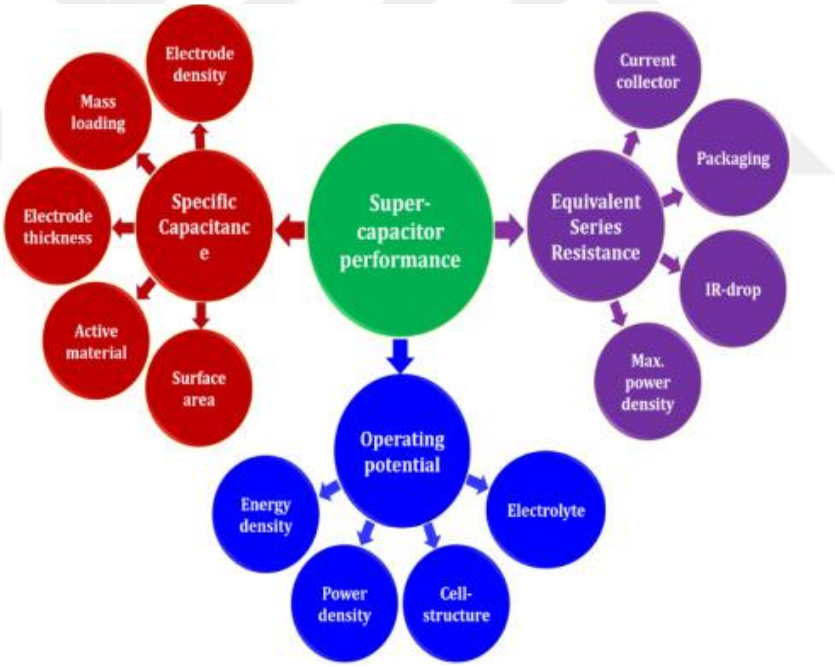

Figure 2.1 Factors influencing supercapacitor performance (Bhojane, 2022).

Table 2.1 Ionic conductivities of different aqueous electrolytes utilized in electrochemical tests (Bhojane, 2022).

Electrolyte	**Conductivity (mS/cm)**
1 M H_2SO_4	265
1 M KOH	191
1 M LiOH	150
1 M NaOH	141
1 M K_2SO_4	100
1 M $KOAc_4$	92
3 M NaOAc	79
1 M $MgSO_4$	51

The overall performance of a supercapacitor relies on the meticulous choice of separator, electrodes, and electrolyte materials. A supercapacitor typically comprises of two electrodes, a separator that is permeable to ions, and an electrolyte that facilitates the ionic connection between the two electrodes during charging and discharging processes while preventing short circuits. Separators such as polyolefin and cellulose enable the transport of ions across electrodes. Two types of electrolytes are used - aqueous (for low voltage) and organic (for high voltage) - with aqueous electrolytes being preferred because of their superior ionic conductivity, which enhances the power density of the supercapacitor. Aqueous electrolytes are also favored over organic electrolytes, as a lower operating voltage in the supercapacitor cell is required to prevent the chemical decomposition of the electrolyte. (S. Sharma & Chand, 2023).

Supercapacitor cells can be assembled in two distinct configurations: the two-electrodes cell and the three-electrodes cell. The two-electrode configuration is commonly utilized in academic research and broader industrial applications, while the three-electrode configuration is primarily employed for precise measurements in scientific investigations,

owing to its improved accuracy. The two-electrode configuration is comprised of two electrodes, metallic current collectors, and separators, while the three-electrode configuration includes a reference electrode to enhance measurement precision. Schematic diagrams of supercapacitor cells in both two-electrode and three-electrode configurations are shown in Figure 2.2 (Olabi et al., 2022).

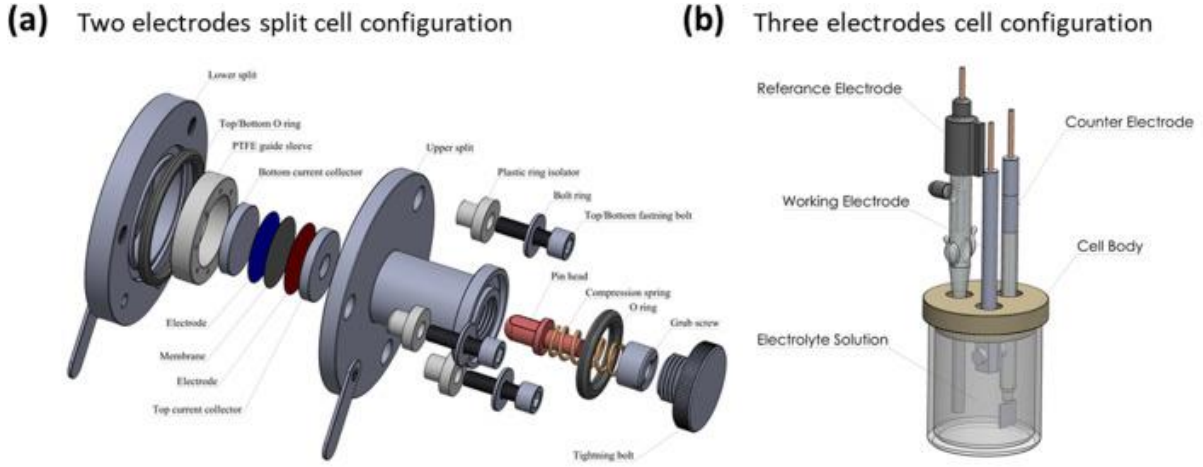

Figure 2.2 Graphical representations of the two-electrode and three-electrode cells (a) the two-electrode configuration (b) the three-electrode configuration (Olabi et al., 2022).

2.2. Types of Supercapacitors

Supercapacitors are categorized into three primary types distinguished by their construction, charge storage mechanism, and the materials utilized for electrodes and electrolytes. These configurations exhibit distinct charge storage mechanisms and display unique characteristics that correspond to each type, namely Electric Double-Layer Capacitors, Pseudocapacitors, and Hybrid Supercapacitors. The classification of supercapacitors is illustrated in Figure 2.3 Although there is extensive literature on all types of supercapacitors, The primary purpose of this concise perspective is to offer an overview of the technological advancements made in supercapacitor technology in recent years, and to investigate the current and future applications of EDLCs as well as the potential uses of newly developed Asymmetric supercapacitors and Hybrid Supercapacitors. Although EDLCs are currently the most widely used supercapacitor technology, ASCs and HSCs designs are actively being investigated and researched, indicating their potential for use in the near future (Olabi et al., 2022).

2.2.1. Electric double layer capacitors (EDLCs)

Supercapacitor electrodes accumulate charge by capitalizing on the electrostatic interaction between ions present in the electrolyte and the charges located at the electrode-electrolyte interface, leading to the creation of oppositely charged layers. Utilizing porous carbon as the electrode material in supercapacitors is advantageous due to the remarkably extensive surface area it offers, enabling effective ion adsorption. A simple explanation of the charge separation that occurs during polarization at the interface between the electrode and electrolyte is provided by the double-layer capacitance theory, which was first introduced by Helmholtz in 1853:

$$C = \frac{\epsilon r\ \epsilon 0\ A}{d} \tag{2.1}$$

The equation above includes the electrolyte's relative permittivity (εr), the vacuum permittivity (ε_0), the thickness of the double layer (d), and the surface area of the electrode (A). However, in highly disordered materials, the quantities εr, d, and A are not well-defined for the interfaces under consideration. Before 2005, the prevailing belief was that the best way to increase capacitance was by maximizing the charging of the electrochemical double-layer. Therefore, researchers focused on developing mesoporous carbon that possess the largest possible surface area. However, research conducted by the Aurbach group in 2011 and 2012 revealed a highly effective storage mechanism in nanopores with pore sizes smaller than 1 nm, which smaller than the dimensions of solvated ions. This discovery caused a shift in thinking, and researchers now understand that pore size, surface area, and carbon nanostructure all play crucial roles in determining electrochemical performance. Since then, significant efforts have been made acquire a basic comprehension of the fundamental charge storage processes at the nano- and subnanoscales, concentrating on the carbon structure and the organization of the electrolyte (Salanne et al., 2016).

The selection of electrode materials for electric double layer supercapacitors is crucial, and typically involves choosing materials with large surface areas and interconnected mesopores. Activated carbon, carbon nanotubes, and graphene are commonly

utilized due to their desirable properties. Activated carbon, for example, has , possesses a substantial surface area and is cost-effective, with a variety of pore sizes ranging from 1 to 20 nanometers in diameter. Mesopores with sizes larger than 1 nm are favorable for ionic motion between electrodes, resulting in enhanced conductivity and higher capacitance values. Micropores with sizes smaller than 2 nanometers, on the other hand, restrict the mobility of ions and are therefore not preferable. For mesoporous carbon, the capacitance per unit area can be determined using equation (2.2) (S. Sharma & Chand, 2023).

$$\frac{C}{A} = \frac{\epsilon r\ \epsilon 0}{r\ ln\frac{r}{a0}} \tag{2.2}$$

In the above equation, A represents the specific surface area of the electrode material, r represents the pore radius, and a_0 represents the effective size of the ion. Macropores are pores with diameters larger than 50 nanometers. However, Large pores that consist mostly of empty space can impede the infiltration of the electrolyte, affecting the efficient movement of ions between current collector electrodes. When the pore size is poorly coordinated with the ion size, such as when the pore diameter is either too small (less than 2 nanometers) or excessively large (over than 50 nanometers), this can result in a reduction in specific capacitance. In general, pore diameter can be arranged in the following order: micropores (< 2 nanometers) < mesopores (2–50 nanometers) < macropores (> 50 nanometers). Mesopores are typically preferred for enhancing the electrochemical performance of supercapacitors because they allow for more efficient utilization of the specific surface area. They facilitate the flow of electrolyte ions across the electrochemical double layer (EDL) of the electric double-layer capacitor (EDLC) (S. Sharma & Chand, 2023).

2.2.2. Pseudocapacitors

The term "pseudocapacitor" is derived from the Greek word "Pseudés," meaning "False" or "Erroneous." It denotes electrode materials with characteristics similar to conventional capacitive electrodes, such as a linear relationship between stored charge Q (in C or mAh/g) and the potential ΔE (in V), which arises from the electrochemical double layer. Pseudocapacitive behavior is mainly observed in transition metal-based materials such as

RuO_2, MnO_2, and conducting polymer-based materials like polyaniline and polythiophene. When protons are stored in the electrolyte, it triggers faradaic charge-transfer reactions in various electrode materials such as RuO_2, MnO_2, and Nb_2O_5. Despite being faradaic in behavior, the resulting cyclic voltammogram and galvanostatic charge-discharge curves display rectangular and triangular shapes, respectively, similar to capacitors. Thus, these materials fall under the classification of innate pseudocapacitive materials. (Bhojane, 2022).

Pseudocapacitor materials have gained significant attention for their capacity to attain substantial energy and power densities, largely due to their ability to facilitate redox reactions through phase transformations, leading to evident redox indicators in cyclic voltammetry and steady states in galvanostatic charging and discharging. Pseudocapacitive materials are generally characterized by two processes: surface redox pseudocapacitance, encompassing charge transfer at the electrode material's surface, and intercalation pseudocapacitance, entailing the swift intercalation and deintercalation of ions into the stratified structure of the electrode material. Redox reactions are integral to both pseudocapacitive charge storage and battery-type charge storage, but the main difference is that pseudocapacitive materials have slower reaction kinetics due to the solid-state diffusion (Lichchhavi et al., 2023).

Efficient electrode materials are crucial for the optimal performance of pseudocapacitors. In particular, low-cost, safe, and effective cathode materials will be essential for the development of various applications, including hybrid electric transportation and smart power grid systems. Over the past few years, researchers have extensively focused on developing battery-type pseudocapacitive materials, which leverage intercalation faradaic mechanisms to enable higher levels of energy storage (Nishchith et al., 2023).

As previously stated, pseudocapacitive electrodes rely on redox reactions and intercalation/de-intercalation processes of electrode materials, specifically RuO_2 and MnO_2, to transfer electrical charges. Within the potential window, these electrodes demonstrate relatively constant capacitance values. A redox reaction is characterized by simultaneous oxidation and reduction, and the charge stored Q varies linearly with the voltage Vas, as expressed in equation (2.3).

$$Q = CV \tag{2.3}$$

Equation (2.4) describes how current (I) is obtained by differentiating charge (Q) concerning time (t).

$$I = C\frac{dv}{dt} \tag{2.4}$$

The proportionality constant C, which is measured in units of Fg^{-1} or Fcm^{-2} is known as the specific capacitance (S. Sharma & Chand, 2023).

The specific capacitance can be derived using the equation (2.5) with the Cyclic Voltammetry (CV) curves, while equation (2.6) can be employed to obtain the specific capacitance from the Galvanostatic Charge/Discharge (GCD) measurements, as demonstrated below (Yazar & Atun, 2022).

$$Cs = \frac{\oint_{V1}^{V2} I\ dV}{m \times v \times \Delta V} \tag{2.5}$$

$$Cs = \frac{I \times \Delta t}{m \times \Delta V} \tag{2.6}$$

where Cs ($F\ g^{-1}$): the specific capacitance, $\oint_{V1}^{V2} I\ dV$: the integrated field from the CV measurement, ΔV (V): the working potential window, m(g): the amount of active substance in the electrode, and v ($mV\ s^{-1}$) refers to the scan rate, I(A) is the discharge current and Δt(s) is the discharge time (Arvas, Gencten, et al., 2021).

2.2.3. Hybrid capacitors

The advancement of sustainable and eco-friendly electrochemical energy storage technologies, including batteries and supercapacitors, has garnered significant attention in modern society. While batteries offer high capacity and energy density, their short cycling lifetime due to irreversibility of complex redox reactions is a limitation. On the other hand, supercapacitors have excellent power density and extended cycling lifetime, whereas their energy density is lower than batteries. To overcome these limitations, the concept of hybrid supercapacitors has emerged, combining capacitor-type and battery-type (or pseudocapacitive) electrodes to achieve high power and energy density (Xing et al., 2023).

Hybrid supercapacitors are a category of energy storage device that utilizes a conducting polymer as the positive electrode (anode) and activated carbon as the negative electrode (cathode). The selection of these electrode materials is crucial to ensure that the kinetics of the charge/discharge process is balanced. There are three categories of hybrid supercapacitors based on the chosen electrode materials: asymmetric hybrids, battery-type hybrids, and composite hybrids (such as Fe_3O_4/graphene and rGO-f/PANI). The cathode of the hybrid supercapacitor stores charges through surface adsorption/desorption, a process known as non-faradic, while the anode stores charges through intercalation, a process known as faradic. Battery-type electrodes store charges through both faradaic and non-faradaic processes, allowing them to have fluctuating specific capacity values depending on the voltage range employed. They possess an advantage over electric double-layer capacitors and pseudocapacitors as they can combine both storage mechanisms. These electrodes are cost-effective, exhibit excellent performance attributes, and can work over a extensive temperature range. As a result, hybrid supercapacitors are commonly employed as power sources in vehicles (S. Sharma & Chand, 2023).

Currently, the assembly of hybrid supercapacitors has emerged as an effective strategy for increasing the voltage window and producing supercapacitors with high performance. Hybrid supercapacitors combine battery-type materials for energy and capacitive-type materials for power. Carbon-based capacitive negative electrodes widen voltage range and improve conductivity, while positive electrode materials with transition metal compounds enable redox reactions and higher capacitance. However, diffusion limits

redox reaction rates in battery-type electrodes, affecting charge balance and energy-storage benefits. The key challenge is obtaining battery-type electrode materials with excellent conductivity and optimal structure to match capacitive-type electrode charge transfer rates and maximize hybrid supercapacitor benefits (Cui et al., 2023).

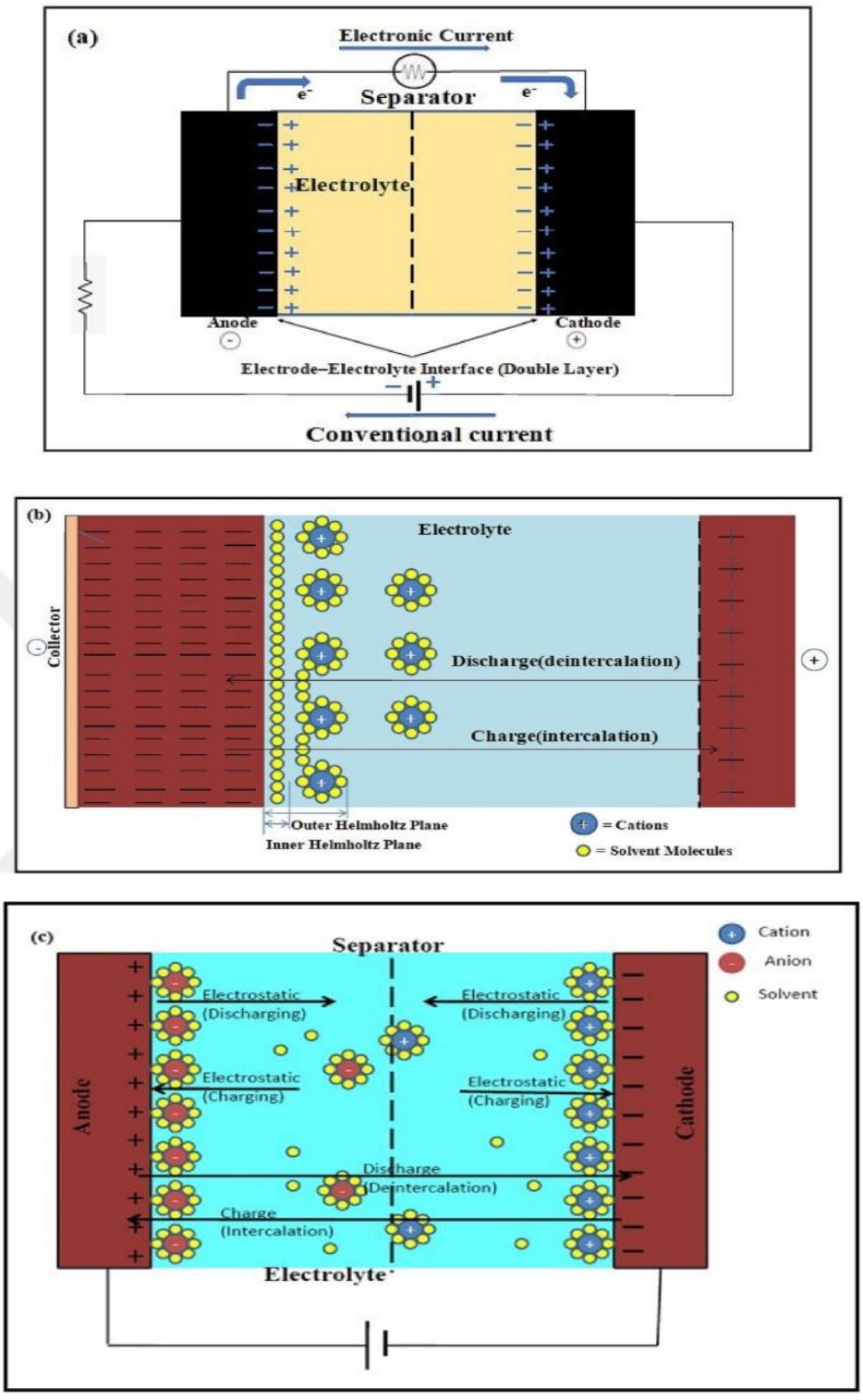

Figure 2.3 Classification of supercapacitor; a) Electric double layer capacitors, b) Pseudo capacitors, c) Hybrid supercapacitors (S. Sharma & Chand, 2023).

Table 2.2 Differences among EDLC, Pseudo-capacitors and hybrid supercapacitors in terms of on charge storage mechanism (S. Sharma & Chand, 2023).

Types	**Electric double layer supercapacitor**	**Pseudocapacitor**	**Hybrid supercapacitor**
classifications		• Redox • Underpotential deposition • Intercalation	Asymmetric • Battery type • Composite based
Charge storage mechanism	Electrostatic	Electrochemical	Electrostatic and Electrochemical
Process	Non-Faradic	Faradic	Faradic and non-faradic
Materials	• Activated Carbon • rGO • CNTs • Carbon aerogel	• Transition Metal Oxides • Conducting Polymer (PANI,PEDOT:PSS)	• CNT//MnO2 • PbO_2//Graphene • TiO_2@rGO//CNT

2.3. Materials of Supercapacitors

Supercapacitors are essential in filling the performance gap between significant energy density batteries or fuel cells and traditional capacitors by providing enhanced power density. To achieve optimal capability, it is crucial to carefully select several components, including active electrode materials, electrolytes, and current collectors. The specific capacitance of supercapacitors primarily relies on electrodes possessing a extensive specific surface area and electronically conducting materials, such as carbon-based materials or oxides/conducting polymers with rapid electrochemical activity. Careful selection of the electrolyte is crucial for device applications, considering its core parameters (Bhat et al., 2023).

The performance of supercapacitors significantly hinges on the electrode material, underscoring its crucial role. As a result, extensive research is being conducted to develop and enhance electrode materials in the supercapacitor domain. High-quality electrode materials are sought-after, characterized by traits like remarkable conductivity, a substantial specific surface area, remarkable stability, robust reversibility, ease of preparation, and the utilization of abundant and cost-effective raw materials (L. Wang et al., 2023).

2.3.1. Carbon based supercapacitors

While supercapacitor (SC) technology has made considerable progress, it still encounters various challenges. One of the primary objectives is to enhance energy density without compromising on rapid charge and discharge capabilities, a lack of reliable design tools to evaluate the influence of different factors on system, and a lack of standardized methods to identify the most suitable applications for different types of SCs. To address these challenges, researchers are working hard to develop innovative and high-performing electrode and electrolyte materials for SCs. Despite ongoing efforts, carbon remains the most widely accepted and popular energy storage electrode material for SCs. Carbon possesses a range of ideal characteristics for supercapacitor (SC) electrodes, including low manufacturing cost, abundance, controllable morphology, large surface area, intercalating capability for electrolyte-ions, high porosity, and high electrical conductivity. Another advantage of carbon is its ability to be post-treated, enabling alterations to its structure and chemical/mechanical properties, thereby improving its SC performance. Due to these features and merits, virtually all SC manufacturers prioritize carbon/activated carbon (AC) as their primary active electrode material component (N et al., 2022).

Carbon-based materials are renowned for their exceptional conductivity, extensive surface area, and hierarchical pore structure, all of which have a crucial role in their exceptional capacitance and cycle stability. Furthermore, these materials possess ample frame structures, which typically results in higher mechanical endurance (Sun et al., 2023).

Carbon-based materials, including graphene, fullerene, carbon fiber (CF), and carbon nanotubes (CNT), have emerged as popular choices for electrode active materials in supercapacitor electrodes. This preference stems from their advantageous features, such as

cost-effectiveness, significant specific surface area, wide operating temperature variation, and remarkable electrical characteristics. Carbon nanotubes (CNTs) are a significant area of research due to their one-dimensional sp^2 hybridized carbon layer arranged in a hexagonal lattice. They hold great potential for diverse applications, particularly in the field of supercapacitors. CNTs offer remarkable attributes such as significant electrical conductivity, and rapid electron transfer, making them highly desirable for supercapacitor applications (Kariper et al., 2022).

Carbon nanotubes (CNTs) offer distinct advantages as nanocomposites for conducting polymers, thanks to their intrinsic high mechanical strength, significant surface area with a high aspect ratio, and exceptional electrical conductivity. By incorporating CNTs, the electrochemical and electromechanical properties of conducting polymers can be significantly improved (Obeidat & Rastogi, 2023).

CNTs are being considered as a viable replacement for metallic current collectors like aluminum due to their superior conductivity and ability to sustain high current density without degradation. Furthermore, the flexibility and lightweight nature of CNT films enable a decrease in the physical size, weight, and cost of supercapacitors(Panasenko et al., 2022).

Graphene, a single-layered two-dimensional material consisting of carbon atoms with sp^2 hybridization, exhibits a remarkable combination of characteristics that make it highly suitable as an electrode material for supercapacitors. These features encompass excellent mechanical properties, substantial surface area, and superior electrical conductivity. Notably, recent research has focused on graphene composites due to their extraordinary electrochemical characteristics (Sahoo et al., 2023).

Graphene, a carbon-based material, is garnering considerable interest as an electrode material for supercapacitors, owing to its remarkable features.including substantial specific surface area, impressive mechanical strength, lightweight nature, and facile functionalization. However, the Van der Waals forces and strong π-π stacking of graphene flakes can cause easy and irreversible restacking, resulting in the loss of key benefits, like an extremely active surface area. Consequently, there is a pressing need to synthesize non-aggregated graphene electrodes with lightweight, robust mechanical properties, and optimal

electrochemical activity, which is crucial to expand the practical application of supercapacitors (Lu et al., 2023).

Graphene-based (GR-based) electrodes come in various forms, including combinations with metal oxides, conductive polymers, nitrides, and phosphides. These combinations result in the design of composite materials based on graphene, which enhances supercapacitor applications. (Sahoo et al., 2023).

2.3.2. Metal oxide based supercapacitors

Transition metal oxides (TMOs) are a class of pseudocapacitance materials that exhibit a redox pseudocapacitive charge storage process. These materials, such as Fe_2O_3, MnO_2, ZnO, NiCo LDH, CoAl LDH, and Co_3O_4, have undergone thorough research as electrode materials. This is primarily owing to their unique characteristics, including a versatile valence state that enables the intercalation of ions and electrons into the metallic compound's lattice, as well as their notable inherent stability. Metal oxides offer superior energy density compared to traditional carbon materials, making them highly suitable for supercapacitor applications. Additionally, they exhibit enhanced electrochemical stability when compared to polymer materials. These metal oxides demonstrate electrochemical faradaic reactions with ions at the electrode-material interface, while simultaneously storing energy through electrostatic mechanisms, similar to carbon materials. Recent efforts have focused on chemical surface modifications of carbonaceous materials to optimize their wettability and enhance their capacitive properties. Enhancing the specific capacitance of electrodes can be achieved through the deposition of metal oxide/hydroxide particles. Notably, materials like ruthenium oxide,cobalt oxide, nickel oxide, and mixed metal compositions have shown significant potential in improving electrode capacitance by facilitating fast faradaic pseudocapacitance effects. Furthermore, ensuring an adequate electrical conductivity of the electrodes is a crucial factor in promoting the capacitive effects of carbon capacitors when incorporating metal components (Delbari et al., 2021).

Ruthenium oxide (RuO_2), an extensively studied transition metal oxide (TMO), shows excellent potential for supercapacitor applications due to its superior specific capacitance (reaching a maximum level of 1580 Fg^{-1}) and favorable electrical conductivity. However, the widespread utilization of RuO_2 has been hindered by challenges such as toxicity, significant cost, and the rarity of ruthenium elements. In addition to RuO_2, other metal oxides like NiO, Co_3O_4, MnO_2, and V_2O_5 have been extensively explored and shown to be plentiful, cost-effective, and ecologically friendly alternatives. Nevertheless, the practical utilization of these metal oxides was hindered by their comparatively lower specific capacitances. Consequently, Recent progress in the field has brought attention to mixed transition metal oxides (MTMOs) as viable and affordable options for supercapacitor utilization. MTMOs enable diverse redox reactions with two metal species in one structure, yielding higher specific capacitance than single-component oxides. Yet, challenges include insufficient conductivity, limited cycling stability, and aggregation during charge-discharge (Low et al., 2019).

Ruthenium oxide (RuO_2) based supercapacitors are gaining attention due to the exceptional electrochemical capacitance exhibited by RuO_2 as an electrode material. Both crystalline and amorphous hydrous forms of RuO_2 show promise, with capacitance values exceeding 700 Fg^{-1} achieved through under-potential hydrogenation in acidic electrolytes or oxygenation in alkaline electrolytes. The capacitance of RuO_2 is remarkably high, ranging from 150–260Fcm^{-2}, approximately ten times greater than that of carbon. This superior performance is attributed to pseudocapacitance arising from the surface reaction between Ru ions and H ions. In an H_2SO_4 electrolyte, the C–V curve of RuO_2 appears mirror-like and lacks distinctive features within a potential range of 1.4 V. Amorphous ruthenium oxides possess advantages, including substantial specific capacitance (Sc), excellent conductivity, and superior electrochemical reversibility. They have demonstrated a maximum specific capacitance of 768 Fg^{-1}, which is more than twice as high as that of other capacitive electrode materials. Additionally, amorphous ruthenium oxides exhibit a broader potential range of around 1.35V in aqueous electrolytes, surpassing the 1.05V range observed for crystalline ruthenium oxides. Focusing on the amalgamation of RuO_2 with various materials, extensive research has been carried out to create bulk composite electrodes, aiming to enhance oxide dispersion. These studies have explored various compositions involving RuO_2 and other oxides, such as TiO_2, MoO_3, CaO, among others (Lokhande et al., 2011).

Manganese oxide (MnO_2) is being explored as a cost-effective and less toxic alternative to ruthenium oxide in supercapacitor applications. Researchers are investigating composite electrodes that combine MnO_2 with carbon nanotubes, polyaniline, and other conductive materials for MnO_2-based supercapacitors. Diverse synthesis methods, including sol-gel and electrochemical deposition, have been used to prepare manganese oxide thin films for these supercapacitors (Lokhande et al., 2011).

Cobalt oxide (Co_3O_4) has emerged as a potential material for supercapacitors attributed to its intercalative pseudocapacitance properties. In studies, a maximum specific capacitance (Sc) of 291 Fg^{-1} was achieved using CoO_x xerogel calcined at 423 K. The cobalt oxide electrode exhibits excellent efficiency, long-term performance, and corrosion stability. The incorporation of MWNTs/Co_3O_4 composites enhances the capacitor properties significantly, with a best specific capacitance of 200.98 Fg^{-1}, surpassing that of pure MWNTs. Additionally, a simple and cost-effective room temperature method known as SILAR was developed for depositing cobalt oxide films onto copper substrates. Cobalt oxide films, formed from $CoCl_2$ and liquor ammonia solution as a cationic precursor, along with H_2O_2 as an anionic precursor, showed a Sc of 165 F g^{-1} in 1.0 M KOH.

Nickel oxide films were prepared using various methods, including thermal treatment of electrodeposited $Ni(OH)_2$, sol-gel, and electrostatic spray deposition. Heat treatment of electrochemically precipitated $Ni(OH)_2$ films in air resulted in the gradual transformation of non-stoichiometric nickel oxide ($Ni1-_xO$) into the stoichiometric NiO structure, leading to defect healing. The presence of defects in nickel oxide contributed to an enhanced specific capacitance, ranging from 200 to 278 Fg^{-1} in 1 M KOH under a potential window of 0.5 V (Lokhande et al., 2011).

2.3.3. Polymer based supercapacitors

In recent years, supercapacitors (SCs) have found application in high-power automotive systems, encompassing diverse functionalities like regenerative braking, intense velocity devices for propulsion, demanding strong power and energy density, as well as flexibility, resilience, and high wear strength. To meet these diverse demands, polymer-based materials have been increasingly used as electrodes and electrolytes in SCs. These materials offer advantages such as intense power density, flexibility, resilience, and lightweight properties relative to carbon-based supercapacitors. However, to improve their cyclic stability, there has been extensive research in the past decade on polymer composites. Furthermore, the biodegradable nature of polyvinyl alcohol has led to its broad exploration in energy storage applications (Gaikwad et al., 2023).

The utilization of polymers as electrodes in energy storage devices offers the possibility of achieving desirable electrochemical properties. These polymers can undergo either n-doped or p-doped, with p-doped variants exhibiting electrochemical stability and providing notable reversibility when undergoing doping. However, in the case of pseudocapacitors, electrodes primarily composed of conducting polymers like polyaniline (PANI), polypyrrole (PPy) and poly(3,4-ethylenedioxythiophene) (PEDOT) have been extensively investigated, showcasing a maximum specific capacitance of up to 1000 Fg^{-1}. Nonetheless, the continuous faradaic electron exchange throughout the charge-discharge process can lead to material deterioration and inadequate capacitance retention in polymer pseudocapacitors. To address this challenge, a promising approach involves the use of hybrid electrodes comprising polymer nanocomposites. This strategy has led to significant advancements in energy storage devices, as the reduction of particle size to the nanoscale has brought about a dramatic change in properties, particularly by greatly Expanding the specific surface area at the interface of the electrode and electrolyte. This breakthrough in nanoscale polymer composites holds great potential for achieving outstanding electrochemical performance in energy storage applications (Gaikwad et al., 2023).

Recently, there has been a notable rise in research focus on conducting polymers (CPs) and their composites, primarily due to their exceptional properties such as superior conductivity in the doping state, excellent charge storage capacity, broad voltage window,

simple synthesis, cost-effectiveness, and eco-friendly. These desirable characteristics have made CPs highly suitable for the development of electrodes in supercapacitors. Among the CPs commonly utilized for supercapacitive applications are polyaniline (PANI), polypyrrole (PPy), polythiophene (PTh), and poly(3,4-ethylenedioxythiophene) (PEDOT) (Ambade & Patil, 2023). The subsequent section provides a more detailed discussion on CPs. Additionally, the electrode's surface morphology significantly influences the performance of a supercapacitor. Therefore, it is essential to design electrodes using porous materials that offer a large surface area, enhanced carrier mobility, excellent chemical compatibility, extended lifespan, thermal stability, and significant capacitance values. Furthermore, these electrodes should possess substantial temperature and chemical stability, superior electrical conductivity, environmental eco-friendly, and cost-effectiveness. Two top-ranked CPs, polypyrrole (PPy) and polyindole (PIn), have been extensively analyzed the context of their application as supercapacitor electrode materials. These CPs have gained prominence as leading contenders for the production of electrodes in cutting-edge and futuristic supercapacitors (Ambade & Patil, 2023).

The practical application of conducting polymers in electrochemical supercapacitors is hindered by their low performance caused by volume changes over extended cycling stability, despite their high intrinsic conductivity and unique properties. Nevertheless, conducting polymers like polyaniline (PANI), polypyrrole (PPy), poly(3,4-ethylenedioxythiophene) (PEDOT), and polythiophene (PTh) persist as favored electrode materials for supercapacitors because they possess unique doping-dedoping characteristics, ease of processing, environmentally friendly nature, and affordability (Ambade & Patil, 2023).

Superabsorbent polymers (SAPs) fall into two categories: natural and synthetic types. Natural SAPs, including cellulose, starch, and chitosan, offer the advantage of being biodegradable. However, they have a drawback of low water absorption, requiring larger quantities for effective use. In contrast, synthetic SAPs like polyacrylic acid (PAA) and polyacrylamide (PAM) possess advantages such as cost-effectiveness, prolonged lifespan, and high water absorption. However, their non-degradable properties can potentially harm the environment and hinder plant growth (Chang et al., 2021).

Polyacrylic acid (PAAc) has recently become a popular topic of interest due to its utilization as a thickening agent in lattices, adhesives, and various formulations such as pharmaceuticals, cosmetics, coatings, and agricultural chemicals. The presence of an carboxylic (-COOH) group in PAA chains enables a variety of bond creation options, including hydrogen, ionic, and coordination bonds. These bonding mechanisms have been utilized in the creation of hydrogels, chelating agents, esters, and complex nanoparticles (NPs). An electrophoretic deposition process was used to create a composite film of Carbon nanotubes (CNTs) and polyacrylic acid (PAAc) in a PAAc aqueous solution. This film was then utilized as a capacitive deionization electrode with the PAAc acting as both a cation-exchange polymer and matrix for CNT incorporation (Nie et al., 2012).

Polyisopropylacrylamide (PNIPAM) is a temperature-sensitive phase transition material that exhibits a lower critical temperature (LCST) ranging from 30 to 35 ℃ (X.-E. Hu et al., 2023). Below the LCST, PNIPAM remains dissolved in water, but above this threshold, it undergoes a transition from a coiled to a spheroidal structure, resulting in precipitation. By graft copolymerizing PNIPAM with chitosan (CS), the chitosan-poly-N-isopropylacrylamide graft copolymer (CS-g-PNIPAM) can be obtained. This graft copolymer not only confers temperature-responsive properties to chitosan but also effectively resolves the issues of weak strength and delayed gelation typically associated with Polyisopropylacrylamide-based gels. The CS-g-PNIPAM gel, synthesized by grafting PNIPAM onto CS, exhibits improved temperature-sensitive reversibility and mechanical strength compared to CS-based gel. The gel has a viscosity of approximately 73 Pa s with a CS content of 0.25 g, and it undergoes gelation at a lower temperature of 30 ℃. The gel demonstrates a phase change within 3 minutes (X.-E. Hu et al., 2023).

S-PNIPAM graft copolymer has an LCST (lower critical solution temperature) of 32 ℃, mirroring the surface temperature of the human eye, making it a potential drug carrier for eye diseases. A PNIPAM composite grafted with bacterial cellulose nanowhiskers has an LCST of 34.3 ℃ and shows promise in transarterial chemoembolization (TACE) treatment with enhanced mechanical strength. (X.-E. Hu et al., 2023) .

2.4. Electrochemical Characterization Techniques of Supercapacitors

In recent times, remarkable advancements have been achieved in the development of electrode materials, leading to an increased demand for more precise and standardized procedures to assess them. However, analyzing these materials poses several challenges, particularly due to their intrinsic complexities compared to bulk materials (for instance, diminutive dimensions and decreased quantities may be observed in certain cases following laboratory-scale production). Nanomaterials exhibit unique properties such as very small dimensions and limited quantities, especially when produced on a laboratory scale. Additionally, the interdisciplinary nature of nanoscience and nanotechnology often limits access to a diverse array of analytical methods for research teams (Baig et al., 2021). Consequently, a comprehensive approach integrating different characterization methods becomes necessary for a more thorough understanding of electrode materials. This raises the question of whether a single characterization method is sufficient to obtain the necessary data or if a combination of techniques, particularly the in-situ approach, is necessary. As nanoscience and nanotechnology continue to advance, It becomes apparent that characterization techniques may differ in their effectiveness when applied to electrode materials compared to standard or traditional applications. Various analytical and electrochemical techniques are employed to characterize electrode materials used in energy storage devices. These methods, while sometimes restricted to specific properties, can be combined for a more comprehensive analysis. The accessibility, applicability, selectivity, nondestructive nature, and ease of implementation of these techniques are carefully considered. Electrochemical techniques like cyclic voltammetry, impedance spectroscopy, and charging/discharging are utilized to investigate the electrochemical performance of electrode materials. Table 2.3 provides a summary of the electrochemical measurements used for characterizing supercapacitors. Additionally, Table 2.3 presents the main parameters that need to be determined for supercapacitors and the corresponding characterization methods. A comprehensive examination of the advantages and drawbacks of each technique was performed to aid scientists in selecting the most suitable technique based on their specific requirements and resources. Current developments in this field indicate the use of a combination of methods to investigate the performance of supercapacitors in the charge/discharge and storage process (Baig et al., 2021).

Table 2.3 Summary of the electrochemical techniques used to assess supercapacitor performance (Baig et al., 2021).

Technique	Key Data Derived
Cyclic voltammetry (CV)	Capacitance; cyclic stability; potential window; charge storage mechanism; kinetic parameters; the exchange current density.
Galvanostatic charge-discharge (GCD)	Capacitance; energy density; cyclic stability; self-discharging; potential window; charge storage mechanism; cell resistance; kinetic parameters.
Electrochemical Impedance Spectroscopy (EIS)	Impedance data; capacitance; Nyquist plot; accurate charge storage mechanism; internal resistances (R_s, R_{ct}, ESR); time constant.

2.4.1. Cyclic Voltammetry (CV)

Cyclic Voltammetry (CV) is a widely used and powerful electrochemical technique that provides valuable insights into the thermodynamic and kinetic behavior of a system. It is a versatile approach for quantifying the current behavior of a redox-active solution and establishing the relationship between current and potential. Cyclic Voltammetry is considered a fundamental tool in electrochemical analysis, offering both potentiometric and voltammetric capabilities. In potentiometry, the electric potential of an electrochemical cell is measured during stable circumstances, while in voltammetry, variations in potential across the electrodes are used to analyze the resulting current. Cyclic Voltammetry measurements are typically performed at various scan rates, expressed in mVs^{-1}, while maintaining a constant current density in Ag^{-1} units. The derivative of charge (Q) with respect to potential (V) yields the differential capacitance (C), providing valuable insights into the underlying processes (S. Sharma & Chand, 2023).

The investigation of charge storage mechanisms in supercapacitors, including electric double-layer capacitors and pseudocapacitors, commonly utilizes the three-electrode system with CV as the preferred method. By examining the profile of the cyclic voltammogram, valuable insights can be obtained. For electric double-layer capacitors and

most pseudocapacitors materials, the CV profiles exhibit a rectangular and symmetrical shape. In contrast, certain pseudocapacitive materials display distinct redox peaks. (Baig et al., 2021).

2.4.2. Galvanostatic Charge/Discharge Cycling (GCD)

Galvanostatic Charge/Discharge (GCD) tests, also known as Constant Current Charging/Discharging, are widely utilized for assessing energy storage systems and materials, particularly in the case of electrochemical capacitors (ECs). These tests involve applying consistent positive and negative currents to charge and discharge a material or device while maintaining a predetermined potential level. Frequently, this procedure is carried out over numerous cycles. Galvanostatic Charge/Discharge profiles serve the purpose of evaluating the capacitive response quality, identifying potential non-reversible Faradaic reactions, and deriving important performance indicators for ECs, including capacitance, energy storage, and power. However, one aspect that remains insufficiently investigated in Galvanostatic Charge/Discharge tests is the impact of charge distribution within the material on the observed response and performance indicators. Throughout the charging or discharging operation, the outer surface of the material shows a rapid reaction, while the bulk material may exhibit significant lag. This phenomenon warrants further investigation to better understand its influence on the observed behavior and key parameters in electrochemical capacitors (Licht et al., 2020).

2.4.3. Electrochemical Impedance Spectroscopy (EIS)

Electrochemical Impedance Spectroscopy (EIS) is a versatile, cost-effective, harmless, and extensive technique prevalently employed for characterizing energy storage devices, sensors, and electrocatalysts. In the context of Supercapacitors (SCs), EIS enables the acquisition of various physical properties that are crucial for understanding the underlying electrochemical processes. These properties include (1) pore structures, (2) electrolyte resistance within the electrode pores, (3) Equivalent Series Resistance (R_{ESR}), (4) interfacial impedance, and (5) charge transport resistance. Understanding these

characteristics is essential for gaining insights into the SC electrochemical process. Additionally, compared to techniques like Cyclic Voltammetry (CV) and Galvanostatic Charge/Discharge (GCD), Electrochemical Impedance Spectroscopy offers the advantage of being a simpler technique, allowing the analysis of various variables in an experiment, arising from disparities in the time constants of the events. This makes Electrochemical Impedance Spectroscopy a more convenient approach for comprehensive characterization of SCs (Pedro Aguiar dos Santos et al., 2023).

3. MATERIALS AND METHODS

3.1. Materials

The majority of reagents employed in this study were acquired from reputable commercial chemical suppliers and utilized without further purification. Specifically, ammonium persulfate (APS) was obtained from Crlo Erba, while N,N'-methylenebis(acrylamide) (MBA) and N,N,N',N'-tetramethylethylenediamine (TEMED) were procured from Sgimga-Aldrich. Carbon felt, on the other hand, was sourced from Mersen.

3.2. Synthesis of PAAc

Polymer and polymer composites were obtained using the radical polymerization method. Acrylic acid (AAc), methylene bisacrylamide (MBA), N, N, N′, N′-Tetramethyl ethylenediamine (TEMED), and ammonium persulfate (APS) were used for polymer synthesis as the monomer, crosslinker, accelerator, and initiator, respectively. PAAc synthesis was first stirred by adding AAc, MBA, and TEMED to deionized water. Then, after adding the APS and mixing again, it was transferred onto the carbon felt with the help of a micropipette and kept at 45 ^{o}C for 12 h.

3.3. Synthesis of PANIPAM

Poly(N-isopropylacrylamide) (PNIPAM) and its composites were synthesized using the radical polymerization method. The monomers used for PNIPAM synthesis were N-isopropylacrylamide. Similar to the synthesis of PAAc, a crosslinker, accelerator, and initiator were utilized, including methylene bisacrylamide (MBA), N, N, N′, N′-Tetramethyl ethylenediamine (TEMED), and ammonium persulfate (APS), respectively. In the synthesis of PNIPAM, the N-isopropylacrylamide monomers were dissolved in water. The crosslinker (MBA) and accelerator (TEMED) were added to the solution, followed by stirring to ensure homogeneity. Similar to PAAc, the radical initiator (APS) was then introduced to initiate the polymerization reaction. The reaction mixture was transferred onto a suitable substrate, such

as carbon felt, and maintained at a specific temperature, typically 45°C, for a designated period, typically 12 h, to allow the polymerization process to occur.

3.4. Synthesis of PAAc/PNIPAM-g-CNT and PAAc/PNIPAM-g-(M/CNT) Composites

The PAAc/PNIPAM-g-CNT, PAAc-g-(Pd, Pt, Ru, Co, Mo, Fe, Ga, Bi, Ni /CNT) and PNIPAM-g-(Ru/CNT) composites were synthesized using the same parameters as the polymer synthesis method. The only variation was the addition of CNT and M/CNT before introducing the initiator (APS). To achieve a uniform dispersion, the CNT and M/CNT were treated in an ultrasonic bath. This ensured that they were homogeneously distributed within the composites, leading to enhanced characteristics and a vast range of potential applications.

3.5. Synthesis of M/CNT Catalysts

The synthesis of M(Pd, Pt, Ru, Co, Mo, Fe, Ga, Bi, Ni /CNT) metals on carbon nanotubes (CNT) was achieved through the reduction method of sodium borohydride ($NaBH_4$). To begin, deionized water and Mo precursor were combined in a beaker and subjected to an ultrasonic bath until uniformly dispersed. Subsequently, CNT was incorporated into the solution. The solution was mixed using both a mixer and an ultrasonic bath for about two hours. Subsequently, the reducing agent NaBH4 was dissolved in deionized water and gradually incorporated into the mixture. Following stirring for around 1 hour, the mixture was filtered, washed, and dried at 85 ^{o}C for 12 hours.

3.6. The Characterization of Polymer Composites

Fourier transform infrared spectrophotometer (FTIR), X-ray diffraction (XRD), Raman spectroscopy, and scanning electron microscopy-energy dispersive X-ray (SEM-EDX) and mapping analyses were conducted to examine the structural and morphology properties of polymer and polymer composites. XRD analysis was realized to determine the crystal structures of polymer composites using a Panalytical EMPYREAN instrument. A Bruker Alfa T spectrometer with a 30° reflection accessory (M112-06/08) was employed to conduct infrared reflection-absorption spectroscopy (IRRAS) analysis of the films. Raman

spectroscopy (Renishaw inVia Raman Microscope) was used to analyze polymer composites' chemical and structural properties. Polymer composites were characterized by SEM-EDX and mapping to analyse the material's surface properties and elemental analysis using the Hitachi Regulus 8230 FE-SEM instrument.

3.7. Electrochemical Analysis of The Electrode Materials

The electrochemical tests were carried out using the Ivium Vertex Instruments Potentiostat/Galvanostat, manufactured by Ivium Technologies B.V, The Netherlands. The methods employed for the electrochemical tests (were cyclic voltammetry (CV), galvanostatic charge/discharge (GCD), and electrochemical impedance spectroscopy (EIS)). A half-cell system comprising a platinum wire as a counter electrode, Ag/AgCl as a reference electrode, and a 0.5 M H_2SO_4 aqueous electrolyte were used to evaluate the capacitance performance of the electrodes. Equation (3.1) was used to determine the value of specific capacitance from the CV curves. The specific capacitance can be determined from the GCD measurements by applying equation (3.2), as shown below (Yazar & Atun, n.d.) :

$$Cs = \frac{\oint_{V1}^{V2} I\, dV}{m \times v \times \Delta V} \tag{3.1}$$

$$Cs = \frac{I \times \Delta t}{m \times \Delta V} \tag{3.2}$$

where Cs (F g^{-1}) is the specific capacitance, $\oint_{V1}^{V2} I\ dV$ is the integrated field from the CV measurement, ΔV (V) is the working potential window, m(g): the amount of active substance in the electrode, and v(mV s^{-1}) refers to the scan rate, I(A) is the discharge current and Δt(s) is the discharge time (Arvas, Gencten, et al., 2021).

4. RESULTS AND DISCUSSION

4.1. FTIR

FTIR (Fourier-transform infrared) spectroscopy is a effective analytical technique commonly employed for the identification and characterization of functional groups in organic and inorganic compounds. In Figure 4.1, the FTIR spectra of various materials are shown: poly(acrylic acid) (PAAc), PAAc-grafted carbon nanotubes (PAAc-g-CNT), PAAc-grafted platinum-decorated carbon nanotubes (PAAc-g-(Pt/CNT)), PAAc-grafted palladium-decorated carbon nanotubes (PAAc-g-(Pd/CNT)), and PAAc-grafted ruthenium-decorated carbon nanotubes (PAAc-g-(Ru/CNT)). The FTIR spectrum of PAAc exhibits peaks at 1100 cm^{-1}, which correspond to C=O stretching vibrations. In the spectrum of PAAc-g-CNT, additional peaks are observed around 3000 cm^{-1}, indicating stretching vibrations of C-H bonds in the carbon nanotubes. The spectra of PAAc-g-(Pt/CNT), PAAc-g-(Pd/CNT), and PAAc-g-(Ru/CNT) show further peaks around 1700 cm^{-1} and 1100 cm^{-1}, indicating stretching vibrations of metal-carbonyl bonds in the metal-decorated carbon nanotubes. Moving on to Figure 4.2, the FTIR spectra of five different materials are depicted: CF/PAAc, CF/PAAc-g-CNT, CF/PAAc-g-(Ni/CNT), CF/PAAc-g-(Fe/CNT), and CF/PAAc-g-(Co/CNT). The FTIR spectra reveal absorption bands corresponding to different chemical bonds present in the samples. CF/PAAc spectrum displays a prominent peak at 1050 cm^{-1}, indicating C=O stretching vibrations in the carboxylic acid functional group. CF/PAAc-g-CNT exhibits additional peaks around 650 cm^{-1}, which correspond to stretching vibrations of C-H bonds in the carbon nanotubes. CF/PAAc-g-(Ni/CNT) spectrum shows a peak at approximately 1630 cm^{-1}, corresponding to the C=C bond stretching vibrations in the carbon nanotubes. Additionally, the presence of a metal-oxygen-carbon (M-O-C) bond is indicated by a peak at around 1600 cm^{-1}, representing the stretching vibrations of the Ni-O bond. The spectrum of CF/PAAc exhibits a peak at around 3300 cm^{-1}, indicating the stretching vibrations of the hydroxyl (-OH) group present in the carboxylic acid functional group of the PAAc polymer (Silverstein & Bassler, 1962)(L. Jiang et al., 2022).

In Figure 4.3, the FTIR spectra of various materials are displayed, including PAAc, PAAc-g-CNT, PAAc-g-(Mo/CNT), PAAc-g-(Ga/CNT), and PAAc-g-(Bi/CNT). The FTIR spectrum of PAAc shows peaks at 1100 cm^{-1} and 1700 cm^{-1}, representing the stretching vibrations of C=O bonds. Both PAAc and PAAc-g-(Mo/CNT) exhibit a peak at 620 cm^{-1}, indicating the stretching vibrations of carbon-hydrogen (C-H) bonds (Feng et al., 2018).

In Figure 4.4, significant peaks at 3289 cm^{-1} and 1600 cm^{-1} are observed, indicating the presence of the secondary amide (N–H) stretching vibration in PNIPAM. Another notable peak at 1670 cm^{-1} corresponds to the stretching of the secondary amide (C=O). Additionally, characteristic peaks at 1366 cm^{-1}, 1457 cm^{-1}, and 2966 cm^{-1} confirm the existence of methyl groups in the PNIPAM structure (X. Yang et al., 2020). Furthermore, the PNIPAM-CNT composite exhibits an additional peak at 1500 cm^{-1}, associated with the stretching vibration of C-C bonds, suggesting the bonding between PNIPAM and CNT.

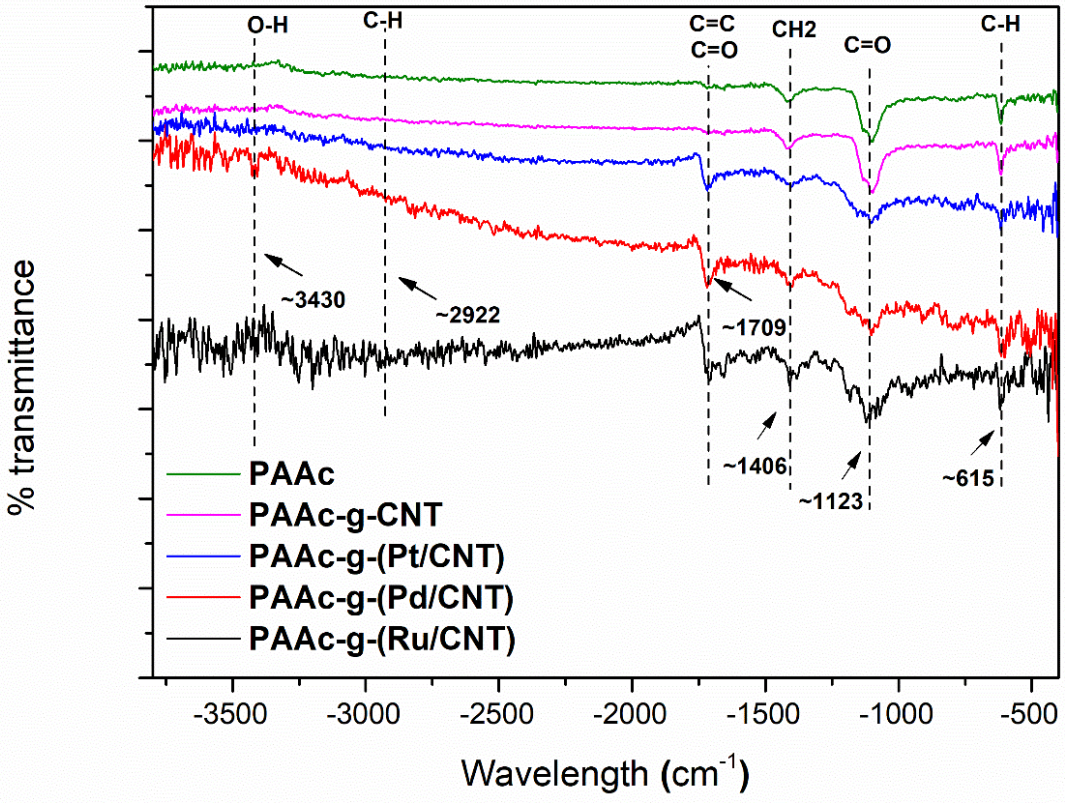

Figure 4.1 The FTIR spectra of PAAc, PAAc-g-CNT, PAAc-g-(Pt/CNT), PAAc-g-(Pd/CNT), and PAAc-g-(Ru/CNT).

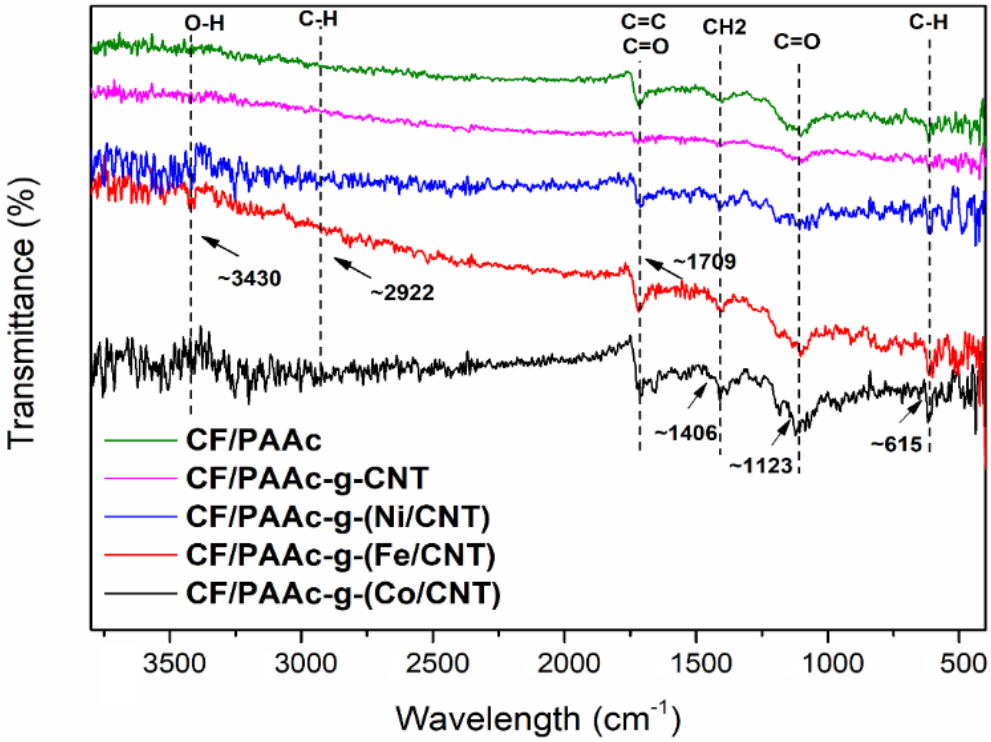

Figure 4.2 The FTIR spectra of CF/PAAc, CF/PAAc-g-CNT, CF/PAAc-g-(Ni/CNT), CF/PAAc-g-(Fe/CNT), and CF/PAAc-g-(Co/CNT).

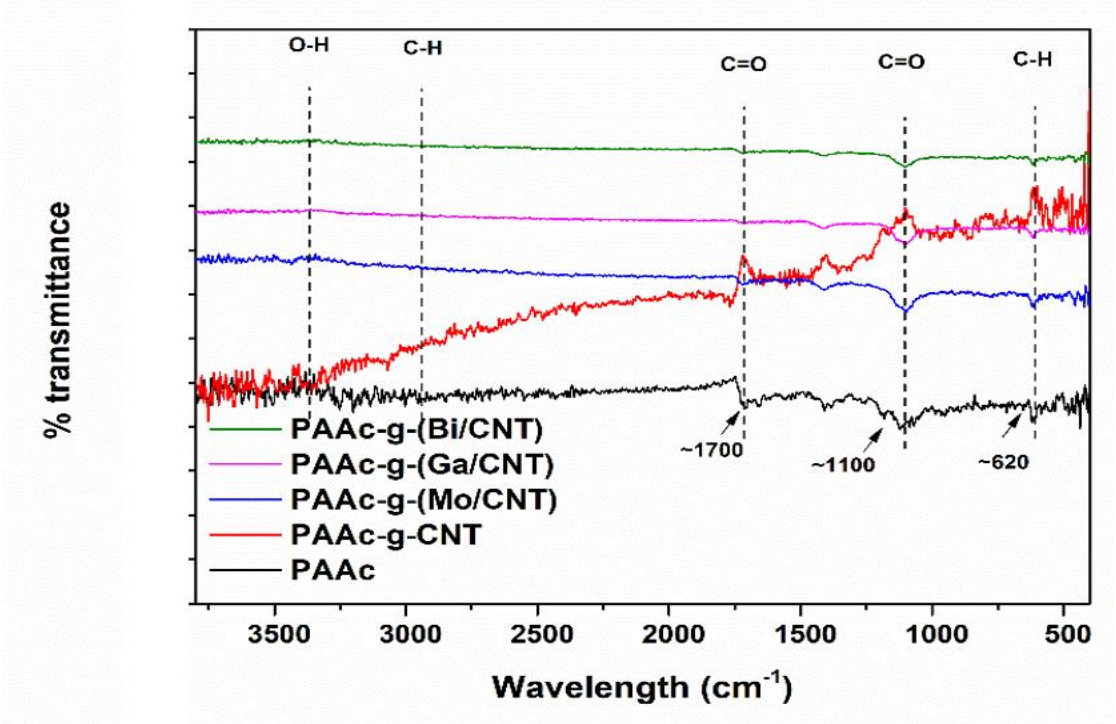

Figure 4.3 The FTIR spectra of PAAc, PAAc-g-CNT, PAAc-g-(Mo/CNT), PAAc-g-(Ga/CNT), and PAAc-g-(Bi/CNT).

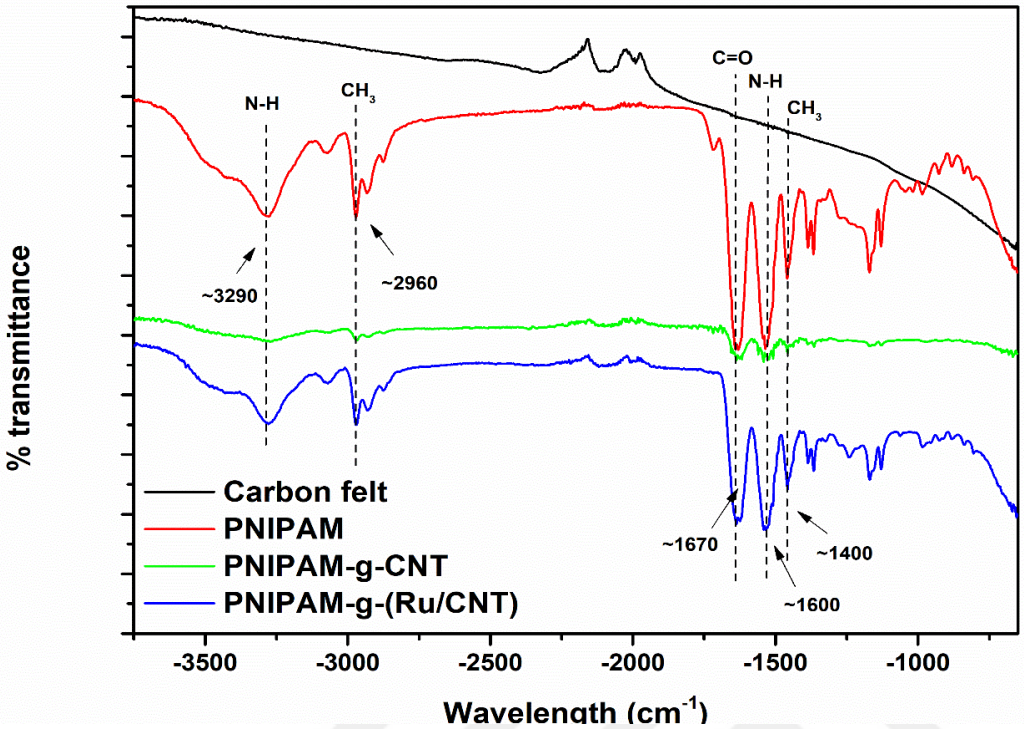

Figure 4.4 The FTIR spectra of carbon felt, PNIPAM, PNIPAM-g-CNT and PNIPAM-g-(Ru/CNT).

4.2. XRD

Figure 4.5 displays the XRD patterns of the PAAc, PAAc-g-CNT, and PAAc-g-(Ru/CNT) polymer composites. The XRD patterns indicate an amorphous structure of hydrogels, evident by the broad peak observed at approximately 2θ=20.4° (Sayed et al., 2022)(Al-Gorair et al., 2022). Comparing the peak densities, it is evident that PAAc-g-CNT and PAAc-g-(Ru/CNT) composites have lower peak densities compared to PAAc polymer. The absence of crystalline peaks corresponding to Ru and C suggests their low concentration in the polymer composites relative to PAAc. The decrease in peak densities of the polymer composites, along with the amorphous structure, suggests the formation of the composites.

Moving on to Figure 4.6, the XRD patterns of the CF/PAAc, CF/PAAc-g-CNT, and CF/PAAc-g-(Ni/CNT) polymer composites are shown. The diffraction peak at around 20.40° indicates the amorphous structure of the hydrogel. Comparing the peak densities, it is observed that CF/PAAc-g-CNT and CF/PAAc-g-(Ni/CNT) composites have lower peak densities compared to CF/PAAc polymer. Moreover, the diffraction peak of the CF/PAAc-g-(Ni/CNT) composite displays a negative shift compared to CF/PAAc and CF/PAAc-g-CNT. Despite the absence of distinct diffraction peaks due to the low concentrations of Ni and C elements, the decrease in peak intensity and the negative shift suggest the formation of the composite.

Furthermore, in Figure 4.7, the XRD patterns of the PAAc, PAAc-g-CNT, and PAAc-g-(Mo/CNT) polymer composites reveal an amorphous hydrogel structure, as indicated by the broad peak observed at around 2θ=20.4°(Sayed et al., 2022)(Al-Gorair et al., 2022). The peak density of PAAc-g-CNT and PAAc-g-(Mo/CNT) composites is lower compared to that of PAAc polymer. Notably, the XRD pattern shows a reduction in the intensity of the diffraction peak for the PAAc-g-(Mo/CNT) composite, despite the low concentration of Mo and C elements. This reduction in peak intensity suggests the formation of the composite.

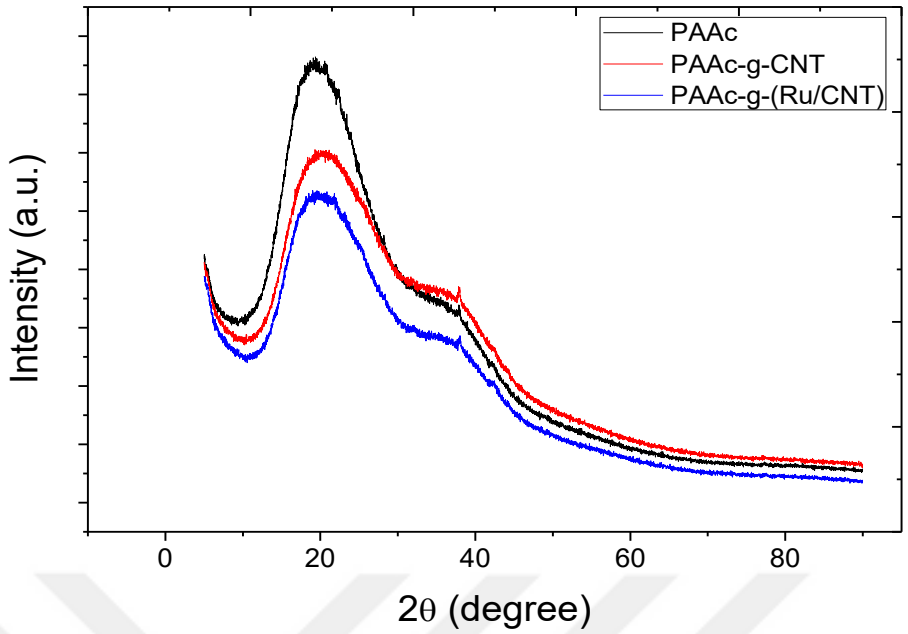

Figure 4.5 XRD patterns of PAAc, PAAc-g-CNT, and PAAc-g-(Ru/CNT) composites.

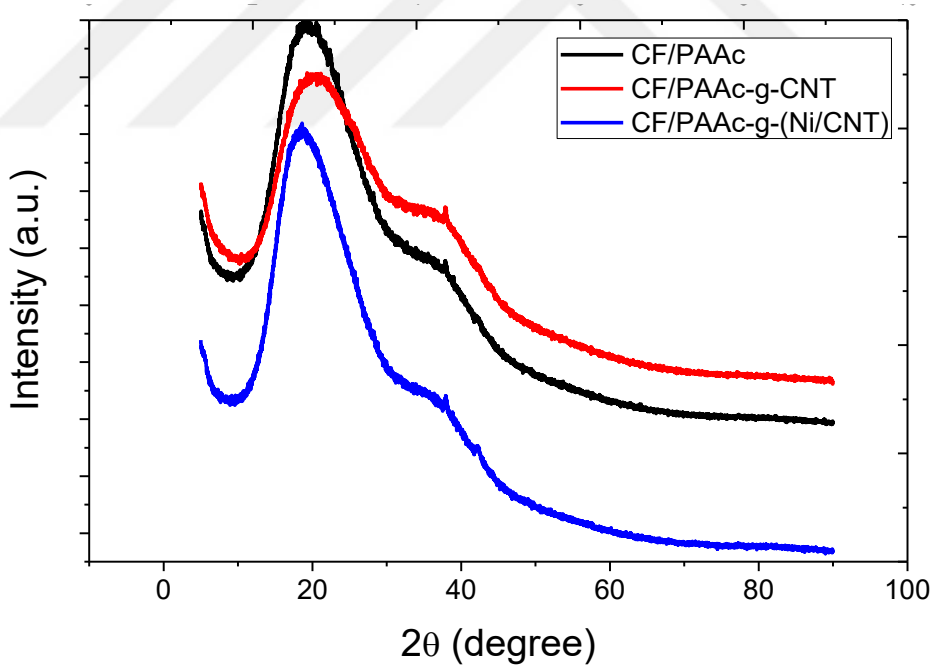

Figure 4.6 XRD patterns of PAAc, PAAc-g-CNT, and PAAc-g-(Ni/CNT) composites.

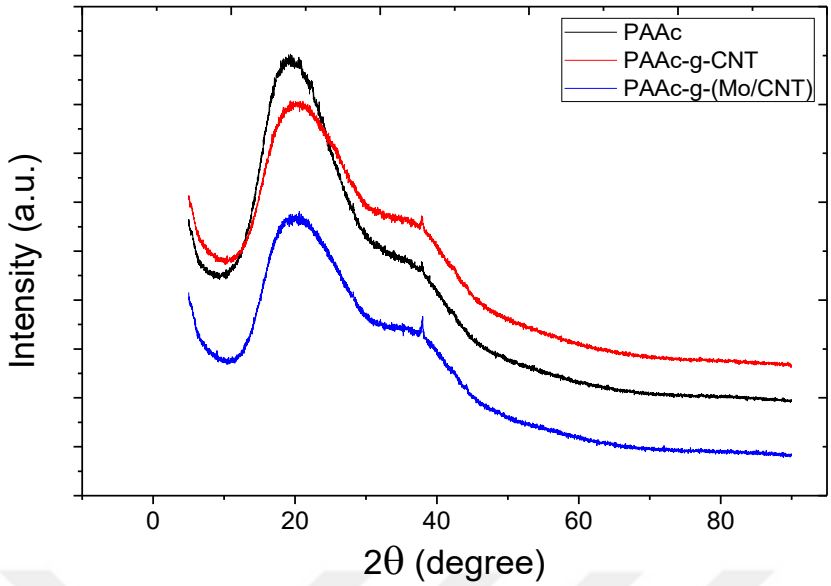

Figure 4.7 XRD patterns of PAAc, PAAc-g-CNT, and PAAc-g-(Mo/CNT) composites.

4.3. SEM-EDX

SEM-EDX and mapping analysis for surface morphology of the PAAc-g-(Ru/CNT) polymer composite was given in Figure 4.8 SEM images of the PAAc-g-(Ru/CNT) polymer composite demonstrate that polymer structures and nanoparticles are formed. Since the amount of Ru metal is very low compared to CNT and PAAc, a low amount of presence was observed in the EDX analysis. Furthermore, mapping analysis indicated the formation of Ru and C elements with blue and red colors, respectively. From the SEM-EDX and mapping analysis, it can be concluded that the desired composite structure formed.

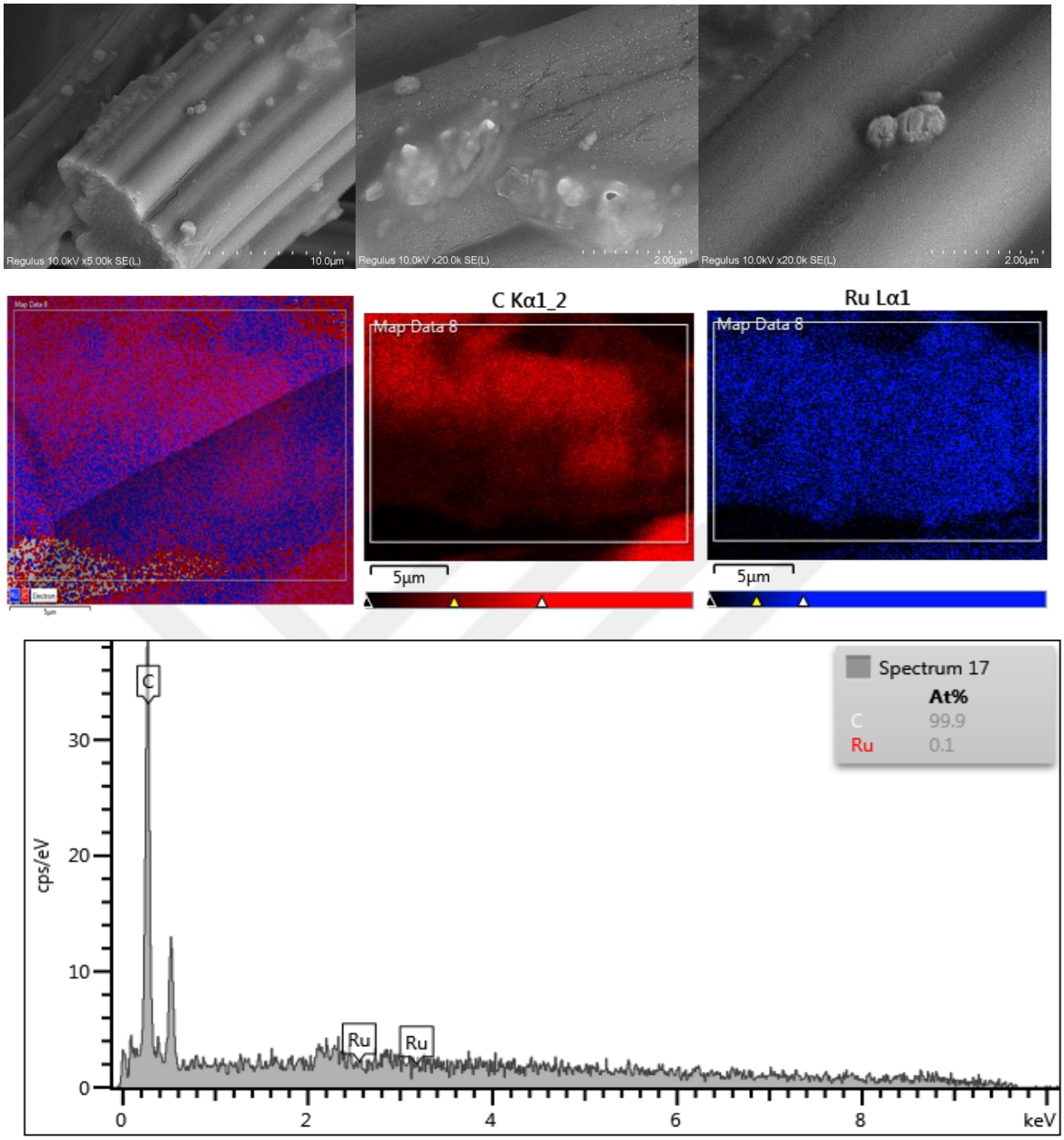

Figure 4.8 SEM-EDX and mapping analysis of PAAc-g-(Ru/CNT) composite.

Figure 4.9 demonstrates the SEM-EDX and mapping analysis for the surface morphology of the CF/PAAc-g-(Ni/CNT) polymer composite. SEM images of the CF/PAAc-g-(Ni/CNT) polymer composite indicate that polymer structures and nanoparticles are composed. It was observed that Ni/CNT nanoparticles formed composites in PAAc. Although the amount of Ni metal is very low compared to CNT and PAAc, EDX analysis shows that Ni metal other than C is formed in the composite structure. Furthermore, mapping analysis illustrated the formation of C and Ni elements with red and blue colors,

respectively. According to the SEM-EDX and mapping results, it can be concluded that the desired composite structure formed.

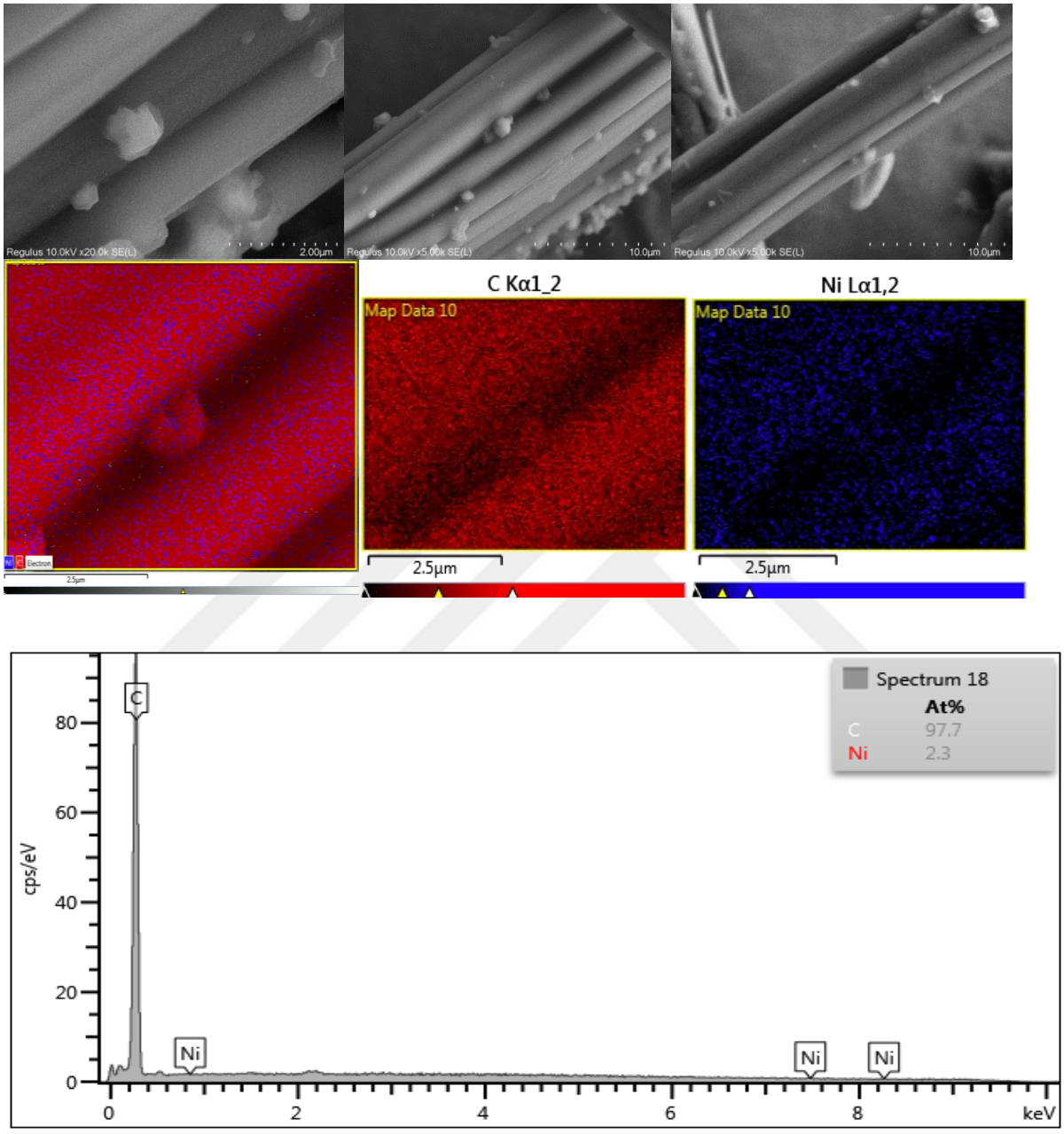

Figure 4.9 SEM-EDX and mapping analysis of CF/PAAc-g-(Ni/CNT) composite.

Figure 4.10 presents SEM-EDX and mapping analysis of the surface morphology of the PAAc-g-(Mo/CNT) polymer composite, showing the formation of polymer structures and nanoparticles. The EDX analysis revealed a low concentration of Mo metal compared to CNT and PAAc, which is consistent with the small amount present in the composite.

Based on the mapping analysis, the formation of Mo and C elements in the PAAc-g-(Mo/CNT) composite was indicated by blue and red colors, respectively. Therefore, the SEM-EDX and mapping analysis findings provide evidence that the composite structure was successfully formed as intended.

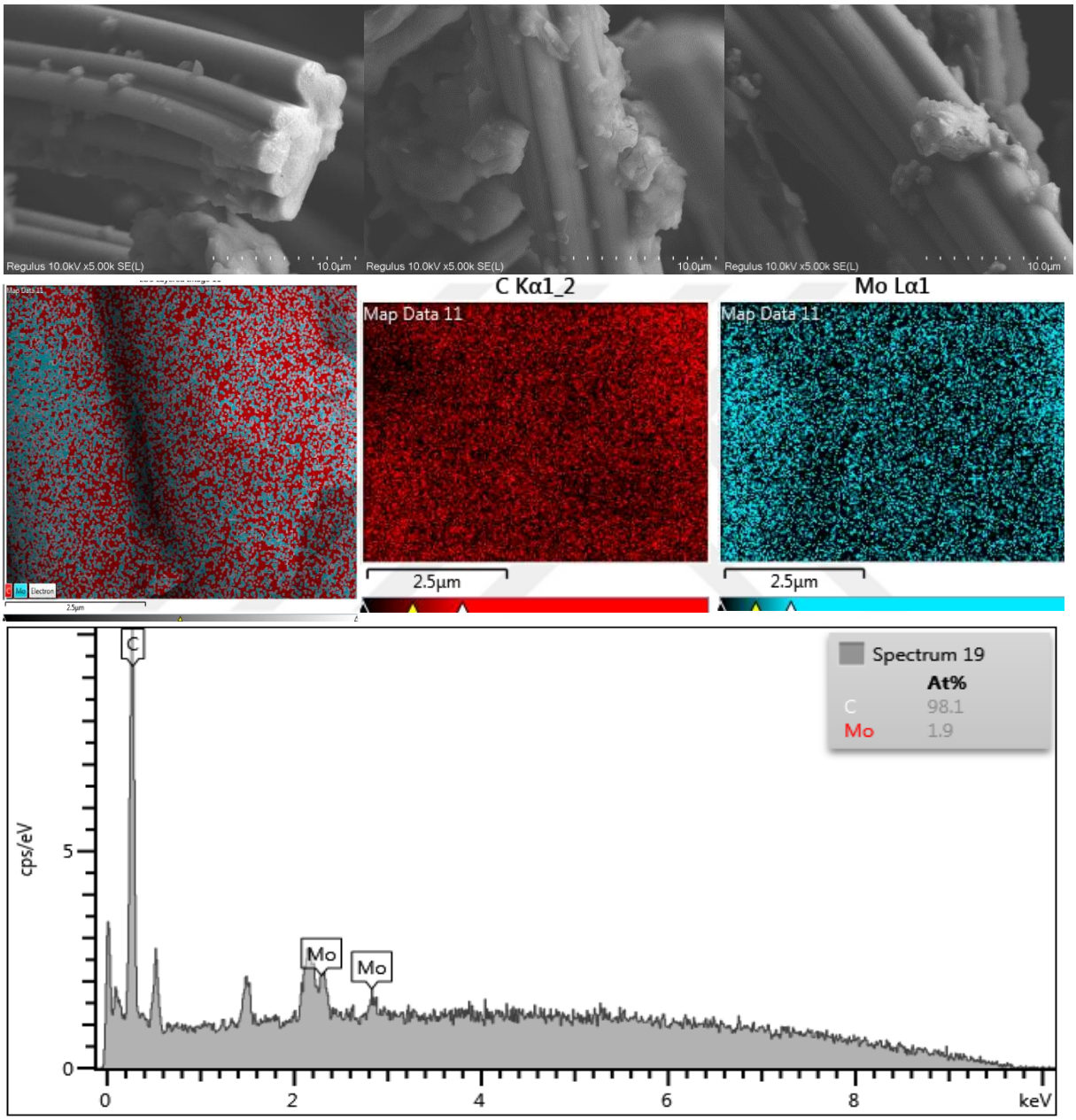

Figure 4.10 SEM-EDX and mapping analysis of PAAc-g-(Mo/CNT) composite.

4.4. Micro-Raman Spectrum

The Micro-Raman spectrums for the PAAc, PAAc-g-CNT, and PAAc-g-(Ru/CNT) polymer composites were illustrated in Figure 4.11 The characteristic Raman peaks of PAAc at 1108 cm^{-1}, 1327 cm^{-1}, 1455 cm^{-1}, and 1700 cm^{-1} can be observed in C-C, C-O-H vibration, CH_2 (vibration), and a carbonyl group (C=O), respectively (Sánchez-Márquez et al., 2015)(Grabowska et al., 2016). The two Raman peaks observed for the PAAc-g-CNT and PAAc-g-(Ru/CNT) polymer composites were 1314 cm^{-1}/1604 cm^{-1} and 1340 cm^{-1}/1611 cm^{-1}, respectively. These peaks can be attributed to the C-O-H vibration and the carbonyl group (C=O) as in PAAc. However, shifts in Raman peaks and low peak intensities can be due to the composite formed. The Micro-Raman spectrums for the CF/PAAc-g-CNT and CF/PAAc-g-(Ni/CNT) polymer composites were given in Figure 4.12 The two Raman peaks observed for the CF/PAAc-g-CNT and CF/PAAc-g-(Ni/CNT) polymer composites were 1314 cm^{-1}/1604 cm^{-1} and 1344 cm^{-1}/1688 cm^{-1}, respectively (Sánchez-Márquez et al., 2015)(Grabowska et al., 2016). These peaks can be assigned to the C-O-H vibration and the carbonyl group (C=O). From Figure 4.12 the positive shift of CF/PAAc-g-(Ni/CNT) compared to CF/PAAc-g-CNT Raman peaks can be considered due to the presence of metal. Figure 4.13 illustrates the Micro-Raman spectra of the PAAc-g-CNT and PAAc-g-(Mo/CNT) polymer composites, which exhibit two distinct Raman peaks at 1314 cm^{-1}/1604 cm^{-1} and 1344 cm^{-1}/1688 cm^{-1} for PAAc-g-(Mo/CNT), respectively. The observed peaks can be attributed to the vibrations of the C-O-H bonds and the carbonyl group (C=O) present in PAAc (Sánchez-Márquez et al., 2015)(Grabowska et al., 2016). However, variations in the Raman peak positions and weak peak intensities may indicate the formation of a composite material.

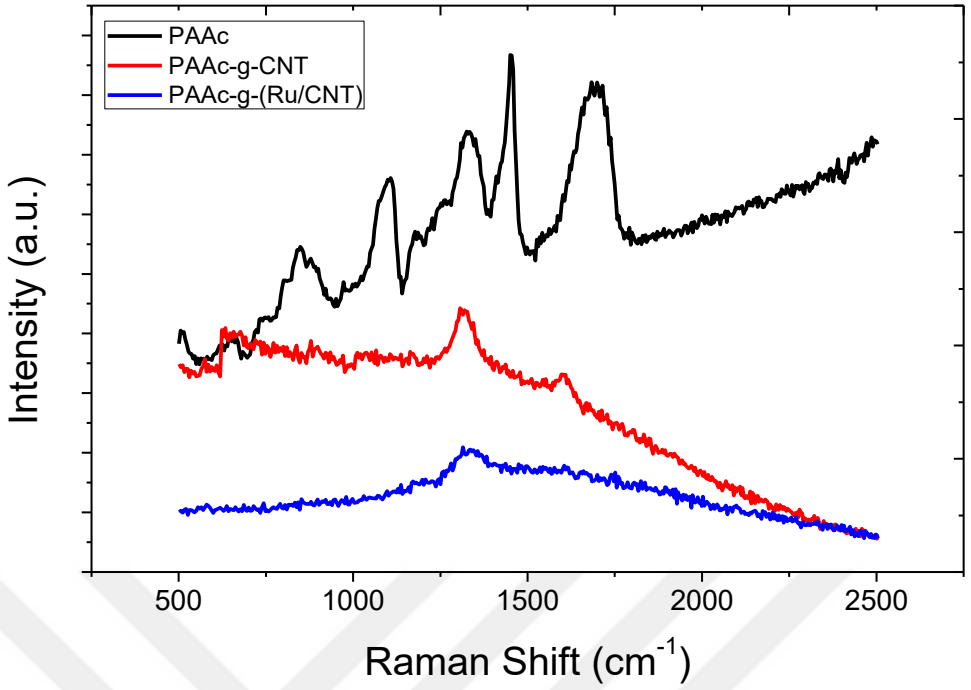

Figure 4.11 Micro-Raman spectra of PAAc, PAAc-g-CNT, and PAAc-g-(Ru/CNT) polymer composites.

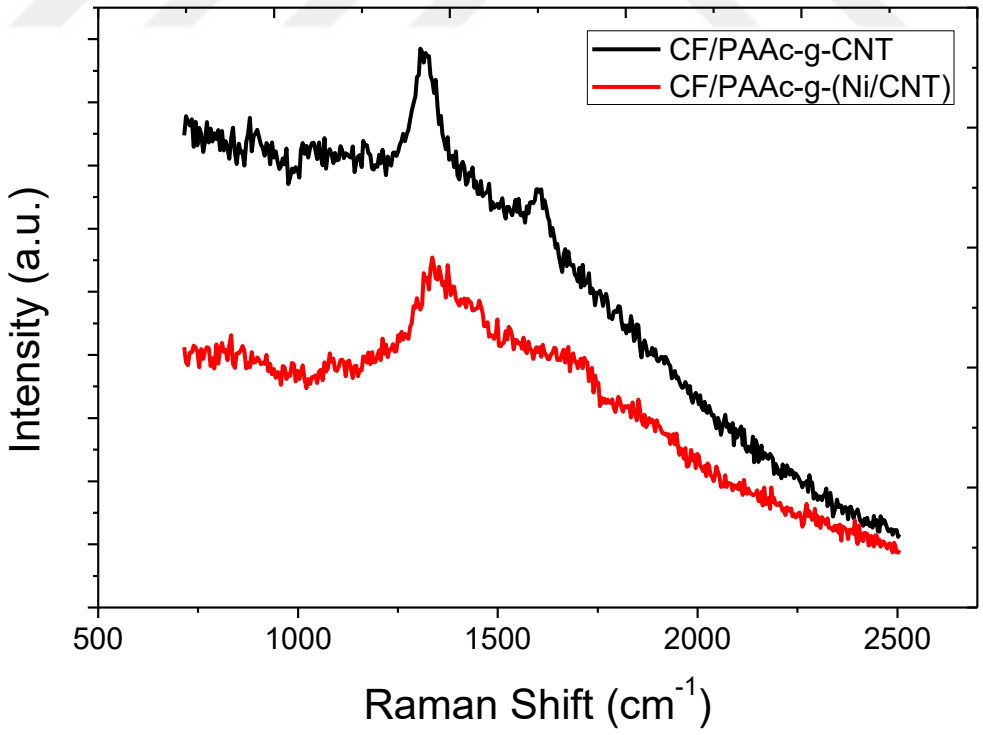

Figure 4.12 Micro-Raman spectra of CF/PAAc-g-CNT and CF/PAAc-g-(Ni/CNT) polymer composites.

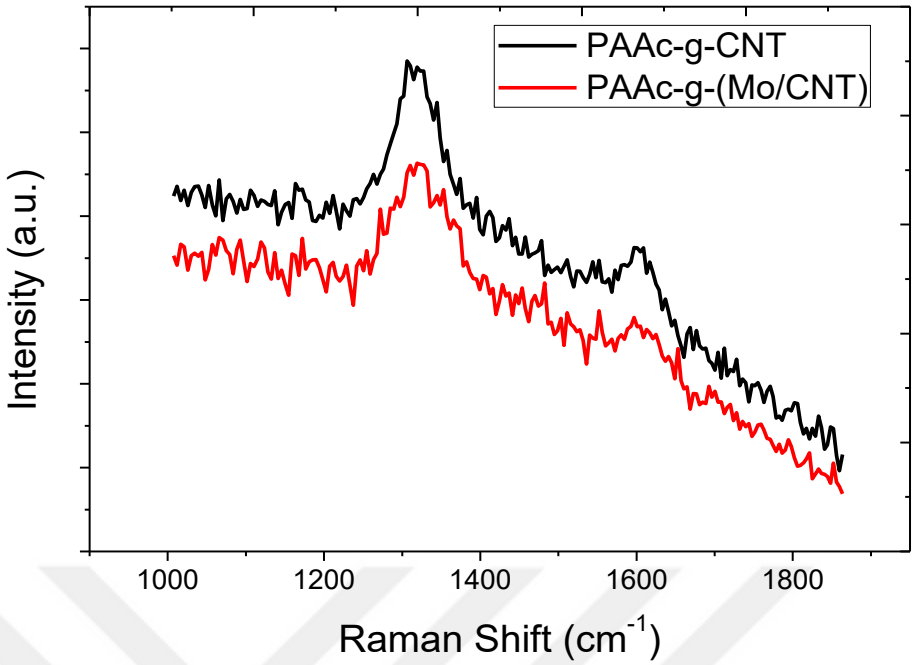

Figure 4.13 Micro-Raman spectra of PAAc-g-CNT and PAAc-g-(Mo/CNT) polymer composites.

4.5. Cyclic Voltammetry Test of Electrodes

In a half-cell setup with 0.5 M H_2SO_4, the electrochemical properties of the produced electrode materials were examined. Cyclic voltammograms of PAAc, PAAc-g-CNT, PAAc-g-(Pt/CNT), PAAc-g-(Pd/CNT), and PAAc-g-(Ru/CNT) at scan rates from 5 to 100 mV s^{-1} were shown in Figure 4.14(a-e), respectively. It was seen that PAAc and PAAc-g-CNT have EDLC type, which was attributed to the establishment of electric double layers as a result of effective electro sorption-desorption of ions. Cyclic voltammetry showed a rectangular I-V curve devoid of any redox peak between -0.2 and 1.0 V. The specific capacitance of the EDLC electrode was closely connected to the electrochemically active region. Notably, PAAc-g-CNT displayed the bigger surrounding area of the CV curve at the same scan rate as PAAc, indicating its superior energy storage capacity. In particular, improved performance supercapacitors electrode material was created when CNTs with novel attributes such as electrical conductivity, enormous surface area, a high charge-carrying capacity, mesoporosity, and electrolyte accessibility were introduced to the medium (Baughman et al., 2002). When PAAc and PAAc-g-CNT were compared at 5 mV s^{-1}, it was determined that the capacitive performance of the electrode increased exactly 3.3 times. The form of the voltammograms changed with the addition of metals to the electrode materials in Figure 4.14(c-e). electrodes The characteristic pseudo-capacitance-type CV curve can be explained by the redox behavior showing reduction and oxidation peaks. Compared to PAAc-g-(Pt/CNT) and PAAc-g-(Pd/CNT), when the PAAc-g-(Ru/CNT) electrode, the current value in the voltammogram and its encircled area reached much higher values. The voltammograms in Figure 4.14(e) can be seen to show anodic and cathodic profiles in the -0.2-1.0 range, which correspond to ruthenium anodic profile to $Ru(OH)_3$ through the interconversion of $Ru(OH)_2$ (Juodkazytė et al., 2007). The cathodic profile of the 5 mV s^{-1} of the cycle showed a current peak centered at 0.4 Volt, indicating the reduction region of $Ru(OH)_3$ to Ru at 0.55 Volt in Figure 4.14(e). RuO_2 surface oxide formation can be explained by the following general reaction (4.1) (Juodkazis et al., 2008).

$$Ru + 2H_2O \Leftrightarrow RuO_2 + 4H^+ + 4e^- \quad (4.1)$$

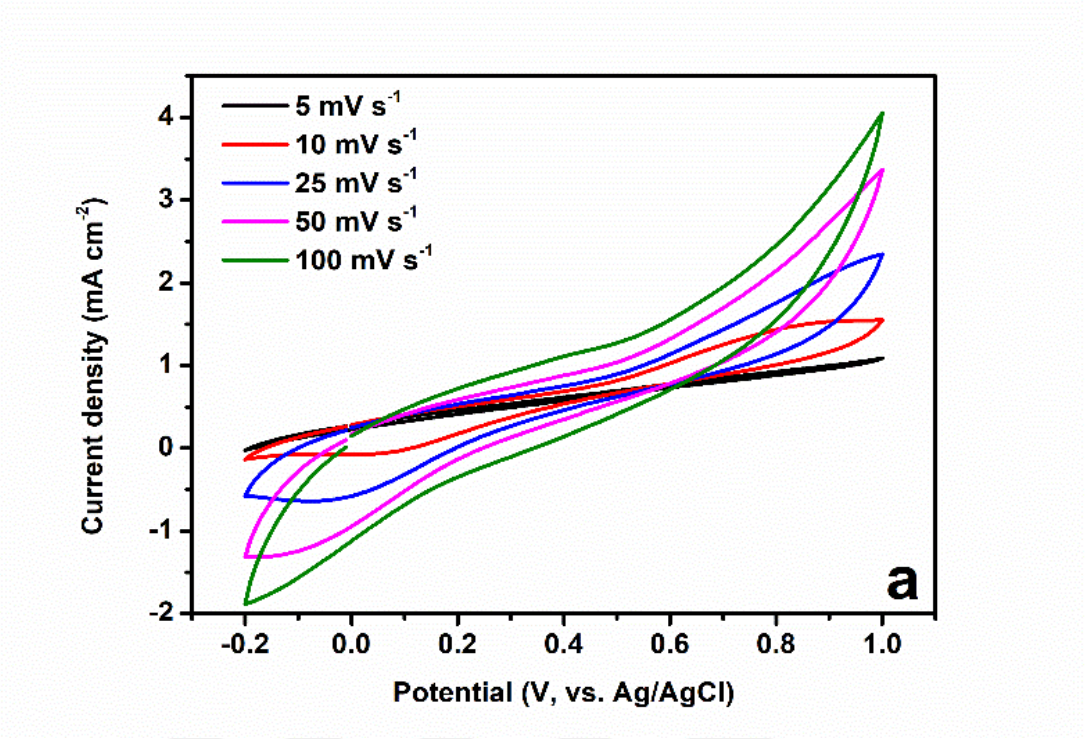
5 mV s-1
10 mV s-1
25 mV s-1
50 mV s-1
100 mV s-1
Current density (mA cm-2)
Potential (V, vs. Ag/AgCl)
a

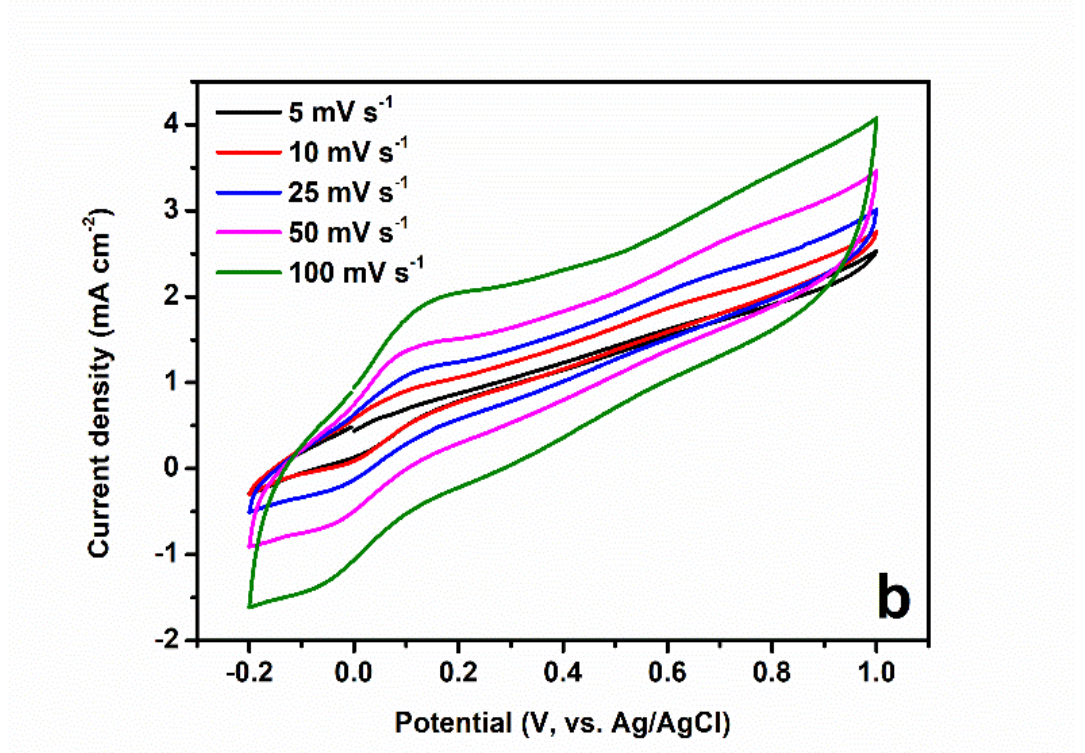
5 mV s-1
10 mV s-1
25 mV s-1
50 mV s-1
100 mV s-1
Current density (mA cm-2)
Potential (V, vs. Ag/AgCl)
b

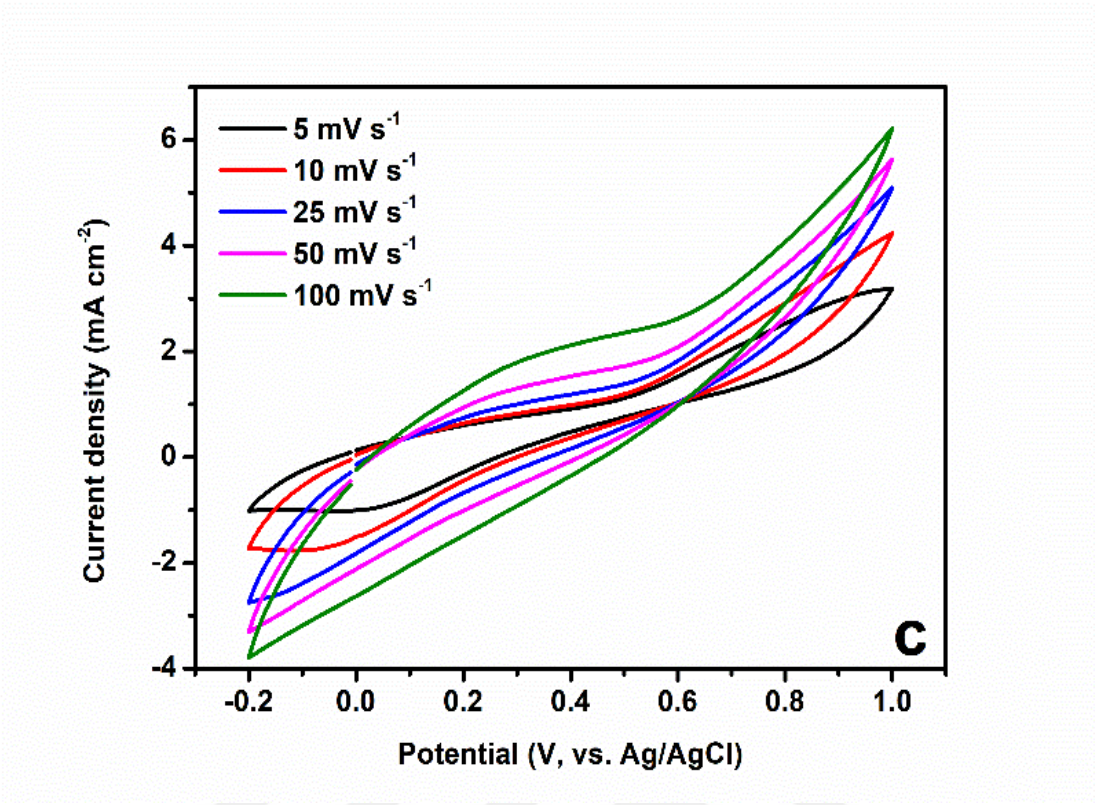
5 mV s-1
10 mV s-1
25 mV s-1
50 mV s-1
100 mV s-1
Current density (mA cm-2)
Potential (V, vs. Ag/AgCl)
c

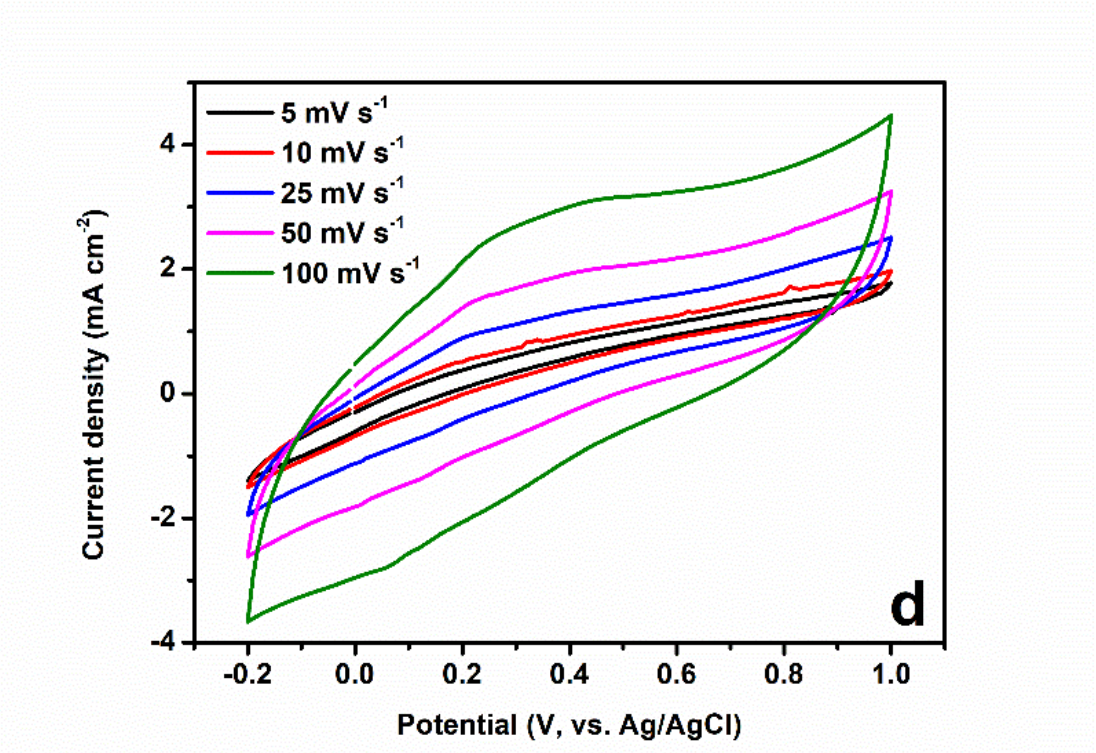
5 mV s-1
10 mV s-1
25 mV s-1
50 mV s-1
100 mV s-1
Current density (mA cm-2)
Potential (V, vs. Ag/AgCl)
d

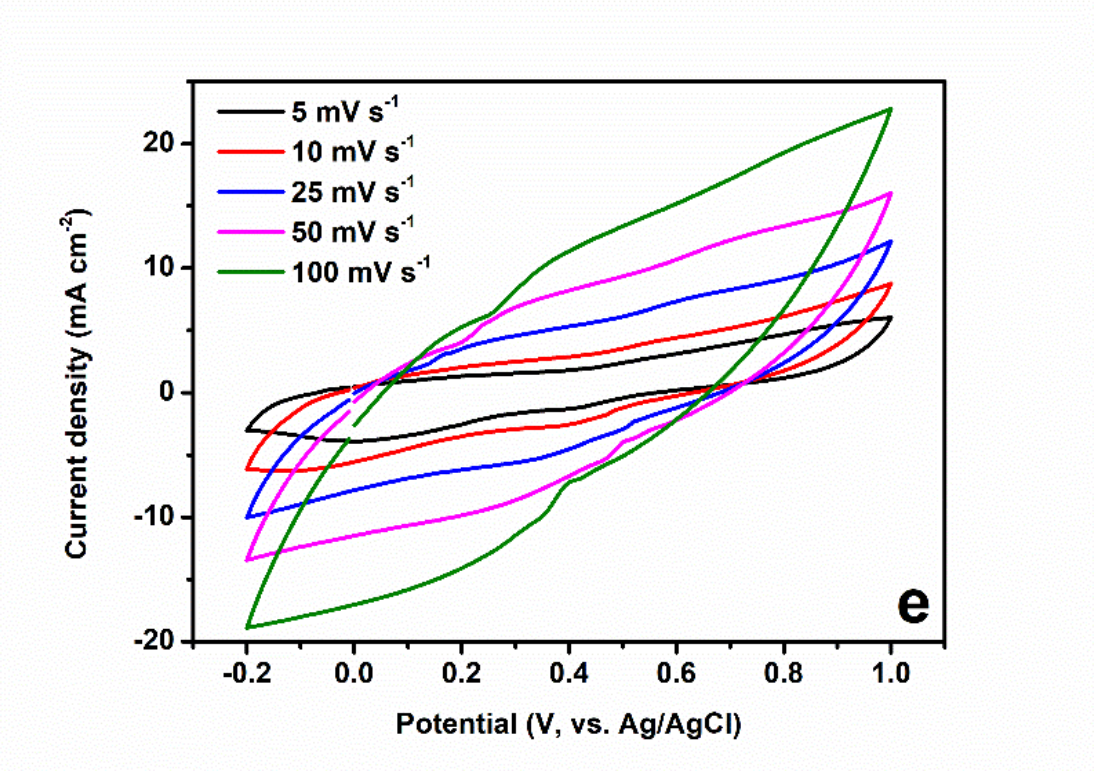

Figure 4.14 Cyclic voltammograms at different scan rates from 5 to 100 mV s^{-1} of electrode materials: a) PAAc, b)PAAc-g-CNT, c) PAAc-g-(Pt/CNT), d) PAAc-g-(Pd/CNT), e) PAAc-g-(Ru/CNT).

The specific capacitance values derived from the cyclic voltammetry tests presented in Table 4.1 reveal important information about the charge storage capacities of PAAc-g-(Ru/CNT), PAAc-g-(Pd/CNT) and PAAc-g-(Pt/CNT) electrodes at various scan rates. Specific capacitance values were calculated according to equation (3.1).

Table 4.1 Specific capacitance values of PAAc-g-(Ru/CNT), PAAc-g-(Pd/CNT) and PAAc-g-(Pt/CNT) obtained from cyclic voltammetry test.

Electrode material	**Scan rate (V s^{-1})**	**ΔV (V)**	**Cs (F g^{-1})**
PAAc-g-(Ru/CNT)	0.005	1.2	1294.46
	0.010	1.2	941.68
	0.025	1.2	598.51
	0.050	1.2	439.96
	0.100	1.2	287.03
PAAc-g-(Pd/CNT)	0.005	1.2	96.81
	0.010	1.2	84.23
	0.025	1.2	78.54
	0.050	1.2	74.07
	0.100	1.2	65.35
PAAc-g-(Pt/CNT)	0.005	1.2	286.75
	0.010	1.2	178.24

Table 4.1 Specific capacitance values of PAAc-g-(Ru/CNT), PAAc-g-(Pd/CNT) and PAAc-g-(Pt/CNT) obtained from cyclic voltammetry test (continued).

Electrode material	Scan rate (V s^{-1})	ΔV (V)	Cs (F g^{-1})
	0.025	1.2	84.36
	0.050	1.2	52.93
	0.100	1.2	36.40

The pseudocapacitive behavior to the total capacitance of the was mostly because of these faradaic redox reactions. The potential range in the charge storage characterization of RuO_2 electrodes where RuO_2 can partially reduce to metallic ruthenium and then be oxidized during anodic scanning was referred to as pseudocapacitance (Choi et al., 2022). When the current densities reached by the enclosed CV areas are compared, it shows that it followed the order PAAc-g-(Ru/CNT)> PAAc-g-(Pd/CNT) > PAAc-g-(Pt/CNT) > PAAc-g-CNT, > PAAc. The PAAc electrode showed some capacitance with the effect of the carbon felt. CNT has been measured to boost the specific capacitance value of the developed electrode 3.3 times since it stores charge with electrostatic interactions. It is clear that the faradaic reaction, which should occurred due to the nature of the metals, was supported on this electrode surface with the metals added to the medium. Pt and Pd that Ru provided an electroactive surface area and an electron transfer between the electrolyte and the electrode compatible with CNT and PAAc. At the scan rate of 5 mV s^{-1}, the value-specific capacitances of electrodes were found to be 15.5, 51.4, 96.8, 286.8, and 1294.5 F g^{-1} for the PAAc, PAAc-g-CNT, PAAc-g-(Pt/CNT), PAAc-g-(Pd/CNT) and PAAc-g-(Ru/CNT), respectively. This result was observed in many electrode materials measured in electrolytes and relates to fast voltage-current change rates (Aoki et al., 2020; Yazar et al., n.d.). It may depend on the ionic conductivity of the polymer and the fast electrochemical dynamic process. While it was noticed that the peak currents intensified and disappeared with increasing scanning rate in Pd and Pt, the voltammogram of the electrode containing Ru showed a more stable result. Furthermore, faster electron transfer and charge storage across the CNT in the PAAc-g-(Ru/CNT) composite provided a large electro-proton switching mechanism (Banik et al., 2022).

In Figure 4.15(a), bare carbon felt (CF), CF/PAAc, CF/PAAc-g-CNT, CF/PAAc-g-(Fe/CNT), CF/PAAc-g-(Co/CNT), and CF/PAAc-g-(Ni/CNT) were taken measurements at scan rate of 10 mV s^{-1} with cyclic voltammetry. When comparing the CV areas of the curves,

a tremendous increase was noticed in the coated electrodes relative to the carbon felt electrode. In cyclic voltammetry, the growing integral area of metal-supported CNT-containing electrode materials indicate higher energy storage capacity. The fact that CNTs have properties like electrical conductivity, large surface area, charge carrying capacity, porosity and electrolyte accessibility, and the incorporation of redox-behaving metals into the electrode material has had a significant effect on obtaining electrode materials for supercapacitors with improved performance(Lekawa-Raus et al., 2014)(Mustaqeem et al., 2022). Then, the capacitive behavior of the CF/PAAc-g-(Fe/CNT), CF/PAAc-g-(Co/CNT), and CF/PAAc-g-(Ni/CNT) electrodes at various scan rates were investigated in Figure 4.15(b-d).

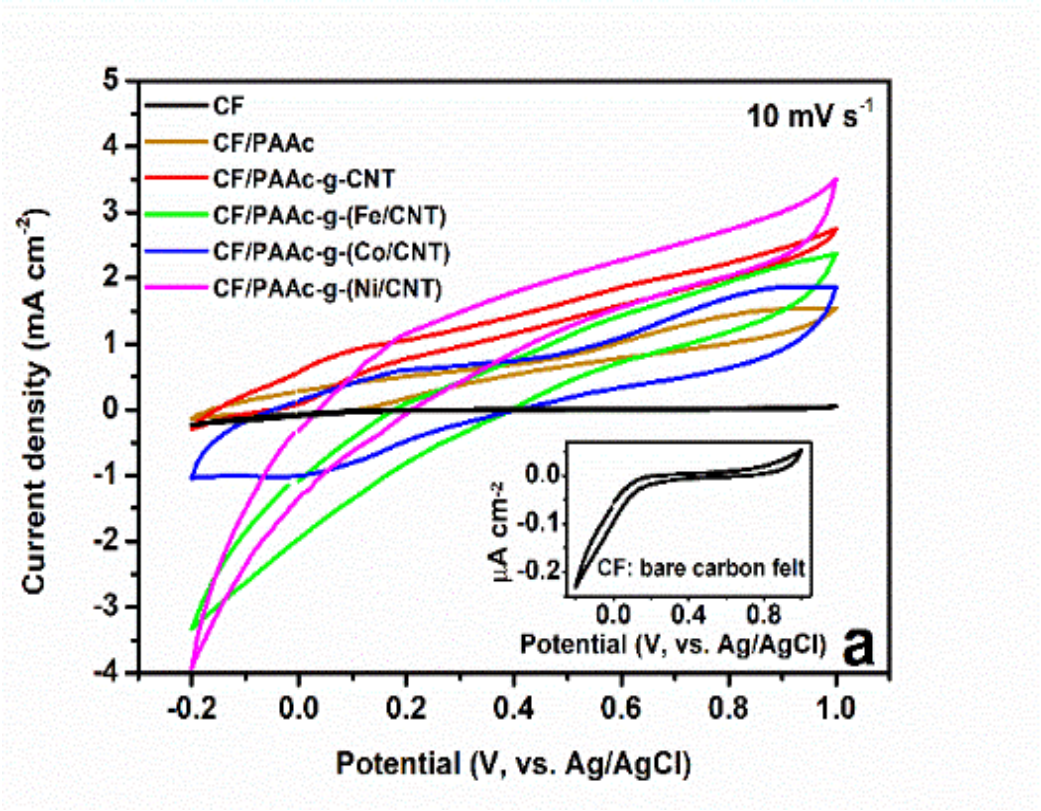

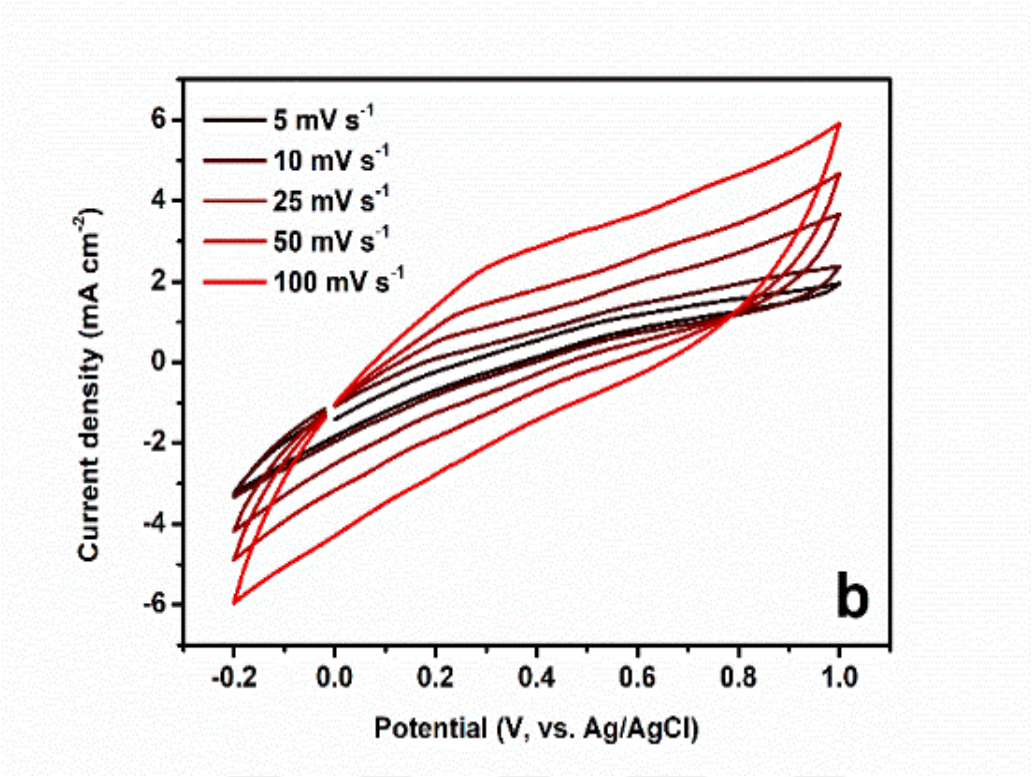
5 mV s-1
10 mV s-1
25 mV s-1
50 mV s-1
100 mV s-1
Current density (mA cm-2)
Potential (V, vs. Ag/AgCl)
b

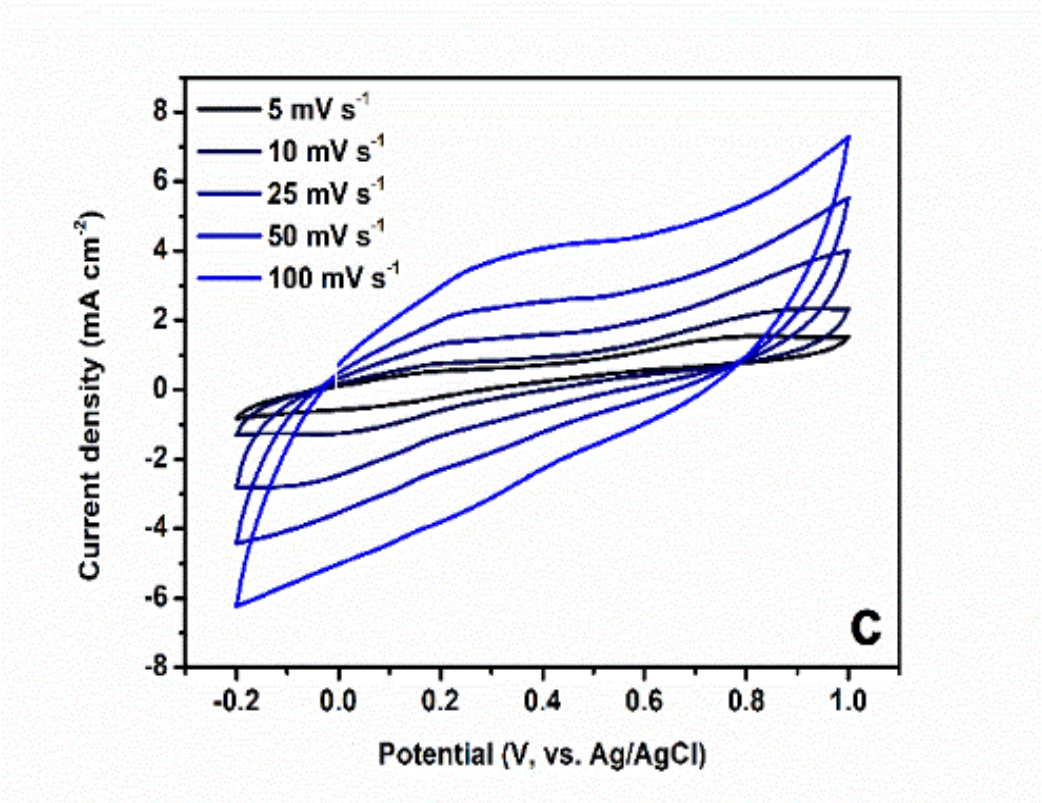
5 mV s-1
10 mV s-1
25 mV s-1
50 mV s-1
100 mV s-1
Current density (mA cm-2)
Potential (V, vs. Ag/AgCl)
c

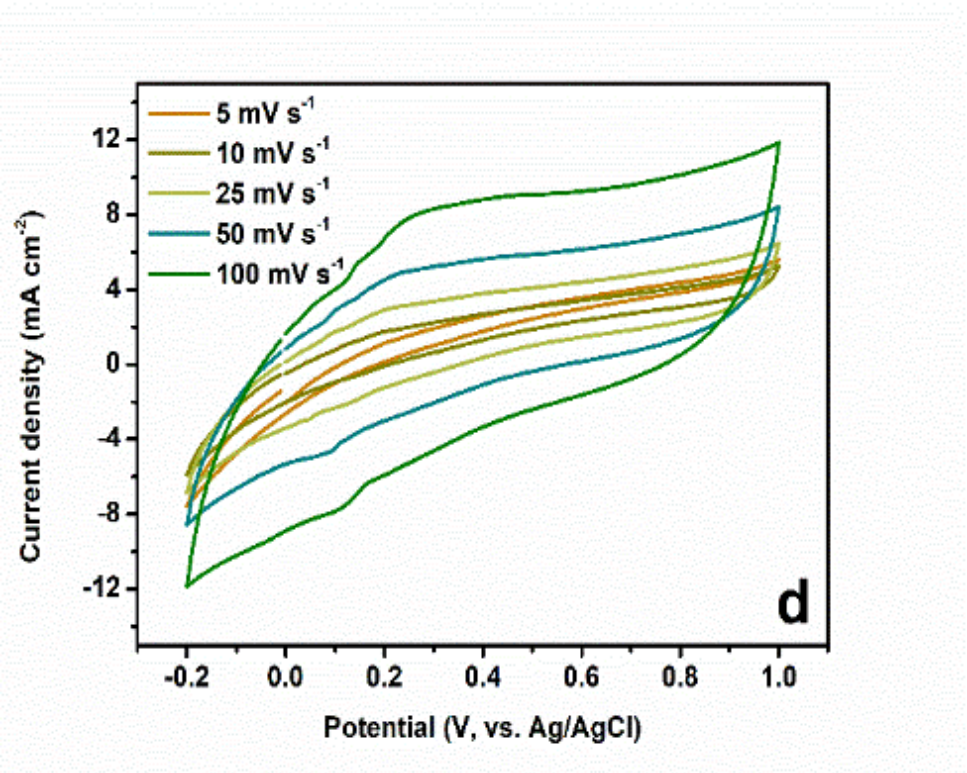
5 mV s-1
10 mV s-1
25 mV s-1
50 mV s-1
100 mV s-1
Current density (mA cm-2)
12
8
4
0
-4
-8
-12
-0.2
0.0
0.2
0.4
0.6
0.8
1.0
Potential (V, vs. Ag/AgCl)
d

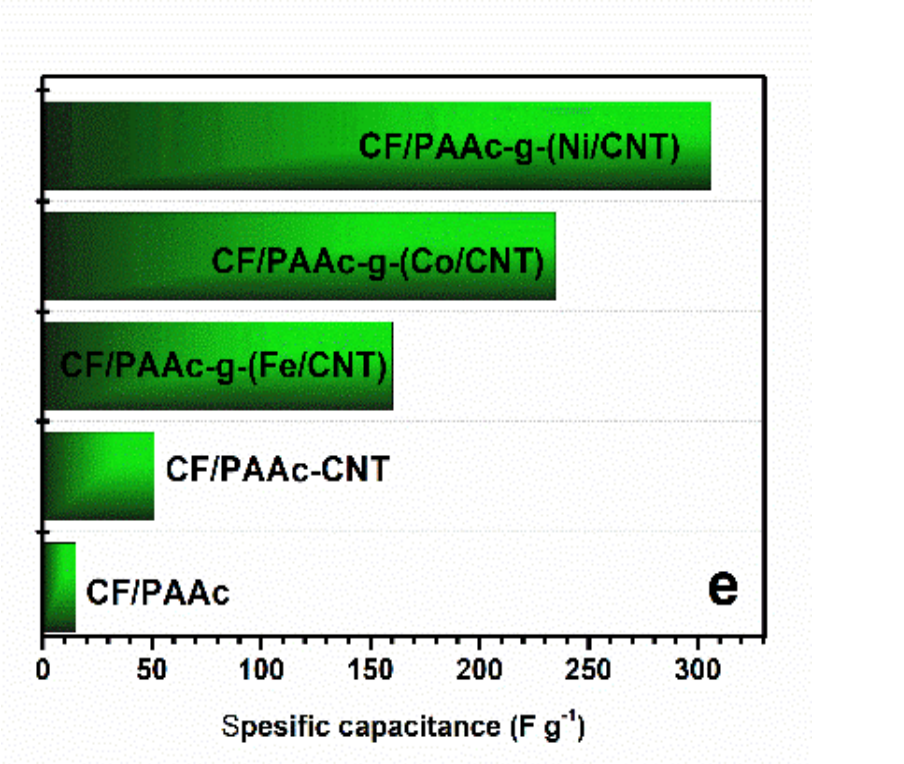
CF/PAAc-g-(Ni/CNT)
CF/PAAc-g-(Co/CNT)
CF/PAAc-g-(Fe/CNT)
CF/PAAc-CNT
CF/PAAc
e
0
50
100
150
200
250
300
Spesific capacitance (F g-1)

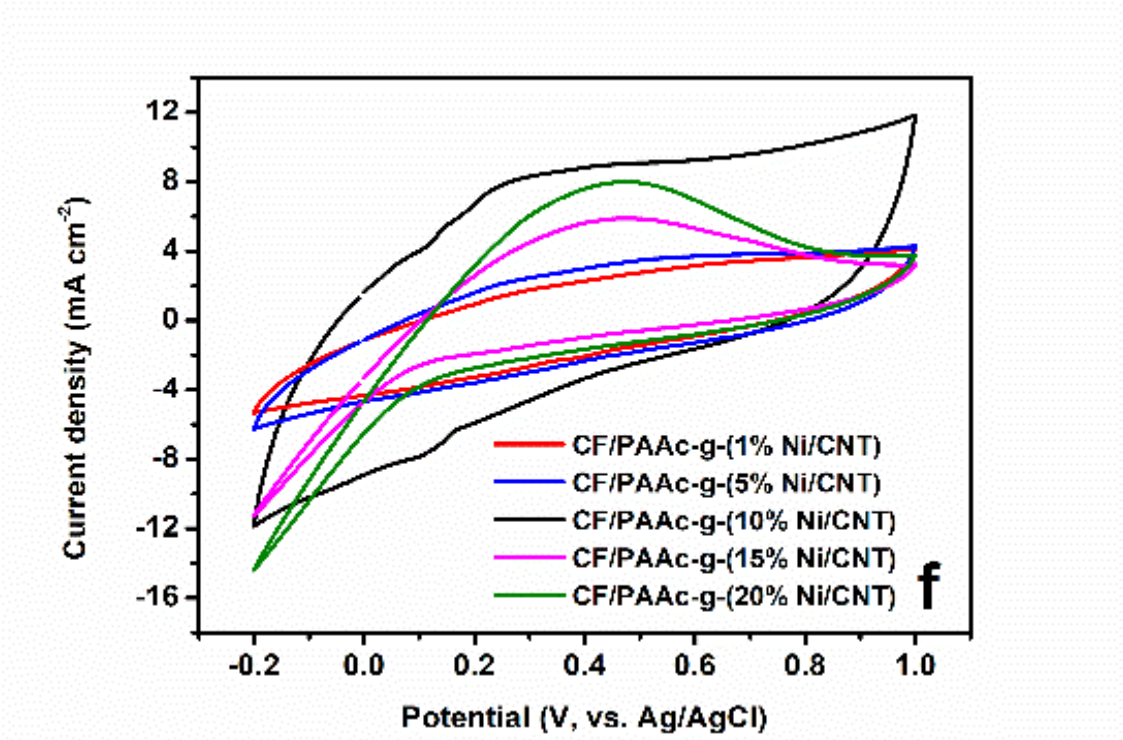

Figure 4.15 a) Cyclic voltammograms of CF/PAAc, CF/PAAc-g-CNT, CF/PAAc-g-(Fe/CNT), CF/PAAc-g-(Co/CNT), and CF/PAAc-g-(Ni/CNT) at 10 mV s^{-1}, b) CV curves of CF/PAAc-g-(Fe/CNT) from 5 to 100 mV s^{-1}, c) CV curves of CF/PAAc-g-(Co/CNT) from 5 to 100 mV s^{-1}, d) CV curves of CF/PAAc-g-(Ni/CNT) from 5 to 100 mV s^{-1}, e) Specific capacitance values of electrodes from CV curves at 5 mV s^{-1}, f) CV curve of CF/PAAc-g-(Ni/CNT) at different concentrations.

Table 4.2 Specific capacitance values of PAAc-g-(Fe/CNT), PAAc-g-(Co/CNT) and PAAc-g-(Ni/CNT) obtained from cyclic voltammetry test.

Electrode material	**Scan rate (V s^{-1})**	**ΔV (V)**	**Cs (F g^{-1})**
PAAc-g-(Fe/CNT)	0.005	1.2	160.5
	0.010	1.2	151.3
	0.025	1.2	112.5
	0.050	1.2	85.6
	0.100	1.2	67.3
PAAc-g-(Co/CNT)	0.005	1.2	235.1
	0.010	1.2	221.7
	0.025	1.2	170.9
	0.050	1.2	132.3
	0.100	1.2	101.6

Table 4.2 Specific capacitance values of PAAc-g-(Fe/CNT), PAAc-g-(Co/CNT) and PAAc-g-(Ni/CNT) obtained from cyclic voltammetry test (continued).

Electrode materia	**Scan rate (V s^{-1})**	**ΔV (V)**	**Cs (F g^{-1})**
PAAc-g-(Ni/CNT)	0.005	1.2	306.8
	0.010	1.2	256.2
	0.025	1.2	248.7
	0.050	1.2	233.4
	0.100	1.2	201.2

When the electrodes were compared, the highest capacitance values of the CF/PAAc-g-(Fe/CNT), CF/PAAc-g-(Co/CNT), and CF/PAAc-g-(Ni/CNT) electrodes were calculated as 160.5 ,235.1 and 306.8 F g^{-1} at the scan rate of 0.005 V s^{-1}, respectively. The rate capability of the CF/PAAc-g-(Fe/CNT), CF/PAAc-g-(Co/CNT), and CF/PAAc-g-(Ni/CNT) were calculated as 41.93%, 43.2% and 65.6% against the 20-times increased scan rate. CF/PAAc-g-(Ni/CNT) was the electrode that exhibited the greatest capacitance value and the best rate capability at different scan rates. Further, when compared to the PAAc-g-CNT electrode in Figure 4.15(e), it was noticed that the supercapacitive performance increased 6-times.

In Figure 4.15(f), cyclic voltammograms of the electrodes prepared at various nickel concentrations are given at a scan rate of 100 mV s^{-1}. Nickel-based compounds with electrochemical activity offer high capacitance but relatively poor reversibility (X. Liu et al., 2018). Compared to the other electrodes, the oxidation peak of nickel can be seen much more clearly in the voltammograms of the electrode materials containing 15% and 20% Ni/CNT. In electrodes containing 1% and 5% Ni/CNT, the square voltammogram, which was similar to the electrochemical double layer supercapacitor type, was effective. According to the literature, it can be represented by equations 4.2 and 4.3 during the reactions that take place by oxidation (El Wanees et al., 2021).

$$Ni \rightarrow Ni^{+} + e \tag{4.2}$$

or

$$Ni + \rightarrow Ni^{2+} + e \tag{4.3}$$

$$Ni^{2+} + H_2O \rightarrow NiO + 2H^{+} + e \tag{4.4}$$

It has been documented in the literature that the oxidation of Ni^{+} to the divalent structure, Ni^{2+} ions, continues at a rate equal to the rate of oxide form (Equation 4.4). This stage continues until the active oxidation of Ni is largely precipitated by nickel oxides on the electrode surface(El Wanees et al., 2021).

In a study, was investigated that PAAc-MWCNT had a successful effect on Ni^{2+} adsorption at low pH. The findings showed that the adsorption of Ni^{2+} was clearly affected by the insertion sequences. Adsorption of Ni^{2+} was mainly attributed to surface complex and ion exchange. The positive effect of PAAc on $Ni+^{2}$ adsorption was enlightened by the complexation of PAAc with nickel ion on the electrode surface. It has been proposed that Ni^{2+} binds to the surface and acts as a PAAc "bridge" between the metal and the electrode surface(S. Yang et al., 2009). When examined in terms of supercapacitor applications, the most important factor that will increase the performance is to enhance the bonding between the electrode and the electrolyte interface and to ensure the realization of electrostatic or faradaic events. Between CF/PAAc-g-(Fe/CNT), CF/PAAc-g-(Co/CNT) and CF/PAAc-g-(Ni/CNT) electrodes, PAAc/CNT showing both pseudocapacitor and EDLC effect CF/PAAc-g-(10% Ni/CNT) was chosen as the highest performance electrode material.

Figure 4.16(a) illustrates the cyclic voltammograms acquired for PAAc, PAAc-g-CNT, PAAc-g-(Mo/CNT), PAAc-g-(Ga/CNT), and PAAc-g-(Bi/CNT) at a scan rate of 100 mV s^{-1}. Furthermore, Figure 4.16(b-d) displays the cyclic voltammograms of PAAc-g-(Mo/CNT),PAAc-g-(Ga/CNT), and PAAc-g-(Bi/CNT) obtained at different scan rates ranging from 5 to 100 mV s^{-1}.

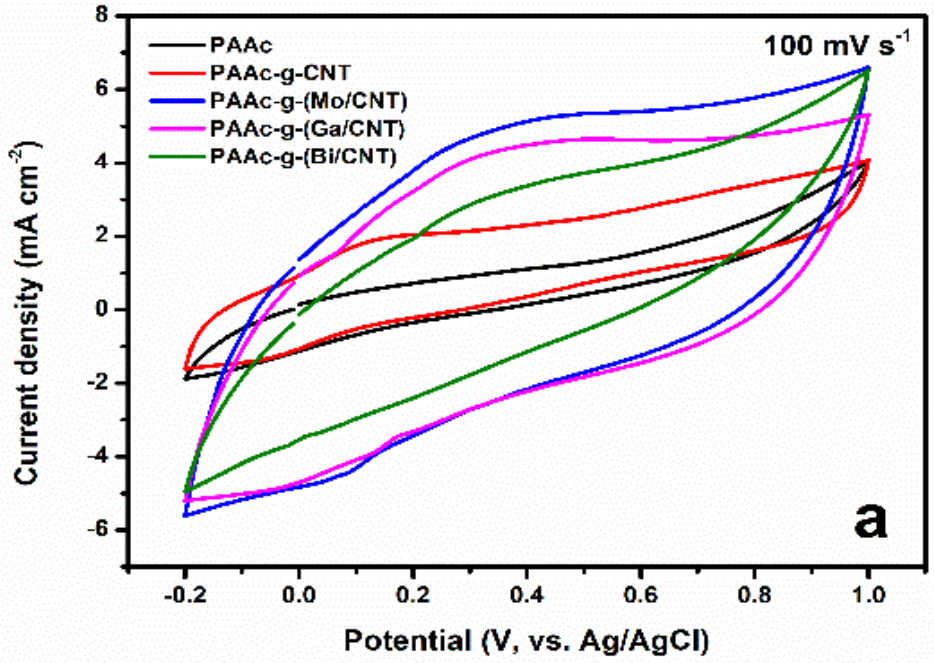
PAAc
PAAc-g-CNT
PAAc-g-(Mo/CNT)
PAAc-g-(Ga/CNT)
PAAc-g-(Bi/CNT)
100 mV s-1
a
Current density (mA cm-2)
Potential (V, vs. Ag/AgCl)

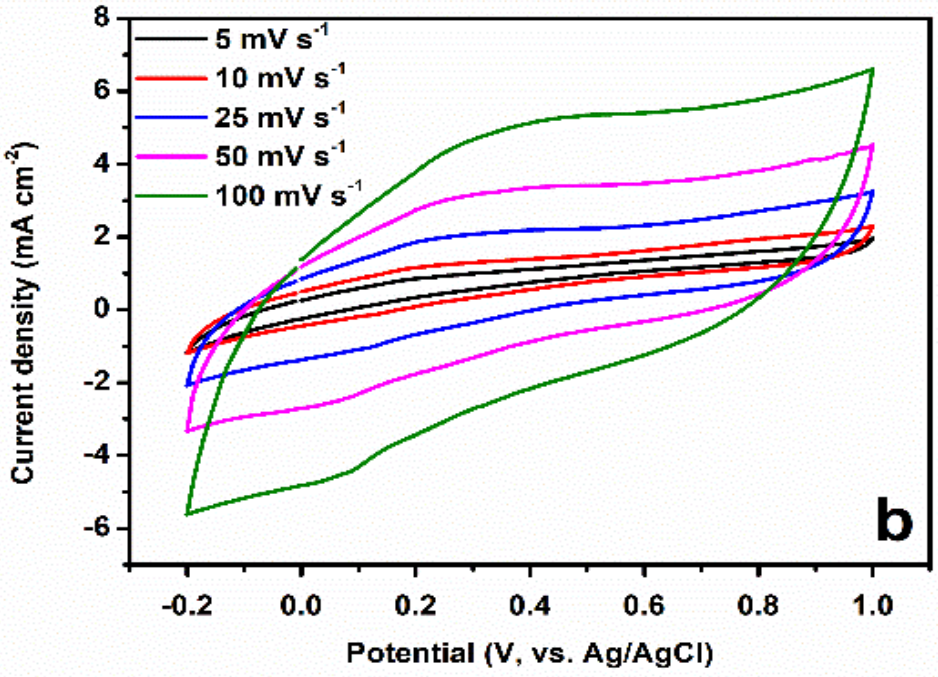
5 mV s-1
10 mV s-1
25 mV s-1
50 mV s-1
100 mV s-1
b
Current density (mA cm-2)
Potential (V, vs. Ag/AgCl)

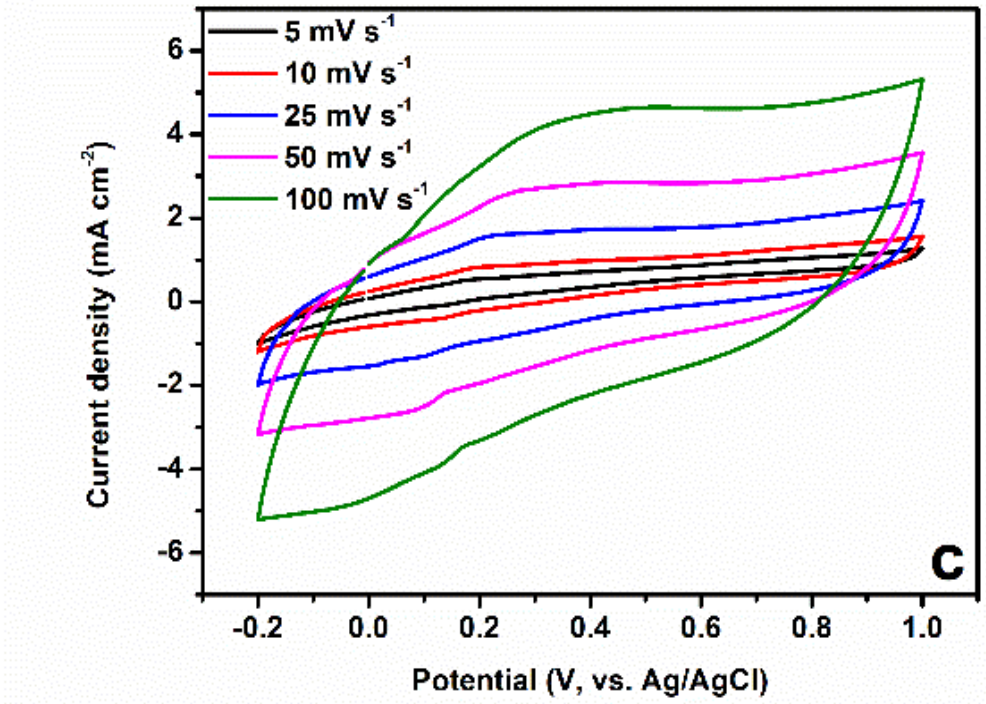
5 mV s-1
10 mV s-1
25 mV s-1
50 mV s-1
100 mV s-1
Current density (mA cm-2)
Potential (V, vs. Ag/AgCl)
c

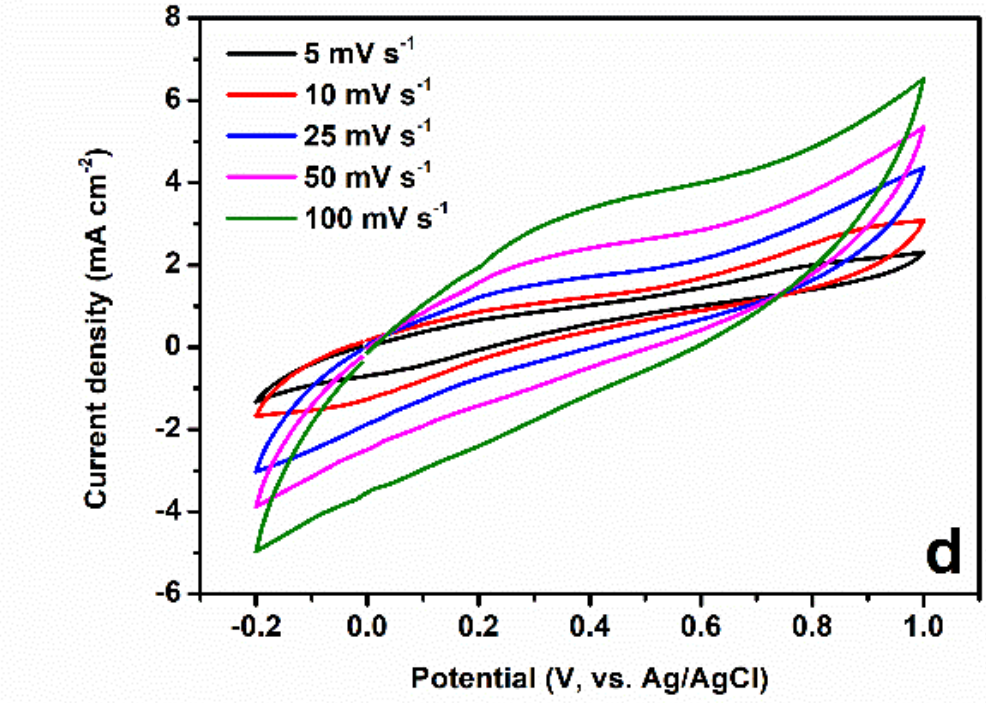
5 mV s-1
10 mV s-1
25 mV s-1
50 mV s-1
100 mV s-1
Current density (mA cm-2)
Potential (V, vs. Ag/AgCl)
d

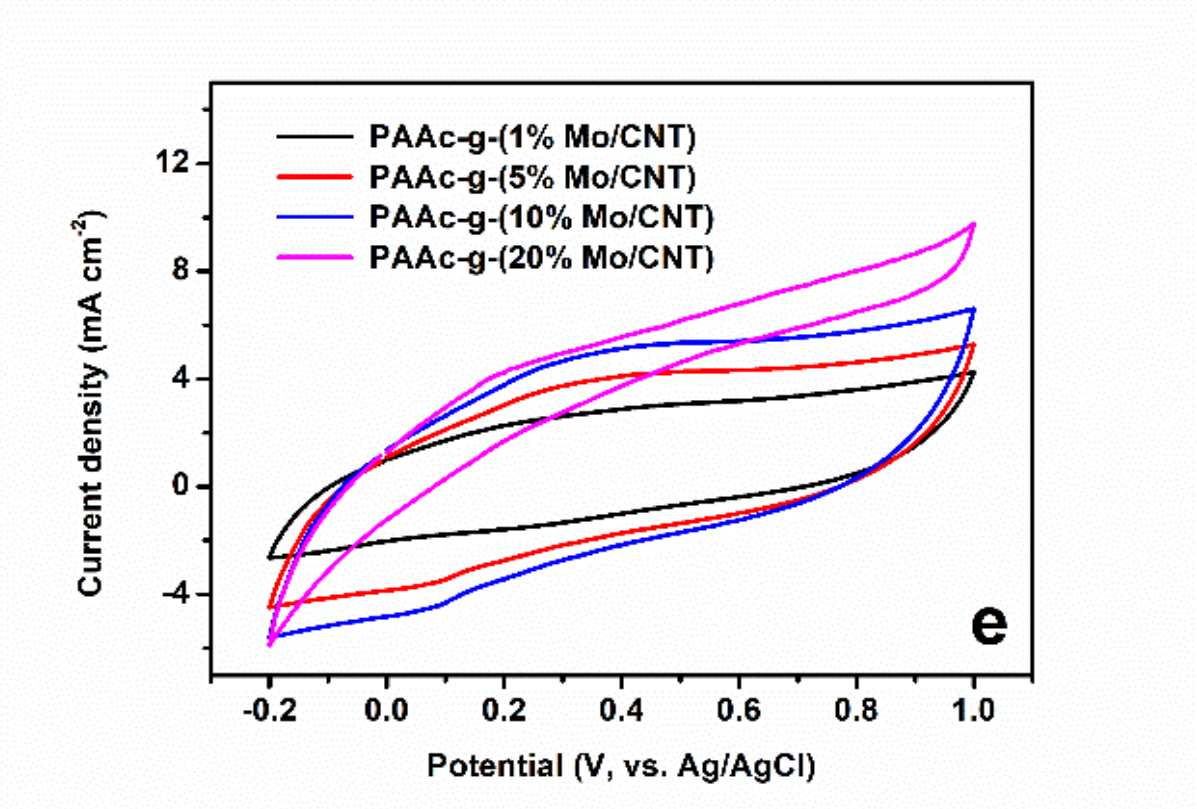

Figure 4.16 a) Cyclic voltammograms of PAAc, PAAc-g-CNT, PAAc-g-(Mo/CNT), PAAc-g-(Ga/CNT), and PAAc-g-(Bi/CNT) at 100 mV s^{-1}, b) CV curves of PAAc-g-(Mo/CNT) from 5 to 100 mV s^{-1}, c) CV curves of PAAc-g-(Ga/CNT) from 5 to 100 mV s^{-1}, d) CV curves of PAAc-g-(Bi/CNT) from 5 to 100 mV s^{-1}, e) Concentration optimization of PAAc-g-(Mo/CNT) from CV curves.

The cyclic voltammograms for these materials exhibited a rectangular I-V curve within the potential range of -0.2 V to 1.0 V, without any appearance of redox peaks. The electrochemically active area was found to have a substantial impact on the specific capacitance of the EDLC electrode. An increasing integral area in cyclic voltammetry measurements for electrode materials containing metal supported CNTs is indicative of a greater capacity for energy storage. The introduction of CNTs with novel attributes, including high electrical conductivity, large surface area, high charge-carrying capacity, mesoporosity, and electrolyte accessibility, to the medium resulted in the creation of a supercapacitor electrode material with enhanced performance(Baughman et al., 2002). Figure 4.16(b-d) demonstrates that the addition of metals to the electrode materials resulted

in a change in the shape of the voltammograms. Table 4.3 presents the capacitance values obtained from the measurements using equation (3.1).

Table 4.3 Specific capacitance values of PAAc-g-(Mo/CNT), PAAc-g-(Ga/CNT) and PAAc-g-(Bi/CNT) obtained from cyclic voltammetry test.

Electrode material	**Scan rate (V s^{-1})**	**ΔV (V)**	**Cs (F g^{-1})**
PAAc-g-(Mo/CNT)	0.005	1.2	149.44
	0.010	1.2	160.80
	0.025	1.2	158.41
	0.050	1.2	142.99
	0.100	1.2	116.89
PAAc-g-(Ga/CNT)	0.005	1.2	139.83
	0.010	1.2	153.09
	0.025	1.2	150.08
	0.050	1.2	132.64
	0.100	1.2	105.39
PAAc-g-(Bi/CNT)	0.005	1.2	146.76
	0.010	1.2	135.67
	0.025	1.2	124.22
	0.050	1.2	91.08
	0.100	1.2	67.91

Comparing the electrodes, the PAAc-g-(Mo/CNT), PAAc-g-(Ga/CNT), and PAAc-g-(Bi/CNT) electrodes displayed the highest capacitance values of 116.9, 105.4, and 67.9 F g^{-1}, respectively, at a scan rate of 0.1 V s^{-1}. The electrode material PAAc-g-(Mo/CNT) demonstrated superior performance compared to the other electrodes, exhibiting the highest capacitance value and excellent rate capability (78.2% maintained) from 5 to 100 mV s^{-1}. scan rates. The electrode's enhanced performance is believed to be due to the excellent electrical conductivity and extensive surface area of CNTs and the redox activity of Mo oxide species. Additionally, the excellent rate capability of PAAc-g-(Mo/CNT) makes it suitable for high-power applications, where rapid charge and discharge rates are required. These results indicate that PAAc-g-(Mo/CNT) is a highly favorable electrode material for supercapacitor applications. In Figure 4.16 (e), cyclic voltammograms of samples prepared at different Mo concentrations at a scanning rate of 100 mV s^{-1} are presented. In electrodes containing 1% and 5% Mo/CNT, square voltammogram similar to electrochemical double-

layer supercapacitor type was effective. The voltammogram of the electrode materials containing 20% Mo/CNT showed too much resistance and deteriorated the capacitive behavior of the electrode. The electrode material containing 10% Mo/CNT exhibited the best performance. The research was carried out on this electrode material for subsequent measurements, and structural and morphological characterizations.

The cyclic voltammograms of PNIPAM, PANIPAM-g-CNT, and PNIPAM-g-(Ru/CNT) obtained at diverse scan rates (5 to 100 mVs^{-1}) in Figure 4.17(a-c) provide valuable insights into their electrochemical behavior and charge storage capacities. The specific capacitance values derived from the cyclic voltammetry test further enhance the understanding of their charge storage capabilities across different scan rates. By establishing correlations between these values and the observed features in the cyclic voltammograms, comprehensive information about the electrochemical performance and charge storage behavior of these electrode materials can be obtained.

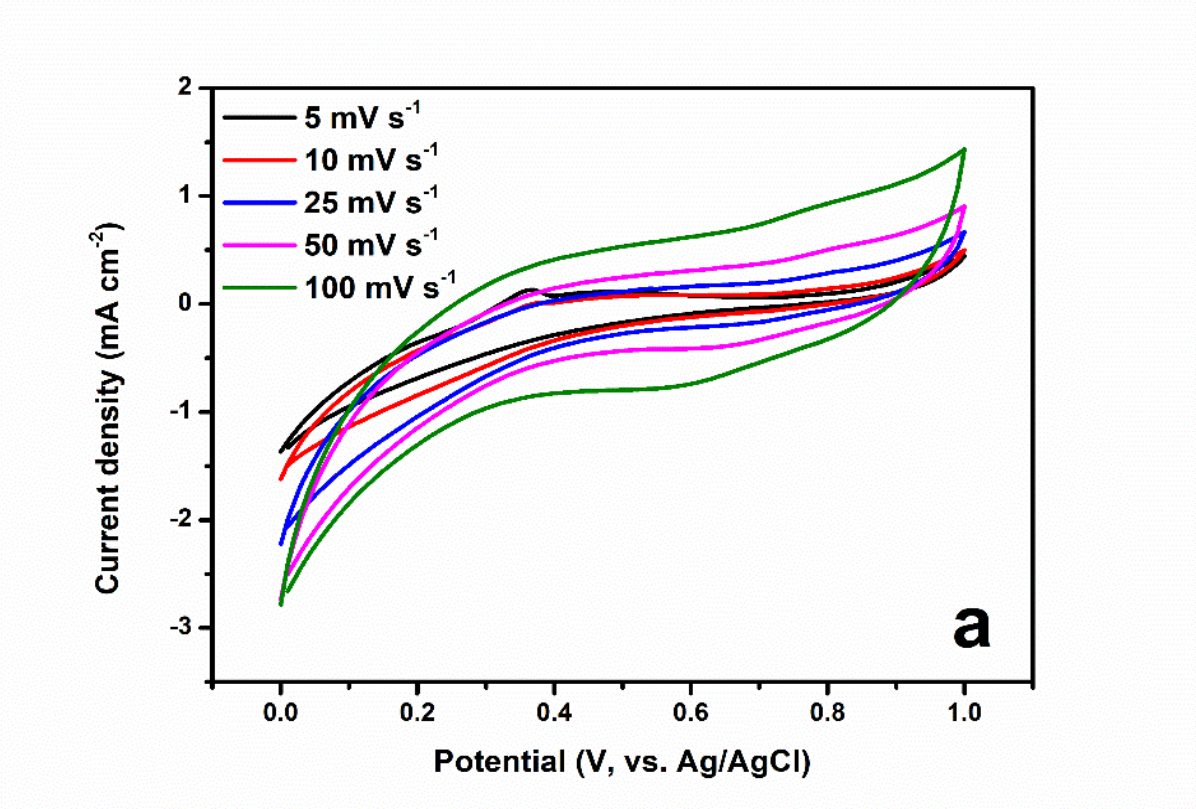

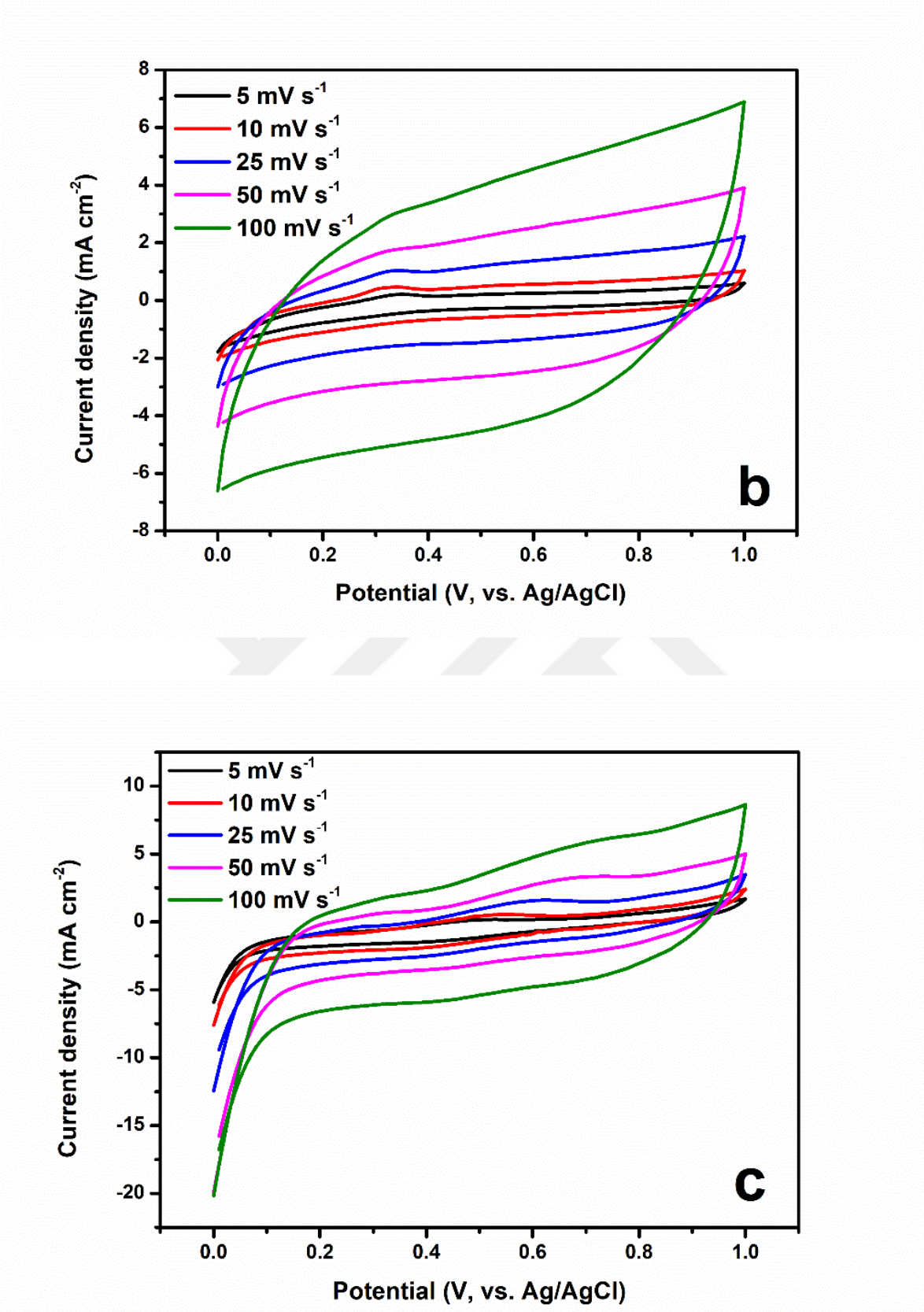

Figure 4.17 a) Cyclic voltammograms of PNIPAM from 5 to 100 mV s^{-1}, b) CV curves of PANIPAM-g-CNT from 5 to 100 mV s^{-1}, c) CV curves of PNIPAM-g-(Ru/CNT) from 5 to 100 mV s^{-1}.

Table 4.4 Specific capacitance values of PANIPAM, PANIPAM-g-CNT and PANIPAM-g-(Ru/CNT) obtained from cyclic voltammetry test.

Electrode material	**Scan rate (V s^{-1})**	**ΔV (V)**	**Cs (F g^{-1})**
PNIPAM	0.005	1.0	80.15
	0.010	1.0	46.64
	0.025	1.0	29.67
	0.050	1.0	23.93
	0.100	1.0	21.45
PNIPAM-g-CNT	0.005	1.0	181.20
	0.010	1.0	193.42
	0.025	1.0	181.79
	0.050	1.0	162.94
	0.100	1.0	137.82
PNIPAM-g-(Ru/CNT)	0.005	1.0	313.57
	0.010	1.0	222.49
	0.025	1.0	168.02
	0.050	1.0	152.34
	0.100	1.0	146.14

The specific capacitance values obtained from the cyclic voltammetry tests presented in Table 4.4 reveal important information about the charge storage capacities of PNIPAM, PANIPAM-g-CNT and PNIPAM-g-(Ru/CNT) electrodes at different scan rates.

Among the materials tested, PNIPAM exhibits the lowest specific capacitance values. The PNIPAM-coated carbon felt electrode has a specific capacitance of 80.15 Fg^{-1} at a scan rate of 0.005 Vs^{-1}, indicating relatively limited charge storage capacity. The current capacitance value here is due to the pure carbon felt. In contrast, PNIPAM-g-CNT shows higher specific capacitance values compared to PNIPAM. PNIPAM-g-CNT has a specific capacitance of 181.20 Fg^{-1} at a scan rate of 0.005 Vs^{-1}. This shows that the incorporation of carbon nanotubes into PNIPAM increases the charge storage capacity. Significantly, PNIPAM-g-(Ru/CNT) exhibits the highest specific capacitance values among the tested materials. PNIPAM-g-(Ru/CNT) indicates a specific capacitance of 313.57 Fg^{-1} at a scan rate of 0.005 Vs^{-1}, indicating superior charge storage performance. The presence of ruthenium and carbon nanotubes in the PNIPAM structure significantly increases the charge

storage capacity. Comparing the materials, PNIPAM-g-(Ru/CNT) consistently shows the highest specific capacitance values, followed by PNIPAM-g-CNT and PNIPAM exhibits the lowest values at all scan rates. These findings emphasise the positive effect of carbon nanotubes and materials exhibiting energy storage capability, such as ruthenium, by allowing electrode-electrolyte interaction in the PNIPAM structure in an ionic conducting polymer environment. It shows that the scanning conditions affect the charge storage behaviour and higher scan rates lead to a decrease in charge storage capacities. Insufficient time for the electrolyte ions in the medium to reach the electrode surface caused the capacitance to decrease. The combination of carbon nanotubes and ruthenium increases the charge storage capacities, making PNIPAM-g-(Ru/CNT) a highly favorable electrode material for energy storage applications. Moreover, the observed dependence of the specific capacitance on the scan rates implies that the electrochemical performance of these materials relies on the diffusion rate (Yazar, Arvas, & Sahin, 2022).

4.6. Galvanostatic Charge-Discharge Test of Electrodes

The electrochemical properties of the produced electrode materials were examined in a three-electrode setup with a 0.5 M H_2SO_4 solution with GCD technic. At the current density of 5 mA cm^{-2}, a comparison of charge-discharge profiles of bare carbon felt, PAAc, PAAc-g-CNT, PAAc-g-(Pt/CNT), PAAc-g-(Pd/CNT) and PAAc-g-(Ru/CNT) was shown in Figure 4.18(a). Based on discharge time from GCD, specific capacitance values were calculated according to equation (3.2) and presented Figure 4.18(f).

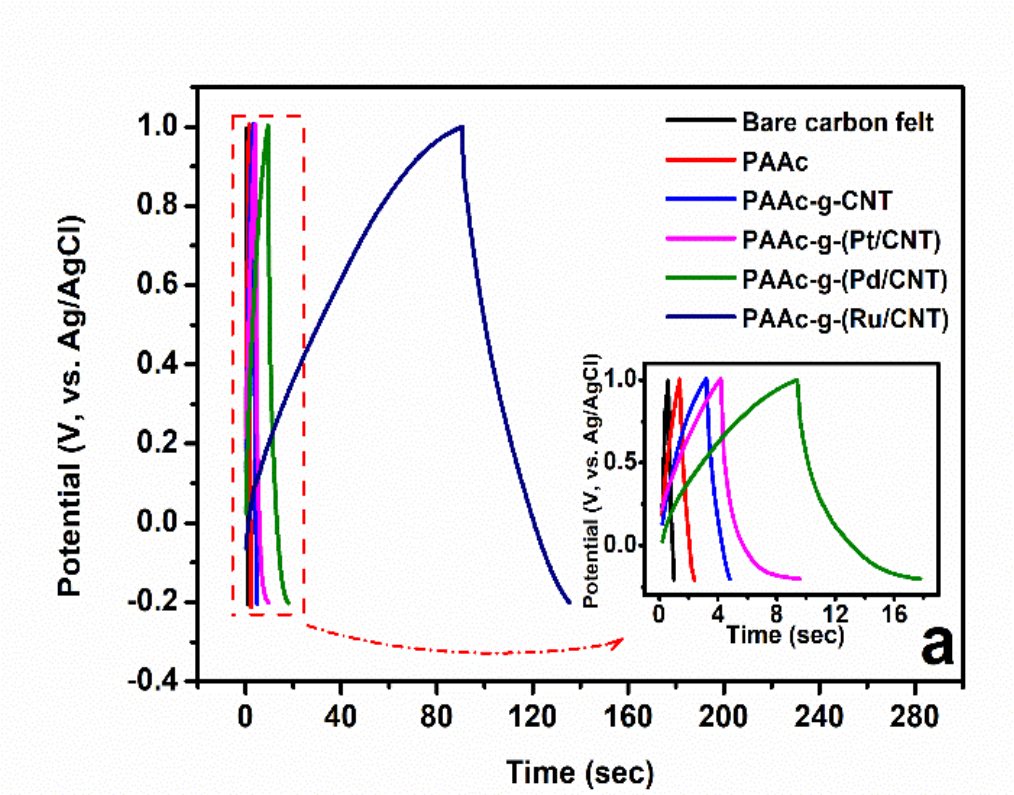
Potential (V, vs. Ag/AgCl)
Time (sec)
Bare carbon felt
PAAc
PAAc-g-CNT
PAAc-g-(Pt/CNT)
PAAc-g-(Pd/CNT)
PAAc-g-(Ru/CNT)
a

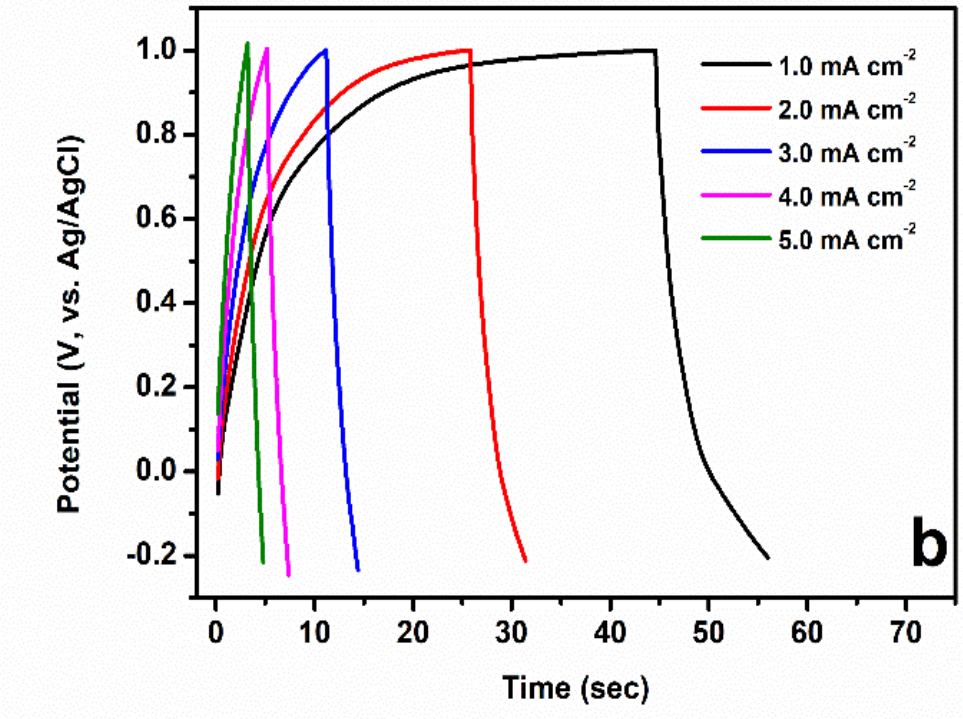
Potential (V, vs. Ag/AgCl)
Time (sec)
1.0 mA cm-2
2.0 mA cm-2
3.0 mA cm-2
4.0 mA cm-2
5.0 mA cm-2
b

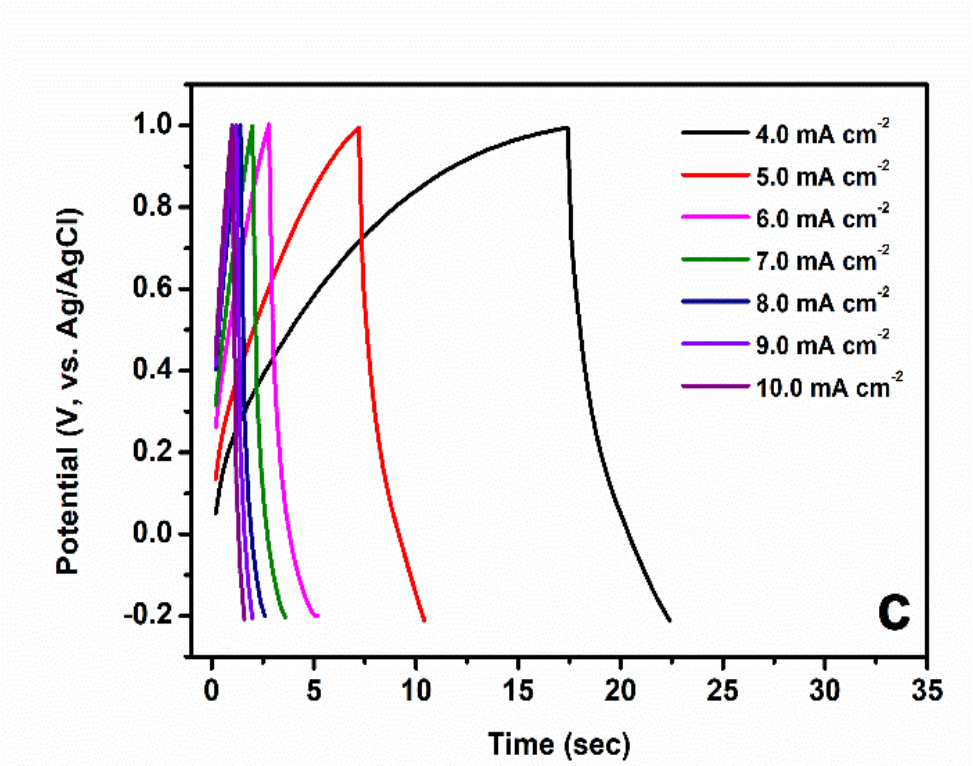
Potential (V, vs. Ag/AgCl)
Time (sec)
4.0 mA cm-2
5.0 mA cm-2
6.0 mA cm-2
7.0 mA cm-2
8.0 mA cm-2
9.0 mA cm-2
10.0 mA cm-2
c

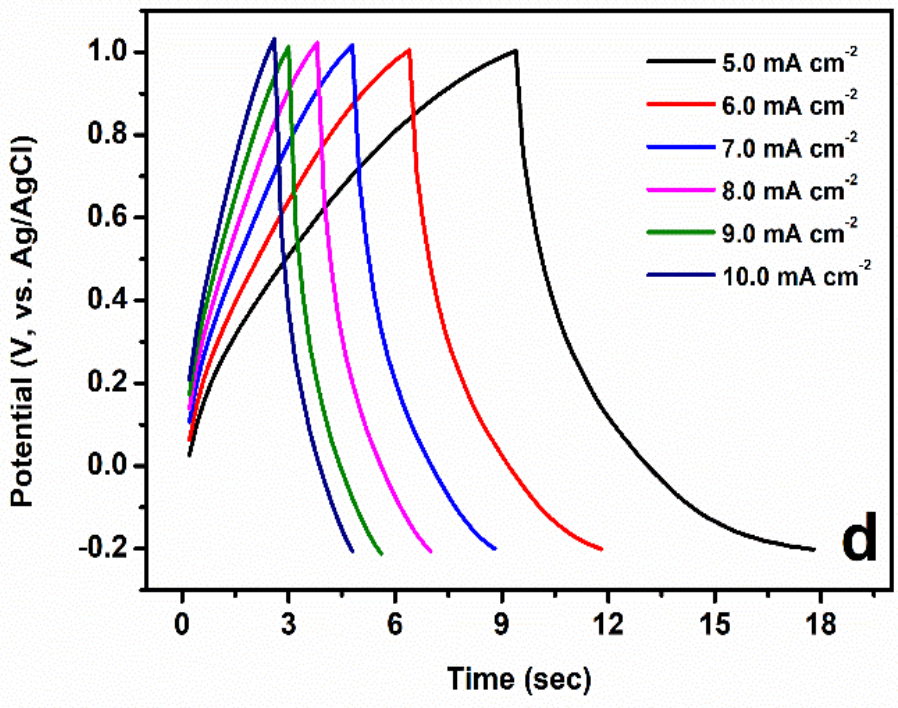
Potential (V, vs. Ag/AgCl)
Time (sec)
5.0 mA cm-2
6.0 mA cm-2
7.0 mA cm-2
8.0 mA cm-2
9.0 mA cm-2
10.0 mA cm-2
d

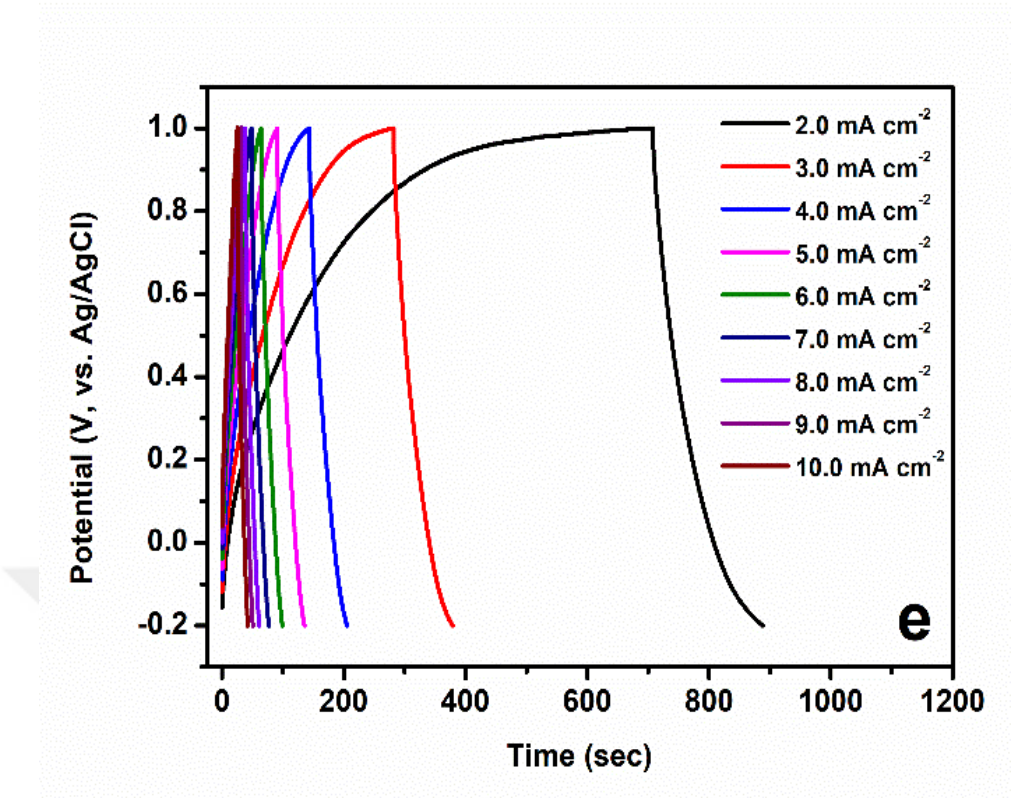

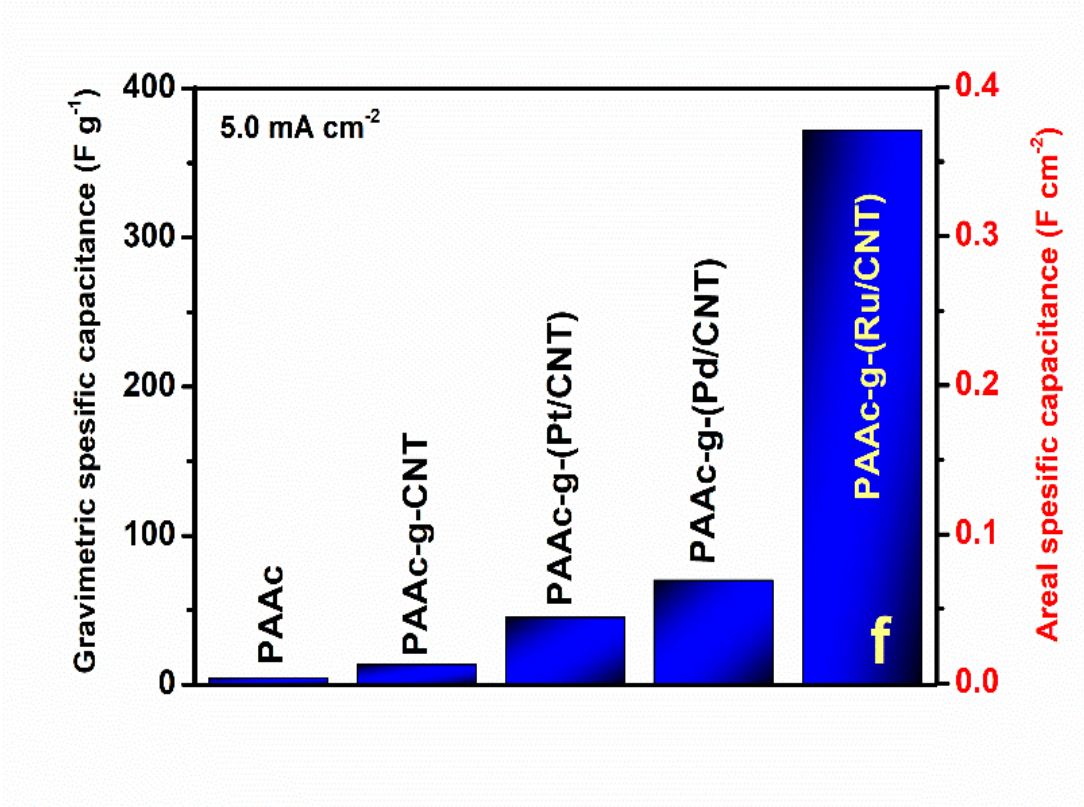

Figure 4.18 a) GCD curves at 5 mA cm^{-2} of bare carbon felt, PAAc, PAAc-g-CNT, PAAc-g-(Pt/CNT), PAAc-g-(Pd/CNT) and PAAc-g-(Ru/CNT), Galvanostatic charge-discharge curves of b) PAAc-g-CNT c) PAAc-g-(Pt/CNT), d) PAAc-g-(Pd/CNT), e) PAAc-g-(Ru/CNT) f) Specific capacitance values of electrodes from GCD curves at 5 mA cm^{-2}.

Table 4.5 Specific capacitance values of PAAc-g-(Ru/CNT), PAAc-g-(Pd/CNT) and PAAc-g-(Pt/CNT) obtained from Galvanostatic charge-discharge test.

Electrode material	**discharge current (A)**	**ΔV (V)**	**Cs (F g^{-1})**
PAAc-g-(Ru/CNT)	0.002	1.2	600.0
	0.003	1.2	484.0
	0.004	1.2	414.7
	0.005	1.2	371.7
	0.006	1.2	350.0
	0.007	1.2	331.3
	0.008	1.2	312.0
	0.009	1.2	297.0
	0.010	1.2	283.3
PAAc-g-(Pd/CNT)	0.006	1.2	54.0
	0.007	1.2	46.7
	0.008	1.2	42.7
	0.009	1.2	39.0
	0.010	1.2	36.7
PAAc-g-(Pt/CNT)	0.004	1.2	21.3
	0.005	1.2	45.0
	0.006	1.2	26.0
	0.007	1.2	21.0
	0.008	1.2	16.0
	0.009	1.2	15.0
	0.010	1.2	16.7

After the addition of CNT to the PAAc electrode, the capacitance value increased 3.2 times, while the Ru/CNT doped electrode showed an extraordinary increase of 27.9 times in Figure 4.18(f). Faradaic reactions that occurred with the help of ions moved from the electrolyte to the electrode surface are important to increase the performance of supercapacitor electrodes(Forouzandeh et al., 2020). Thus, the charge storage performance was improved by augmenting the surface area of the electrode containing PAAc-g-(Ru/CNT). The electrode containing catalyst Ru/CNT provided the highest capacitance performance and the longest discharge time with GCD and CV tests in harmony. It was observed that the PAAc polymer facilitated the transport of ions in the electrode material, and the best synergistic interaction with Ru/CNT was achieved.

In Figure 4.18(c-e), the behavior of PAAc-g-(Pt/CNT), PAAc-g-(Pd/CNT), and PAAc-g-(Ru/CNT) electrodes at different current densities, respectively, was investigated. The PAAc-g-(Pt/CNT), electrode exhibited supercapacitor behaviours in the current density range of 4.0 and 10.0 mA cm^{-2}. Because it exhibited plateau-like discharge at current densities less than 4.0 mA cm^{-2}, the supercapacitor deviated from behaviours and limited measurement in this range of current densities. Although it can protect 78.1% of the capacitance value from 4.0 to 10.0 mA cm^{-2}, the greatest capacitance value was measured as 21.3 F g^{-1} at 4.0 mA cm^{-2}. PAAc-g-(Pd/CNT, on the other hand, was able to exhibit supercapacitor behavior in a much narrower range. It showed a plateau after 6.0 mA cm^{-2}. The highest capacitance value was measured as 54.0 F g^{-1} at the current density of 6.0 mA cm^{-2}. The PAAc-g-(Ru/CNT) electrode showed the ability to take measurements in a wider current density range compared to the other electrodes. It managed to preserve ~50% of its capacitance at current values ranging from 2.0 mA cm^{-2} to 10.0 mA cm^{-2}. It can also be seen in Figure 4.18(e) that the total charge-discharge time reaches ~900 seconds compared to other electrodes. At a current density of 2.0 mA cm^{-2} between -0.2 and 1.0 V showed an IR drop of only 0.04 V in the GCD test and the maximum capacitance value was determined to be 600.0 F g^{-1}.

Both CNT and metals contributed to the capacitance, and ruthenium's benefit to the capacitance was much higher. This indicated that Ru/CNT achieved wider current values, helping to increase the conductivity of the electrode. Likewise, higher current densities were observed in CV voltammograms. In addition, it was thought that PAAc ionic conductive polymer exhibited the best compatibility with Ru and can help increase the electrochemical performance thanks to its ion transport feature.

Table 4.6 Comparison of some supercapacitor electrodes containing polyacrylic acid and ruthenium materials.

Electrode Material	Electrolyte	Measurement type	Maximum capacitance	Cycling life	Ref.
Polyacrylic acid/polypyrrole/silver composite	0.1 M H_2SO_4	3-electrode	226 F g^{-1}, 10 mV s^{-1}	2000 (% 63)	(Patil et al., 2013)
Porous carbons from carboxylated coal-tar pitches functional poly(acrylic acid)	6.0 M KOH	2-electrode	292 F g^{-1}, 1.0 A g^{-1}	10000 (% 94.2)	(H. Wang et al., 2020)
Polyaniline/poly (acrylic acid)-modified carbon nanotube	1.0 M H_2SO_4	3- electrode 2- electrode	612.5 F g^{-1}, 0.5 A g^{-1} 382.9 F/g, 0.5 A g^{-1}	1500 (% 81.5) 2000 (% 71.8)	(Q. Liu et al., 2018)
Nitrogen-doped graphene (NG)-polyacrylic acid/polyaniline (NG-PAA/PANI)	1.0 M H_2SO_4 H_2SO_4-PVA	3- electrode 2- electrode	521 F g^{-1}, 0.5 A g^{-1} 68 F g^{-1}, 1.0 A g^{-1}	2000 (% 83.2)	(Y. Wang et al., 2016)
Cu–poly(acrylic) acid (PAA)	1.0 M H_2SO_4	3- electrode	65 F g^{-1}, 20 mV s^{-1}	-	(Shaikh, Pawar, Tarwal, et al., 2011)
10 wt% RuO_2 /MWCNT	1.0 M H_2SO_4	3- electrode	130 F g^{-1} 50 mV s^{-1}	-	(Choi et al., 2022)
Ruthenium nanohybrid-compounds	0.5 M H_2SO_4	3- electrode	797.7 F g^{-1}, 0.5 A g^{-1}	2000 (% 90.2)	(Guo et al., 2020)
Ru NPs embedded self-templated mesoporous carbons.	6.0 M KOH	3- electrode	656.3 F g^{-1}, 10 A g^{-1}	5000 (% 100)	(Aftabuzzaman et al., 2019)

Table 4.6 Comparison of some supercapacitor electrodes containing polyacrylic acid and ruthenium materials (continued).

Electrode Material	Electrolyte	Measurement type	Maximum capacitance	Cycling life	Ref.
Oxide of ruthenium (IV)/MWCNTs	1.0 M H_2SO_4	3- electrode	457.6 F g^{-1}, 100 mV s^{-1}	-	(Yan et al., 2008)
Poly(acrylic) acid -g-(Ru/CNT)	0.5 M H_2SO_4	3- electrode	1294.5 F g^{-1}, 5mV s^{-1} 600.0 F g^{-1}, 4.0 A g^{-1}	1000 (% 97.7)	[this work]

The capacitance values and various parameters of some supercapacitor materials using polyacrylic acid as the electrode material and containing ruthenium were given in Table 4.6 This value was one of the best reported among electrodes containing Ruthenium/carbonous based electrode materials. This work not only provided insight into the idea strategy and creation for high-performance supercapacitors in combination with ionic conductive polymers but also offered a novel approach to production metal/carbon based materials in energy storage applications.

Figure 4.19(a-c) shows the behavior of the CF/PAAc-g-(Fe/CNT), CF/PAAc-g-(Co/CNT), and CF/PAAc-g-(Ni/CNT) electrodes, respectively, at various current densities. At the current density range of 5.0 and 1.0 mA cm^{-2}, the CF/PAAc-g-(Fe/CNT) electrode displayed supercapacitor behaviors. The supercapacitor deviated from capacitive behavior as it exhibited plateau-like discharge at current densities less than 1.0 mA cm^{-2}. In addition, since the material above *5.0* cm^{-2} could not charge, this density could not be *exceeded,* and the measurement was limited in this range of current densities. After the current density was increased 5 times, it was able to maintain only 44.7% of the capacitance value. A measurement of 78.3 F g^{-1} at 1.0 mA cm^{-2} yielded the greatest capacitance result. Specific capacitance values based on GCD discharge were computed using equation (3.2).

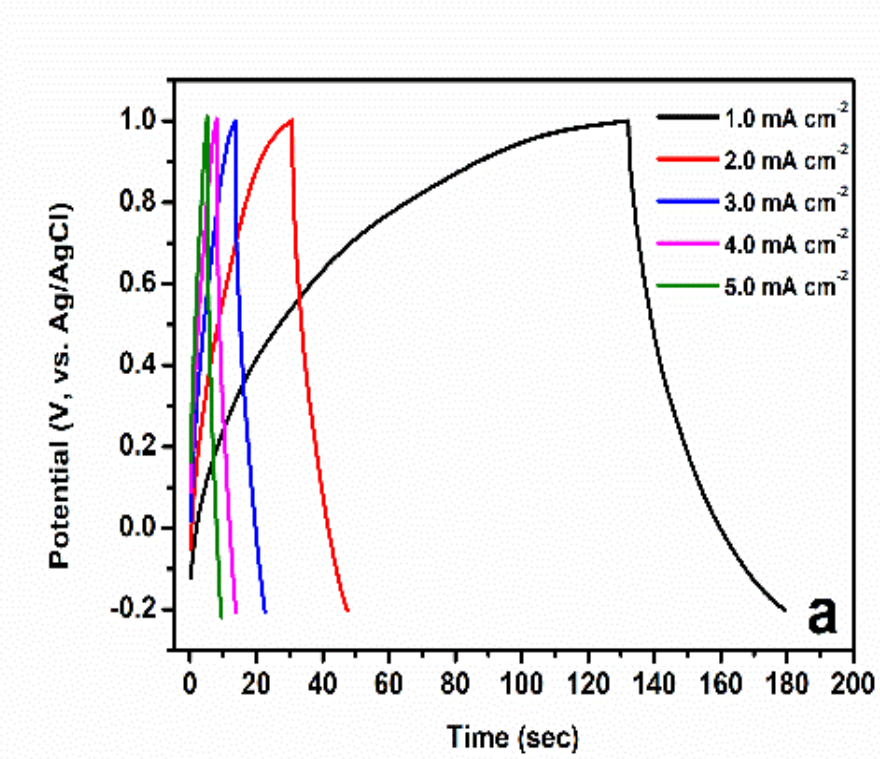
Potential (V, vs. Ag/AgCl)
Time (sec)
1.0 mA cm-2
2.0 mA cm-2
3.0 mA cm-2
4.0 mA cm-2
5.0 mA cm-2
a

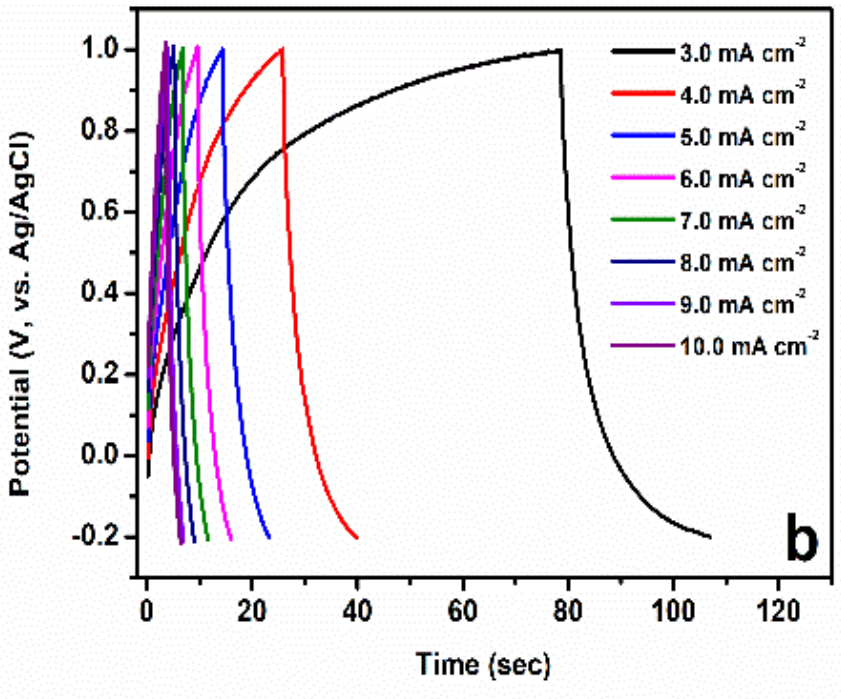
Potential (V, vs. Ag/AgCl)
Time (sec)
3.0 mA cm-2
4.0 mA cm-2
5.0 mA cm-2
6.0 mA cm-2
7.0 mA cm-2
8.0 mA cm-2
9.0 mA cm-2
10.0 mA cm-2
b

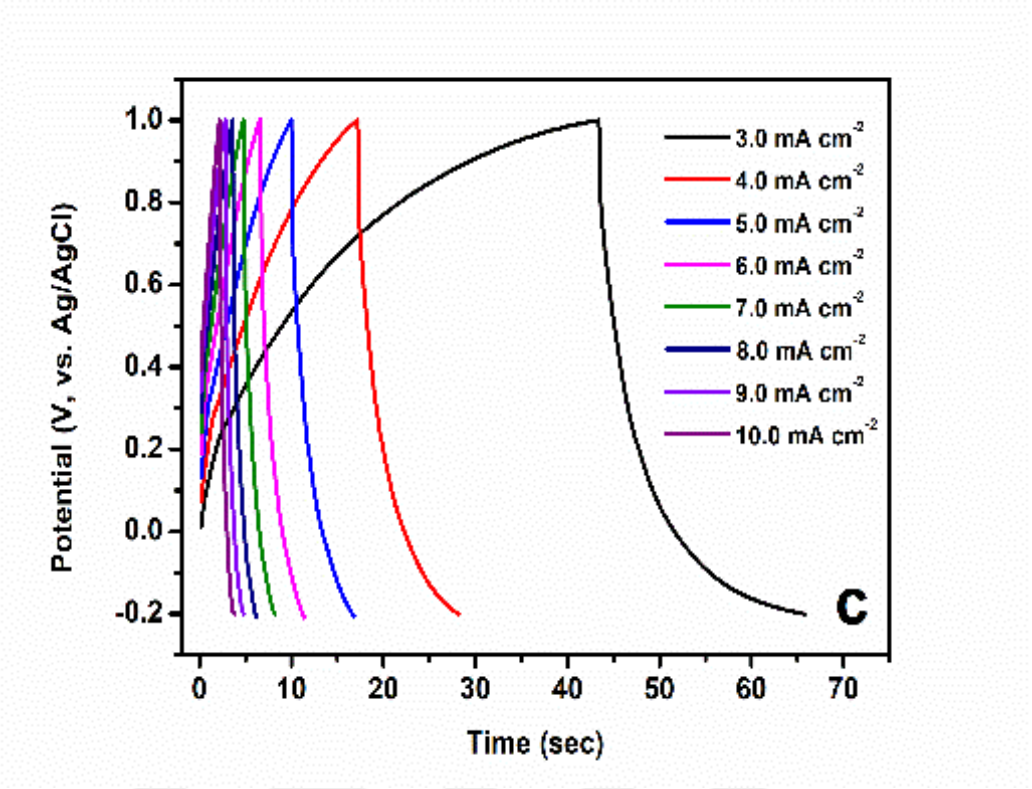
Potential (V, vs. Ag/AgCl)
Time (sec)
3.0 mA cm-2
4.0 mA cm-2
5.0 mA cm-2
6.0 mA cm-2
7.0 mA cm-2
8.0 mA cm-2
9.0 mA cm-2
10.0 mA cm-2
c

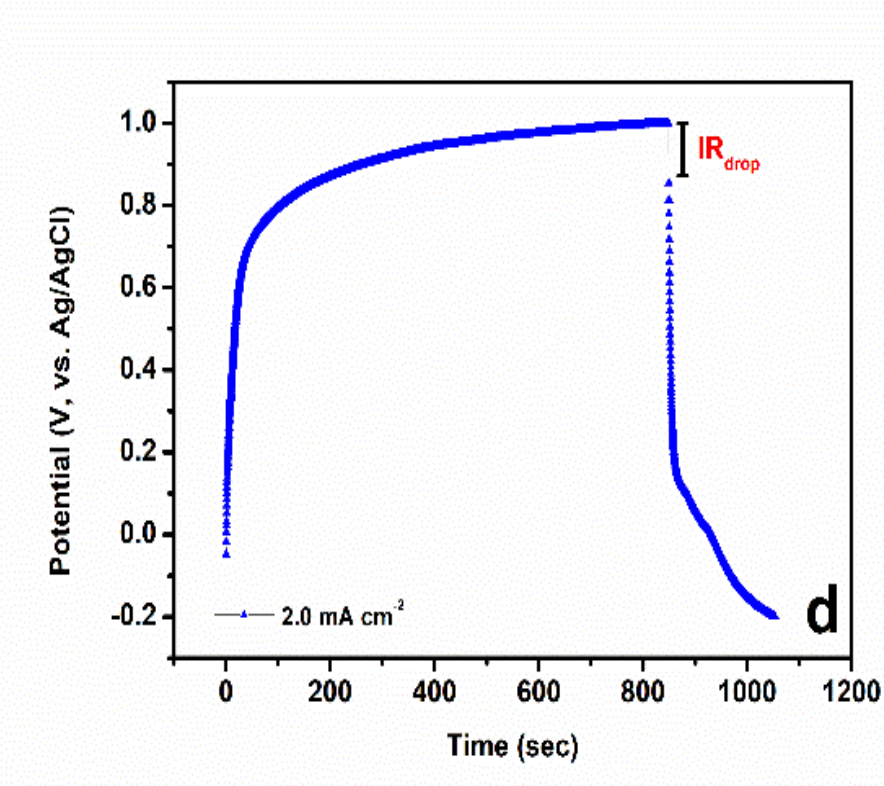
Potential (V, vs. Ag/AgCl)
Time (sec)
IRdrop
2.0 mA cm-2
d

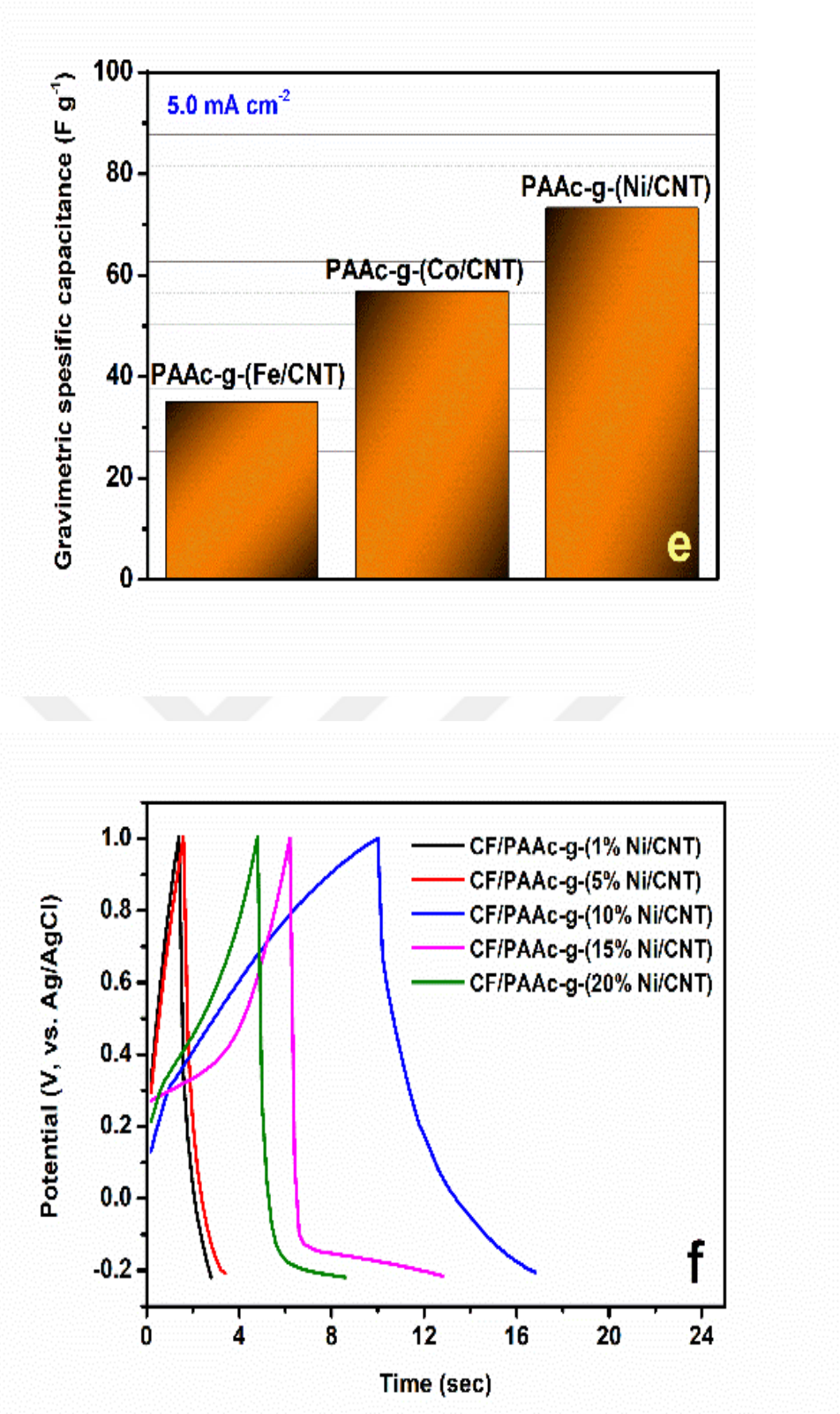

Figure 4.19 Galvanostatic charge-discharge curves of a) CF/PAAc-g-(10% Fe/CNT), b) PAAc-g-(10% Co/CNT), c) PAAc-g-(10% Ni/CNT), d) PAAc-g-(10% Ni/CNT) at 2 mA cm^{-2} e) Specific capacitance values of electrodes from GCD curves at 5 mA cm^{-2}, f) CF/PAAc-g-(Ni/CNT) at different concentrations.

Table 4.7 Specific capacitance values of PAAc-g-(Fe/CNT), PAAc-g-(Co/CNT) and PAAc-g-(Ni/CNT) obtained from Galvanostatic charge-discharge test.

Electrode material	**discharge current (A)**	**ΔV (V)**	**Cs (F g^{-1})**
PAAc-g-(Fe/CNT)	0.001	1.2	78.3
	0.002	1.2	55.3
	0.003	1.2	45.0
	0.004	1.2	38.7
	0.005	1.2	35.0
PAAc-g-(Co/CNT)	0.003	1.2	142.0
	0.004	1.2	93.3
	0.005	1.2	73.3
	0.006	1.2	64.0
	0.007	1.2	56.0
	0.008	1.2	50.7
	0.009	1.2	45.0
	0.010	1.2	46.7
PAAc-g-(Ni/CNT)	0.002	1.2	680.0
	0.003	1.2	112.0
	0.004	1.2	73.3
	0.005	1.2	56.7
	0.006	1.2	48.0
	0.007	1.2	42.0
	0.008	1.2	34.7
	0.009	1.2	33.0
	0.010	1.2	26.7

CF/PAAc-g-(Co/CNT) exhibited charge-discharge behavior in a wider current density range compared to CF/PAAc-g-(Fe/CNT). The highest capacitance value was measured as 142.0 F g^{-1} at the current density 3.0 mA cm^{-2}. It was able to maintain 32.9% of its capacitance between current levels of 3.0 mA cm-2 and 10.0 mA cm^{-2}. CF/PAAc-g-(Ni/CNT) was the electrode that offered measurement in the widest current density range. Moreover, Figure 4.19(d) shows that when compared to other electrodes, the overall charge-discharge time was around 1060 seconds. The highest capacitance was computed as 680.0 F g^{-1} at a current density of 2.0 mA cm^{-2} demonstrating an IR drop of ~0.1 V in the GCD test. To enhance the performance of supercapacitor electrodes, faradaic and electrostatic reactions

that took place with the aid of ions moved from the electrolyte to the electrode surface are crucial (Forouzandeh et al., 2020). As seen in Figure 4.19(e), CF/PAAc-g-(Ni/CNT) proved to provide the highest capacitance performance and the longest discharge time with GCD and CV tests. It can be said that PAAc polymer acted as a bridge by facilitating the transport of ions in the electrode material and the best effect was achieved with 10% Ni/CNT. When the charge-discharge behaviors of the electrode materials synthesized at different nickel concentrations were compared, it was seen that the results were compatible with the CV measurements. It showed improved performance with a similar GCD profile from 1% to 10%, while after 15% the discharge time was reduced and the GCD profile changed. In cyclic voltammetry, it was mentioned that in the energy storage mechanism of CF/PAAc-g-(Ni/CNT) electrode active oxidation of Ni^{2+} will continue until it is largely precipitated by nickel oxides on the electrode surface. Since NiO was a non-ionic oxide, it was slightly soluble. Depending on the applied current densities and the nickel concentration in the environment, a higher amount of oxide may have accumulated compared to other electrodes after a certain period. At low pH values, some studies have mentioned that oxides such as NiO, Ni_2O_3 and Ni_3O_4 can form (El Wanees et al., 2021; Real et al., 1980; Sato & Okamoto, 1963).

In addition, supercapacitor performance comparisons of polyacrylic acid-based Ni-containing electrode materials are presented in the literature (Table 4.8). This study provided information on the creation of new ideas in the choice of ionic conductive polymers as electrode materials other than electrolyte materials.

Table 4.8 Performance comparison of some supercapacitor electrodes containing polyacrylic acid and some forms of nickel.

Electrode Material	Electrolyte	Measurement type	Maximum capacitance	Cycling life	Ref.
Graphene doped polyacrylic acid/polyaniline	1 M H_2SO_4 H_2SO_4–PVA	3- electrode 2- electrode	399 Fg^{-1}, 10 mV s^{-1} 93 Fg^{-1}, 10 mV s^{-1}	-	(Y. Wang et al., 2015)
PAA-coated N-doped graphene	2 M Li_2SO_4	2-electrode	-	100000 (86%)	(Dong et al., 2020)
Polyacrylic acid-b-polyacrylonitrile-b-polyacrylic acid	4 M KOH	3-electrode	256.3 Fg^{-1}, 0.5 Ag^{-1}	80000 (90%)	(Dong et al., 2019)
Nitrogen-doped porous carbons - poly(acrylic acid)/melamine resin	1 M H_2SO_4	3-electrode	280 Fg^{-1}, 0.2 A g^{-1}	9000 (100%)	(J. Jiang et al., 2015)
NiO/C@CNF	3.0 M KOH	3-electrode	742.2 Fg^{-1}, 1.0 A g^{-1}	-	(Shin & Shin, 2021)
NiO/ZnO hollow spheres	1.0 M H_2SO_4	3-electrode	497 Fg^{-1} 1.3 A g^{-1}	2000 (117.1%)	(G.-C. Li et al., 2016)
NiBPDC/GO	6.0 M KOH	3-electrode	630 Fg^{-1}, 1.0 A g^{-1}	10000 (56.5%)	(He et al., 2020)
RGO/Ni-MOF/metallic fabric electrode	6.0 M KOH	3-electrode	260 $mFcm^{-2}$,4 mA cm^{-2}	2000 (80%)	(Cheng et al., 2019)
CF/PAAc-g-(Ni/CNT)	0.5 M H_2SO_4	3-electrode	680.0 F g^{-1}, 4.0 A g^{-1}	1000 (94.1%)	[this work]

Figure 4.20 presents the performance of PAAc-g-(Mo/CNT), PAAc-g-(Ga/CNT), and PAAc-g-(Bi/CNT) electrodes at different current densities, evaluated using the GCD technique.

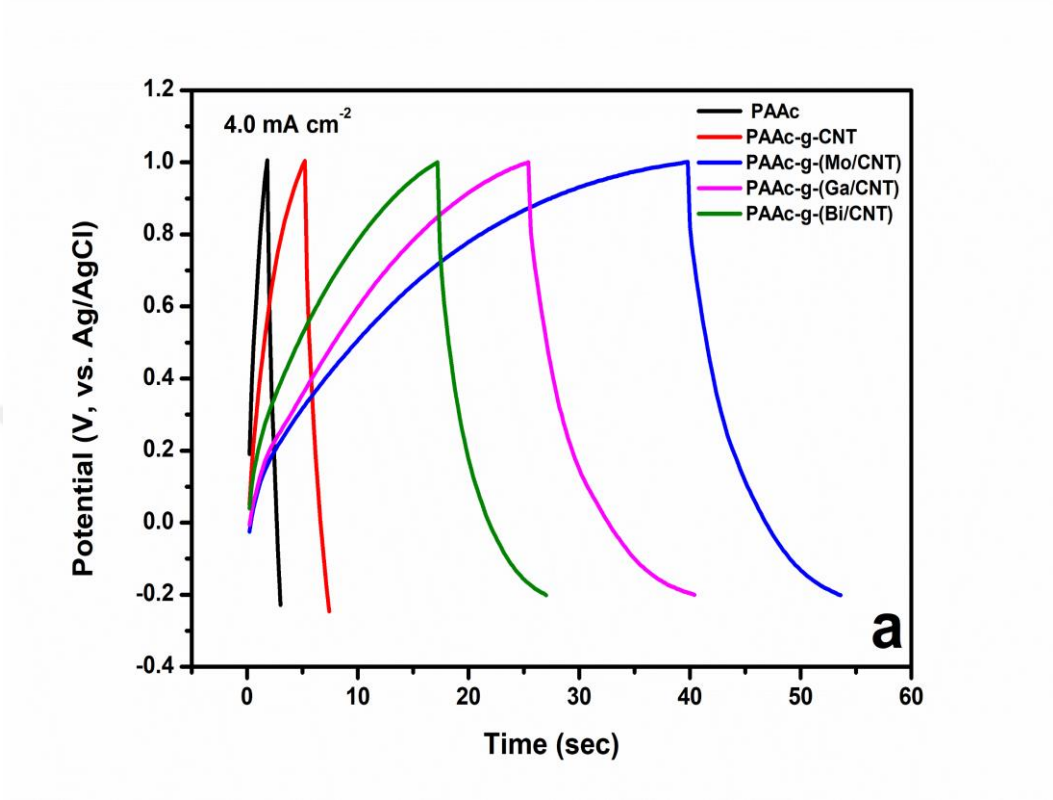

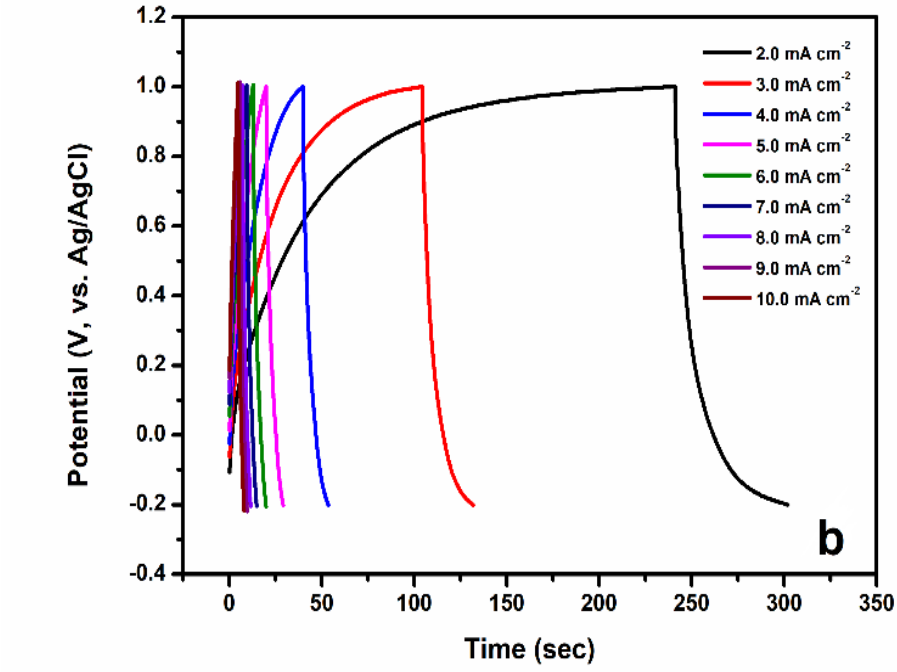

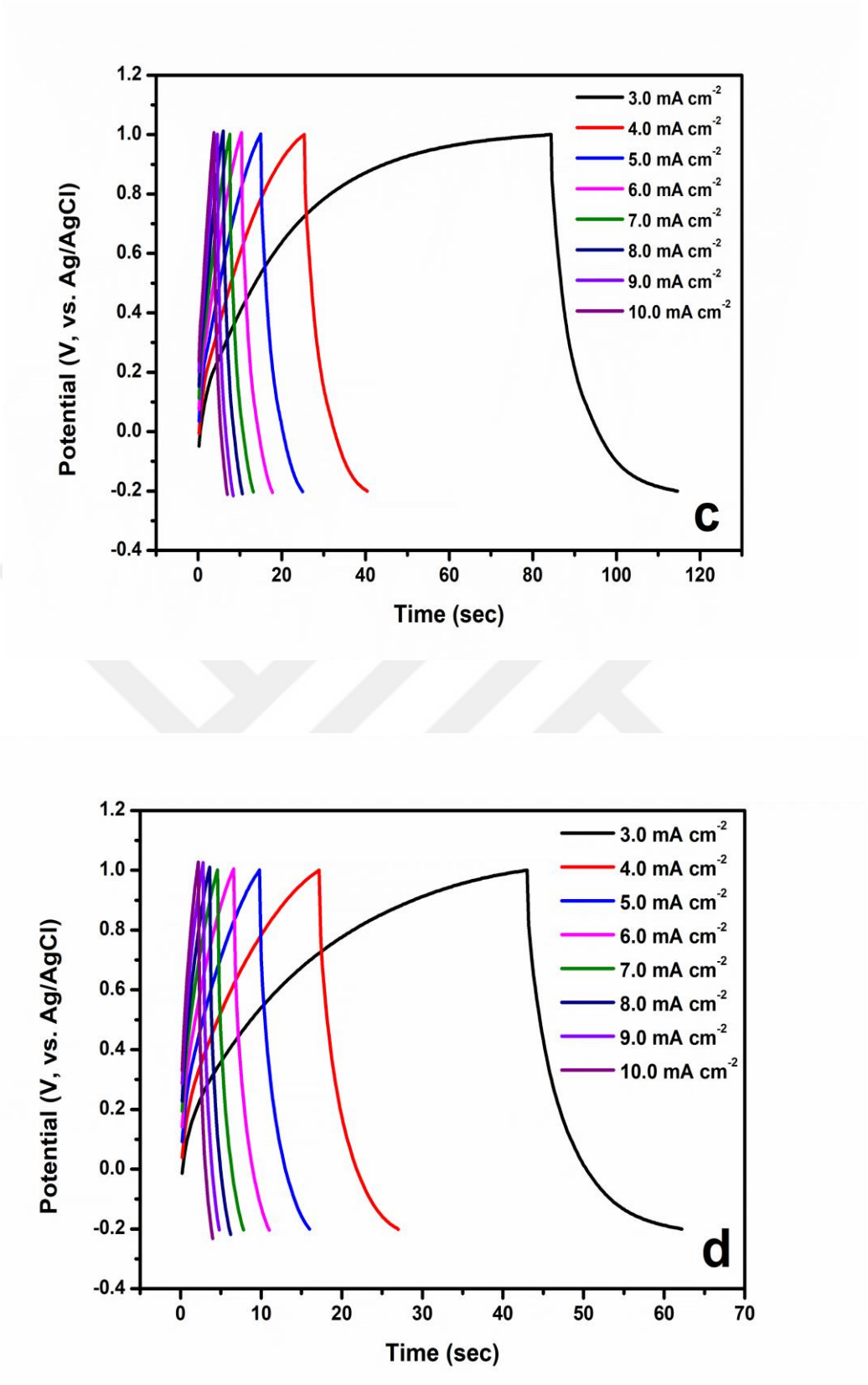

Figure 4.20 a) Galvanostatic charge-discharge curves of PAAc, PAAc-g-CNT, PAAc-g-(Mo/CNT), PAAc-g-(Ga/CNT), and PAAc-g-(Bi/CNT) at 4 mA cm^{-2}, b) GCD curves of PAAc-g-(Mo/CNT), c) GCD curves of PAAc-g-(Ga/CNT), d) GCD curves of PAAc-g-(Bi/CNT) at different current densities.

The behavior of PAAc-g-(Mo/CNT), PAAc-g-(Ga/CNT), and PAAc-g-(Bi/CNT) electrodes was studied at various current densities in Figures 4.20(b-d). Among these electrodes, the PAAc-g-(Mo/CNT) electrode demonstrated excellent supercapacitor characteristics within the range of 3.0 mA cm^{-2} and 10.0 mA cm^{-2} current density. Compared to the other electrodes, PAAc-g-(Mo/CNT) demonstrated the widest range of current density measurement. The overall charge-discharge time for this electrode was approximately 300 seconds. At a current density of 3.0 mA cm^{-2}, it exhibited the highest capacitance of 137.0 F g^{-1} during the GCD test. Through enhancing the surface area of the electrode comprising PAAc-g-(Mo/CNT), the charge storage performance was enhanced. The capacitance values obtained by using the equation (3.2) as a result of the measurements are given in Table 4.9

Table 4.9 Specific capacitance values of PAAc-g-(Mo/CNT), PAAc-g-(Ga/CNT) and PAAc-g-(Bi/CNT) obtained from Galvanostatic charge-discharge test.

Electrode material	**discharge current (A)**	**ΔV (V)**	**Cs (F g^{-1})**
PAAc-g-(Mo/CNT)	0.003	1.2	137.0
	0.004	1.2	92.0
	0.005	1.2	76.7
	0.006	1.2	70.0
	0.007	1.2	63.0
	0.008	1.2	58.7
	0.009	1.2	57.0
	0.010	1.2	53.3
PAAc-g-(Ga/CNT)	0.003	1.2	126.0
	0.004	1.2	89.0
	0.005	1.2	83.3
	0.006	1.2	74.0
	0.007	1.2	65.3
	0.008	1.2	61.3
	0.009	1.2	57.0
	0.010	1.2	53.3
PAAc-g-(Bi/CNT)	0.003	1.2	96.0
	0.004	1.2	65.3
	0.005	1.2	51.7
	0.006	1.2	44.0
	0.007	1.2	37.3

Table 4.9 Specific capacitance values of PAAc-g-(Mo/CNT), PAAc-g-(Ga/CNT) and PAAc-g-(Bi/CNT) obtained from Galvanostatic charge-discharge test (continued).

Electrode material	**discharge current (A)**	**ΔV (V)**	**Cs (F g^{-1})**
	0.008	1.2	34.7
	0.009	1.2	30.0
	0.010	1.2	30.0

The electrode containing the Mo/CNT catalyst exhibited the highest capacitance performance, as demonstrated by both GCD and CV tests. Moreover, the PAAc polymer was found to aid in the transport of ions within the electrode material, and the optimal synergistic interaction was observed between PAAc and Mo/CNT. Overall, the use of PAAc ionic conductive polymer in combination with Mo is promising for improving electrochemical performance due to the polymer's high compatibility with Mo and its ability to facilitate ion transport.

Table 4.10 Performance comparison of some supercapacitor electrodes containing polyacrylic acid and some forms of molybdenum.

Electrode Material	**Electrolyte**	**Measurement type**	**Maximum capacitance**	**Cycling life**	**Ref.**
Poly(acrylonitrile-co-acrylic acid)	3 M KOH	3- electrode	156 Fg^{-1}, 10 A g^{-1}	16000 (99%)	(J. Li et al., 2020)
Polyacrylic acid/polypyrrole/silver composite	0.1 M H_2SO_4	3-electrode	226 Fg^{-1}, 10 mV s^{-1}	2000 (63%)	(Patil et al., 2013)
Polyacrylic acid-b-polyacrylonitrile-b-polyacrylic acid	4 M KOH	3-electrode	256.3 Fg^{-1}, 0.5 Ag^{-1}	80000 (90%)	(Dong et al., 2019)
Cu–poly(acrylic) acid (PAA)	1 M H_2SO_4	3-electrode	65 Fg^{-1}, 20 mV s^{-1}	-	(Shaikh, Pawar, Tarwal, et al., 2011)
Mo/Mn mixed oxide	0.5 M Na_2SO_4	2-electrode	190.9 Fg^{-1}, 5 mV s^{-1}	-	(Nakayama et al., 2005)

Table 4.10 Performance comparison of some supercapacitor electrodes containing polyacrylic acid and some forms of molybdenum (continued).

Electrode Material	Electrolyte	Measurement type	Maximum capacitance	Cycling life	Ref.
α-$MnMoO_4$	1 M Na_2SO_4	3-electrode	180 Fg^{-1}, 5 mV s^{-1}	-	(Yesuraj et al., 2017)
α-$MnMoO_4$ symmetric device	2 M NaOH	3-electrode	81 Fg^{-1}, 5 $mAcm^{-2}$	1000 (91%)	(Gao et al., 2021)
$MoS_2/BiVO_4$	2 M NaOH	2-electrode	610 Fg^{-1}, 1 Ag^{-1}	200 (80%)	(Arora et al., 2016)
PAAc-g-(Mo/CNT)	0.5 M H_2SO_4	3-electrode	160.80 F g^{-1}, 10 mV s^{-1}	1000 (81.8%)	[this work]

Within the current density range of 1.0 and 5.0 mA cm^{-2}, Figure 4.21(a,b) demonstrates the Galvanostatic charge-discharge curves of PNIPAM and PNIPAM-g-CNT electrodes. Figure 4.21(c) depicts the GCD behavior of the PNIPAM-g-(Ru/CNT) electrode, observed at current density ranges of 5.0 and 10.0 mA cm^{-2}.

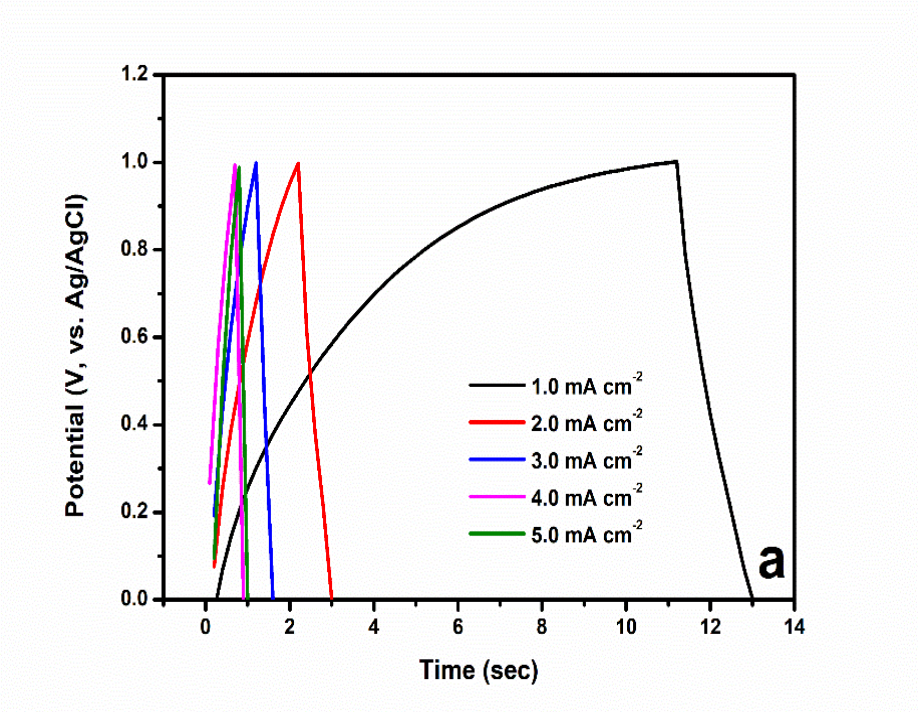

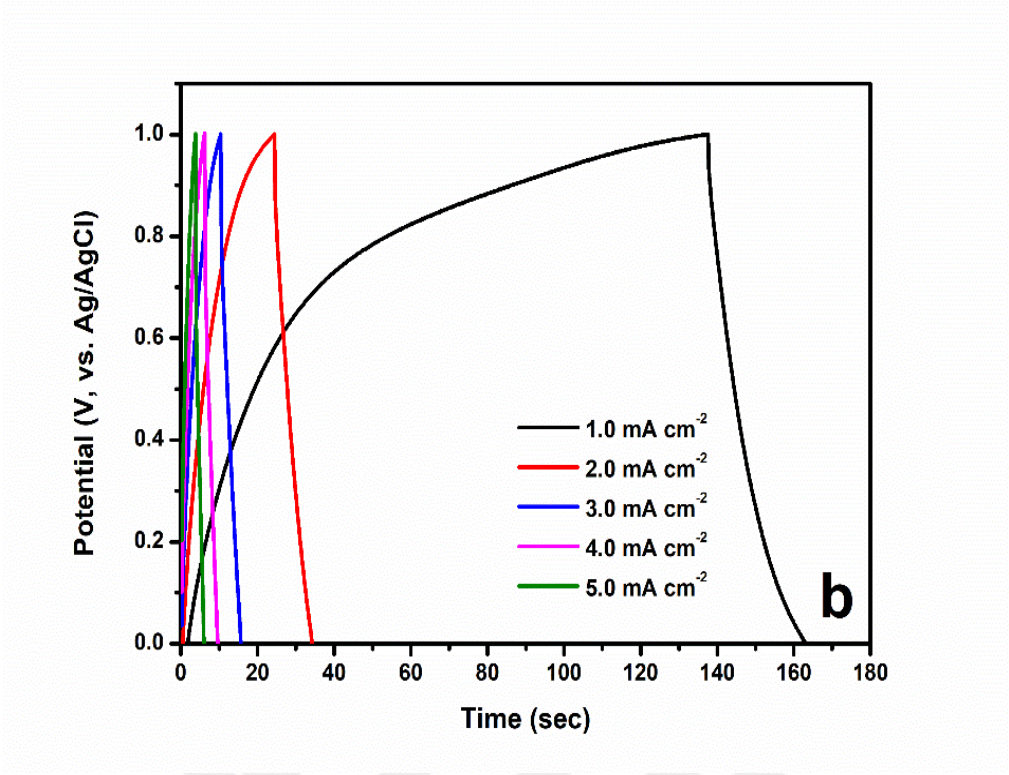

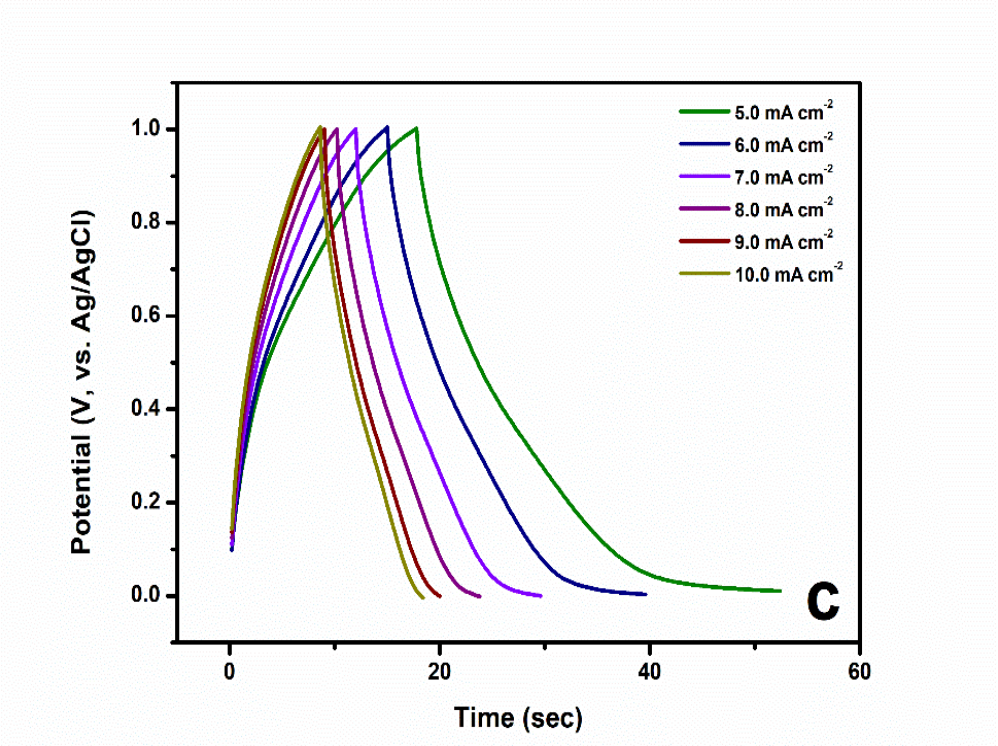

Figure 4.21 a) Galvanostatic charge-discharge curves of PNIPAM at current density ranges of 1.0 and 5.0 mA cm^{-2}, b) GCD curves of PNIPAM-g-CNT at current density ranges of 1.0 and 5.0 mA cm^{-2}, c) GCD curves of PNIPAM-g-(Ru/CNT) at current density ranges of 5.0 and 10.0 mA cm^{-2}.

Table 4.11 Specific capacitance values of PANIPAM, PANIPAM-g-CNT and PANIPAM-g-(Ru/CNT) obtained from Galvanostatic charge-discharge test.

Electrode material	**discharge current (A)**	**ΔV (V)**	**Cs (F g^{-1})**
PNIPAM	0.001	1.0	3.2
	0.002	1.0	3.2
	0.003	1.0	2.4
	0.004	1.0	1.6
	0.005	1.0	2.0
PNIPAM-g-CNT	0.001	1.0	51.2
	0.002	1.0	39.2
	0.003	1.0	31.2
	0.004	1.0	27.2
	0.005	1.0	22.0
PNIPAM-g-(Ru/CNT)	0.005	1.0	346.0
	0.006	1.0	295.2
	0.007	1.0	246.4
	0.008	1.0	217.6
	0.009	1.0	198.0
	0.010	1.0	196.0

The results from the Galvanostatic charge-discharge test, as shown in Table 4.11, provide insights into the specific capacitance values of three different electrode materials: PNIPAM, PNIPAM-g-CNT, and PNIPAM-g-(Ru/CNT). For PNIPAM electrodes, the specific capacitance remains relatively consistent across different discharge currents, ranging from 1.6 F g^{-1} to 3.2 F g^{-1}. This indicates a moderate capacitance performance for PNIPAM alone. In contrast, PNIPAM-g-CNT electrodes demonstrate significantly higher specific capacitance values, ranging from 22.0 F g^{-1} to 51.2 F g^{-1}. The inclusion of carbon nanotubes (CNT) in the electrode composition enhances its capacitance performance, leading to improved energy storage capabilities. Further enhancement is observed in PNIPAM-g-(Ru/CNT) electrodes, which exhibit specific capacitance values ranging from 196.0 F g^{-1} to 346.0 F g^{-1}. This significant enhancement in capacitance performance suggests that the combination of ruthenium (Ru) and CNT further enhances the energy storage capacity of the electrode. In conclusion, the results highlight the positive impact of incorporating carbon nanotubes and the combination of ruthenium with carbon nanotubes in

PNIPAM-based electrodes. PNIPAM-g-(Ru/CNT) electrodes demonstrate the highest specific capacitance values, indicating their potential for efficient energy storage applications.

Table 4.12 Comparison of some supercapacitor electrodes containing PNIPAM.

Electrode Material	**Electrolyte**	**Measurement type**	**Maximum capacitance**	**Cycling life**	**Ref.**
PEDOT-PNIPAm composite	3.0 M KOH	3-electrode	248 F g^{-1}, 2mV s^{-1}	(%98.81)	(A. K. Sharma et al., 2015)
PNIPAm−PPyNTs	0.1 M H_2SO_4	3-electrode	360 F g^{-1}, 100mV s^{-1}	200 (% 92)	(Elashnikov et al., 2021)
GO/PNIPAM hydrogel	1.0 M H_2SO_4	2-electrode	292 F g^{-1}, 1 Ag^{-1}	10000 (% 96)	(Zhao et al., 2017)
PNIPAM-g-(Ru/CNT)	0.5 M H_2SO_4	3- electrode	313.57 F g^{-1}, 5mV s^{-1}	1000 (108.8%)	[this work]

Based on the results, the comparison between PAAc-g-(Ru/CNT) and PNIPAM-g-(Ru/CNT) electrodes reveals interesting insights into their respective performance as electrode materials for energy storage applications. While both hydrogels incorporate carbon nanotubes (CNT) and ruthenium (Ru) to enhance energy storage capacity, they exhibit distinct characteristics that influence their suitability for such applications. The PAAc-g-(Ru/CNT) electrode demonstrated excellent performance, surpassing both PAAc and CNT individually. With an impressive specific capacitance of 1294.5 F g^{-1} at a scan rate of 5 mV s^{-1}, it exhibited impressive energy storage capabilities. On the other hand, the PNIPAM-g-(Ru/CNT) electrode demonstrated a specific capacitance value of 346.0 F g^{-1} at 5.0 mA cm^{-2}. When considering the conductivity of the electrolyte, PAAc-g-(Ru/CNT) hydrogel outperforms PNIPAM-g-(Ru/CNT). PAAc has been known to possess higher ionic conductivity compared to PNIPAM, indicating that PAAc-based gels offer better pathways

for ion transport within the electrode material. This superior conductivity of PAAc-g-(Ru/CNT) hydrogel enables efficient charge transfer during electrochemical reactions, resulting in improved performance and stability. Therefore, in light of the results and acknowledging the conductive nature of PAAc-g-(Ru/CNT) hydrogel, it is preferred to be used as an electrode material for energy storage applications. The higher ionic conductivity of PAAc-based gels facilitates better ion transport within the electrode, leading to enhanced performance and long-term cycling stability.

4.7.Electrochemical Impedance Spectroscopy and Long Life Test of Electrodes

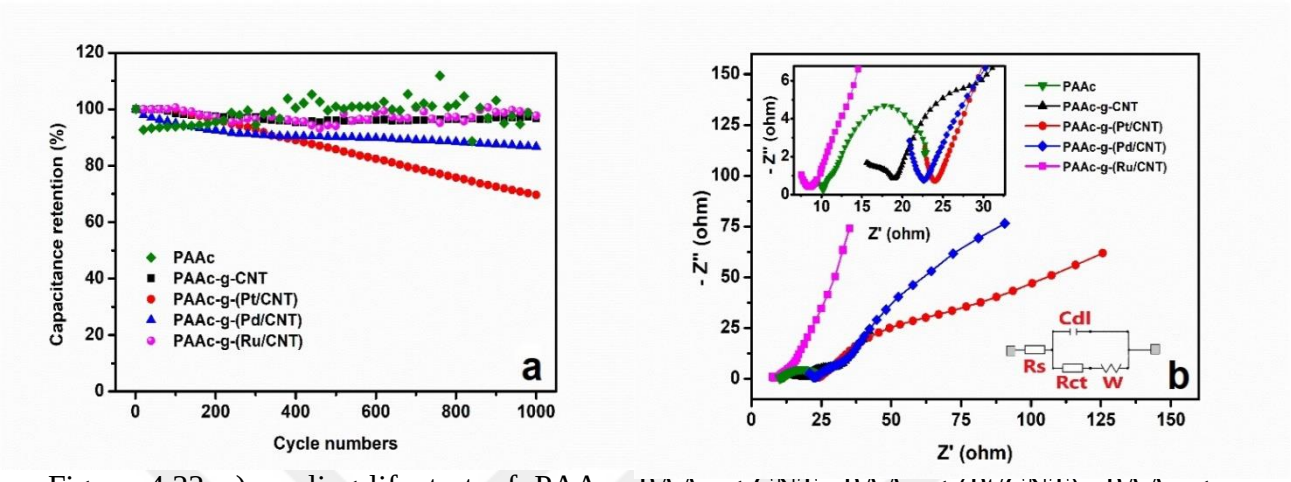

Figure 4.22 a) cycling-life test of PAAc, PAAc-g-CNT, PAAc-g-(Pt/CNT), PAAc-g-(Pd/CNT) and PAAc-g-(Ru/CNT). b) Nyquist plot of PAAc, PAAc-g-CNT, PAAc-g-(Pt/CNT), PAAc-g-(Pd/CNT) and PAAc-g-(Ru/CNT).

Figure 4.22(a) presents the cycling stability study of PAAc, PAAc-g-CNT, PAAc-g-(Pt/CNT), PAAc-g-(Pd/CNT) and PAAc-g-(Ru/CNT) were performed over 1000 cyclic voltammetry cycles, the potential window of 1.2 V at 100 mV s^{-1} scan rate. PAAc, PAAc-g-CNT, PAAc-g-(Pt/CNT), PAAc-g-(Pd/CNT) and PAAc-g-(Ru/CNT) showed excellent capacitance retention of 94.3 %, 96.9 %, 69.6 %, 86.7 % and 97.7 %, respectively. It was observed that the capacitance of the polyacrylic acid-coated carbon felt electrode (PAAc) was maintained over the long cycle time, but unstable measurements occurred a lot. Considering that this material has a hydrogel structure that shows ionic conductivity, it can be said that an imbalance occurs in the number of ions reaching the carbon felt electrode as a result of swelling in the electrolyte environment (Yaseen et al., 2021). The hydrogel material may have exhibited unstable swelling with the applied current. PAAc-g-(Pt/CNT) was the electrode with the fastest drop. Since platinum is a noble metal, it did not have a long life in the electrode material due to the low physical and chemical interaction with its chemical environment (Pan et al., 2020). Since the energy storage capabilities of metals depend on the redox reaction, they have shorter cycle lives than conducting polymers and carbon-based materials (Kausar, 2017). It is clear that the good interaction between Ru-doped CNT persists even after 1000 cycles of testing and exhibits good capacitance retention.

The electrochemical properties of PAAc, PAAc-g-CNT, PAAc-g-(Pt/CNT), PAAc-g-(Pd/CNT), and PAAc-g-(Ru/CNT) were examined using electrochemical impedance spectroscopy analyses. The values were derived by using the simple equivalent circuit model presented in Figure 4.22(a) and presented in Table 4.13.

Table 4.13 Fitted data for EIS test of PAAc, PAAc-g-CNT, PAAc-g-(Pt/CNT), PAAc-g-(Pd/CNT), and PAAc-g-(Ru/CNT) electrodes.

Electrode	**Rs, Ω**	**Rct, Ω**	**Cdl, F**	**W**
PAAc	10.68	11.15	$3.025e^{-6}$	$0.021e^{-3}$
PAAc-g-CNT	15.90	3.685	$4.922e^{-6}$	$36,59e^{-3}$
PAAc-g-(Pt/CNT)	24.72	24.97	$0.591e^{-3}$	$12.37e^{-3}$
PAAc-g-(Pd/CNT)	21.53	2.371	$1.012e^{-3}$	$9.399e^{-3}$
PAAc-g-(Ru/CNT)	5.730	3.182	$1.456e^{-3}$	$48.18e^{-3}$

The parameters Rs, Rct, Cdl, and W characterized the solution resistance, charge transfer resistance, double-layer capacitance, and ion diffusion rates, respectively. PAAc-g-(Ru/CNT) exhibited the lowest charge transfer and highest Cdl value according to the EIS data Figure 4.22(b). In Nyquist diagrams, as the diameter of the semicircle had smaller, the charge transfer resistance decreased and thus the energy storage activity increased. The addition of CNT to the carbon felt electrodes generally reduced the charge transfer resistance of the supercapacitor electrodes (H. Wang et al., 2010). A higher active surface area and lower charge transfer resistance offered a better electron transfer ratio between the electrolyte/electrode interface. In Nyquist plots, the slope of the line was higher than at low frequency and the smaller diameter of the semicircle at high frequency indicated that the redox couple reaction in the electrode material is simultaneously controlled by diffusion and charge transfer resistance, respectively (Laschuk et al., 2021). The EIS analysis's results and the electrodes' CV and GCD analyses' results were both in accord.

The cycling stability analysis of CF/PAAc-g-(Fe/CNT), CF/PAAc-g-(Co/CNT), and CF/PAAc-g-(Ni/CNT) is shown in Figure 4.23(a). In supercapacitor applications, the stable

cycling performance is crucial. The study was carried out 1000 cycles of cyclic voltammetry with a potential window of 1.2 V and a scan rate of 100 mV s^{-1}. Capacitance retention was 76.7%, 81.5%, and 94.1% for CF/PAAc-g-(Fe/CNT), CF/PAAc-g-(Co/CNT), and CF/PAAc-g-(Ni/CNT), respectively. The specific capacitance drops of CF/PAAc-g-(Fe/CNT), CF/PAAc-g-(Co/CNT) after prolonged cycling can be mainly attributed to the mechanical instability of the electrodes, which was caused by the detachment of active materials from the electrode surface. The specific capacitance of CF/PAAc-g-(Fe/CNT) gradually increased over the first 100 cycles and then decreased rapidly. This may be due to the activation process, in which more electrode material is added to the surface redox reaction. Then the electrode began to deteriorate mechanically (Q. Wang et al., 2015). For CF/PAAc-g-(Ni/CNT), the specific capacitance was slightly decreased in the first cycles, attributable to the equilibration of the active material (Q. Hu et al., 2021). CF/PAAc-g-(Ni/CNT) displayed best capacitance retention even after 1000 testing cycles.

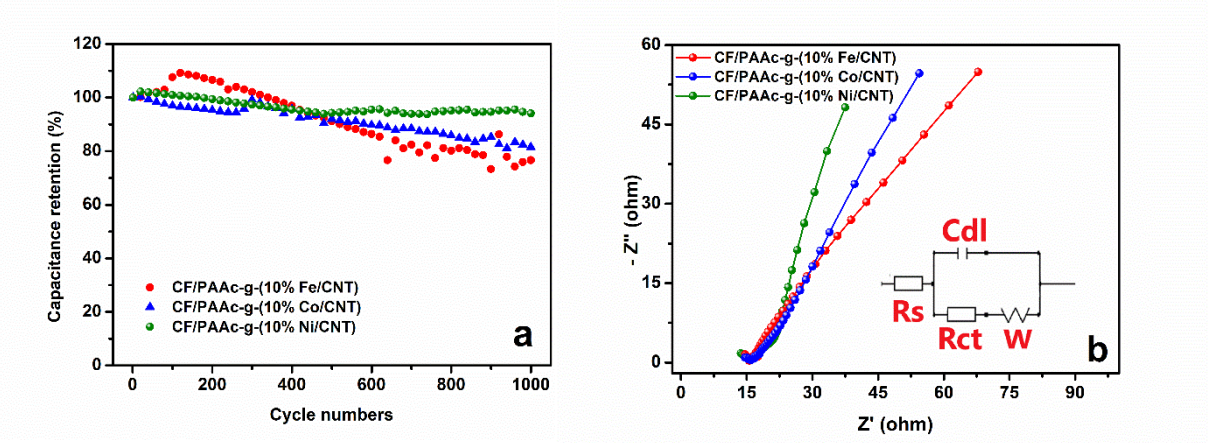

Figure 4.23 a) Cycling-life test of CF/PAAc-g-(10% Fe/CNT), PAAc-g-(10% Co/CNT) and PAAc-g-(10% Ni/CNT) electrodes, b) Nyquist plot of CF/PAAc-g-(10% Fe/CNT), PAAc-g-(10% Co/CNT) and PAAc-g-(10% Ni/CNT) electrodes.

Using electrochemical impedance spectroscopy studies, the electrochemical characteristics of CF/PAAc-g-(Fe/CNT), CF/PAAc-g-(Co/CNT), and CF/PAAc-g-(Ni/CNT) were investigated. Using the basic equivalent circuit model shown in Figure 4.23(a), the values were determined in Table 4.14.

Table 4.14 Fitted data for EIS test of CF/PAAc-g-(Fe/CNT), CF/PAAc-g-(Co/CNT), and CF/PAAc-g-(Ni/CNT) electrodes.

Electrode	Rs, Ω	Rct, Ω	Cdl, F	W
CF/PAAc-g-(Fe/CNT)	15.64	0.017	0.851e-3	16.95e-3
CF/PAAc-g-(Co/CNT)	16.08	0.662	1.493e-3	21.50e-3
CF/PAAc-g-(Ni/CNT)	15.54	0.011	3.502e-3	31.03e-3

Moreover, the EIS tests were carried out in the frequency range between 0.1 Hz and 100 kHz. After fitting, the Nyquist plot shows the presence of a slash at low frequency and a very small semicircle at high frequency, as shown in Figure 4.23(b). The values Rs, Rct, Cdl, and W described the solution resistance, charge transfer resistance, double-layer capacitance, and ion diffusion rates, respectively (H. Wang et al., 2010). According to the EIS data, CF/PAAc-g-(Ni/CNT) displayed the lowest charge transfer and highest Cdl value. In Nyquist diagrams, the charge transfer resistance reduced as the semicircle's diameter grew smaller, increasing the activity of energy storage. More electron transfer between the electrolyte/electrode contact was made possible by the reduced charge transfer resistance. According to the Nyquist plots, it can be said that the redox couple reaction in the electrode material occurs simultaneously with diffusion and charge transfer, with steep slope in the high frequency region and smaller semicircle diameter in the low frequency region. The absence and shrinkage of the semicircle indicates rapid diffusion of charges at the working electrode/electrolyte interface (Saravanan et al., 2015). Here, both the electrodes' CV and GCD studies and the EIS analysis produced consistent results.

The stability of PAAc-g-(Mo/CNT), PAAc-g-(Ga/CNT), and PAAc-g-(Bi/CNT) electrodes during cycling was evaluated in Figure 4.24(a). In supercapacitor applications, it is essential to maintain stable performance over extended cycles. The electrodes underwent 1000 cycles of cyclic voltammetry with a scan rate of 100 mV s^{-1} and a potential window of 1.2 V. The retention of capacitance for PAAc-g-(Mo/CNT), PAAc-g-(Ga/CNT), and PAAc-g-(Bi/CNT) was investigated after 1000 cycles of testing. The results indicated that PAAc-g-(Mo/CNT) exhibited the highest capacitance retention of 81.8%, making it the most reliable and stable material for energy storage applications. In contrast, PAAc-g-(Ga/CNT) and PAAc-g-(Bi/CNT) showed decreased capacitance retention and loss of electroactive

features. These findings suggest that PAAc-g-(Mo/CNT) is a favorable candidate for long-term energy storage applications, while further improvement is needed for the other materials.

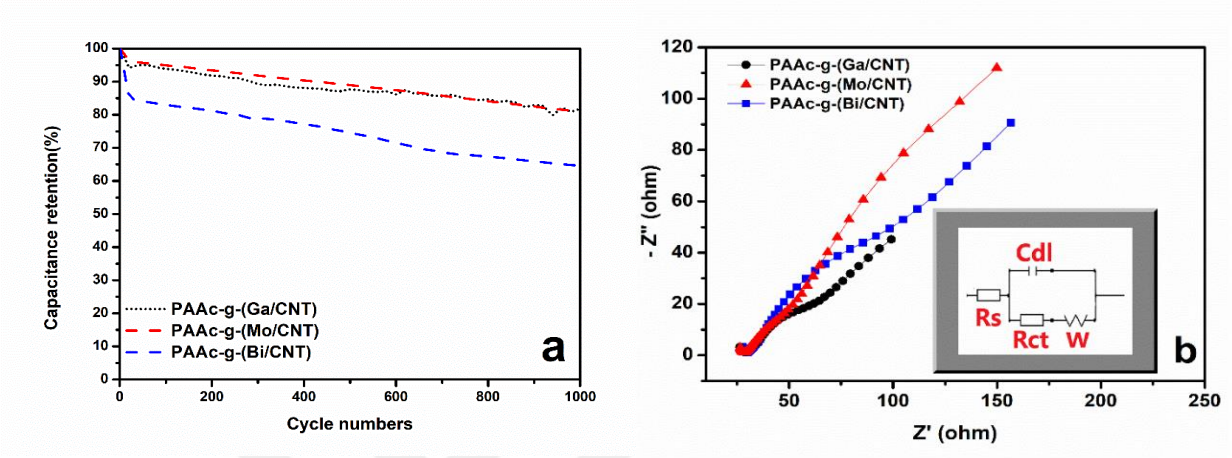

Figure 4.24 a) Cycling-life test of all electrodes of PAAc-g-(Mo/CNT), PAAc-g-(Ga/CNT) and PAAc-g-(Bi/CNT). b) Nyquist plot of of PAAc-g-(Mo/CNT), PAAc-g-(Ga/CNT) and PAAc-g-(Bi/CNT).

The electrochemical characteristics of PAAc-g-(Mo/CNT), PAAc-g-(Ga/CNT), and PAAc-g-(Bi/CNT) were investigated using electrochemical impedance spectroscopy studies (Figure 4.24(a)), and the corresponding values were determined and presented in Table 4.15.

Table 4.15 Fitted data for EIS test of PAAc-g-(Mo/CNT), PAAc-g-(Ga/CNT), and /PAAc-g-(Bi/CNT) electrodes.

Electrode	Rs, Ω	Rct, Ω	Cdl, F	W
PAAc-g-(Mo/CNT)	26.79	4.834	382.7e-6	9.274e-3
PAAc-g-(Ga/CNT)	29.31	16.53	294.9e-6	6.631e-3
PAAc-g-(Bi/CNT)	29.84	9.147	237.0e-6	7.509e-3

EIS measurements are one of the most widely used methods to study charge transfer kinetics, electrode capacitance and diffusion properties (Arvas, Gürsu, et al., 2021). The frequency range between 0.1 Hz and 100 kHz was used for the EIS experiments. The electrochemical characteristics of PAAc-g-(Mo/CNT), PAAc-g-(Ga/CNT), and PAAc-g-

(Bi/CNT) were investigated using electrochemical impedance spectroscopy studies (Figure 4.24(b)), and the corresponding values with equivalent circuit fitted results were determined and presented in Table 4.15. In Nyquist diagrams, the smaller the diameter of the semicircle, the lower the load transfer resistance and the higher the energy storage performance (Laschuk et al., 2021). Although the Rs and Rct values for all samples are not very different from each other, it supports the idea of faster diffusion and movement of ions within the porous structure of the PAAc-g-(Mo/CNT) electrode, which offers the lowest Rs and Rct values compared to other electrodes (Yazar, Arvas, Yilmaz, et al., 2022).

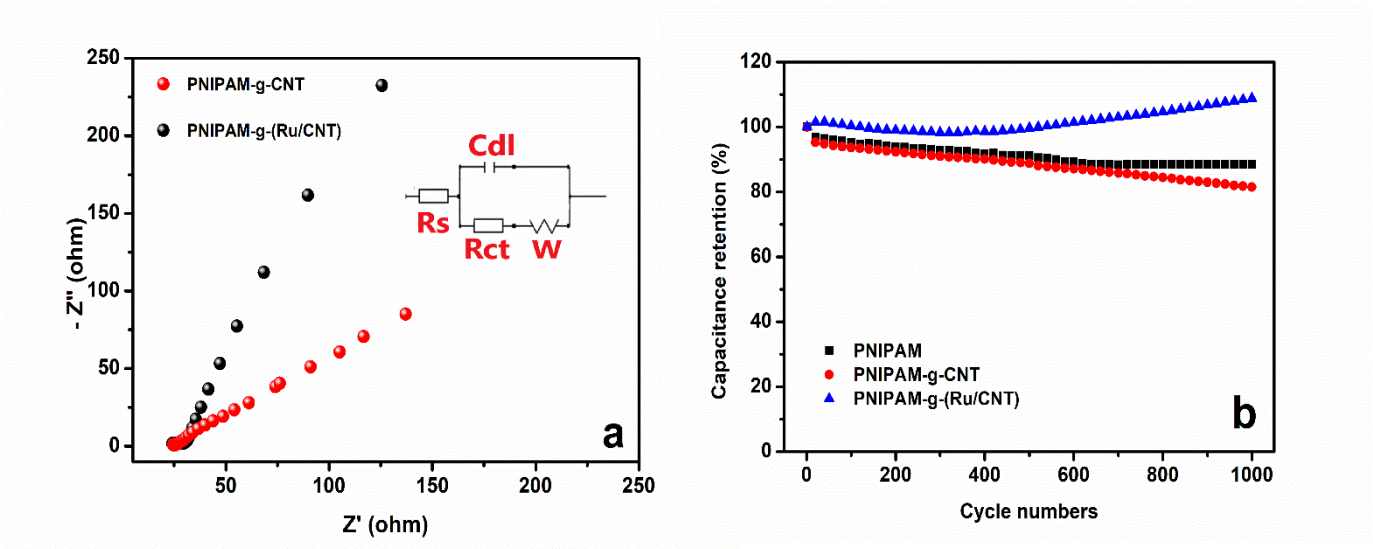

Figure 4.25 a) Nyquist plot of PNIPAM-g-CNT and PNIPAM-g-(Ru/CNT). b) Cycling-life test of all electrodes of PNIPAM, PNIPAM-g-CNT and PNIPAM-g-(Ru/CNT).

Figure 4.25(b) presents the cycling stability study of PNIPAM, PNIPAM-g-CNT, and PNIPAM-g-(Ru/CNT) were performed over 1000 cyclic voltammetry cycles, the potential window of 1 V at 100 mV s^{-1} scan rate. The PNIPAM demonstrates a retention of 81.5%, PNIPAM-g-CNT exhibits a retention of 88.4%, while the PNIPAM-g-(Ru/CNT) composite displays the highest retention at 108.8%. As the number of cycles increases, the capacitance also increases as more electrolyte ions enter and interact with the CNT and Ru components of the PNIPAM-g-(Ru/CNT) composite. This increased capacitance can be credited to the active utilizing of the entire material's surface over time. Moreover, the durable surface of the composite prevents any significant drop in capacitance. The denseness of the material contributes to reaching a larger surface area, facilitating greater interaction with electrolyte ions and consequently resulting in increased capacitance.

The electrochemical properties of PNIPAM, PNIPAM-g-CNT and PNIPAM-g-(Ru/CNT), were examined using electrochemical impedance spectroscopy analyses. The values were derived by using the simple equivalent circuit model presented in Figure 4.25(b) and presented in Table 4.16**.**

Table 4.16 Fitted data for EIS test of PNIPAM-g-CNT, PNIPAM-g-(Ru/CNT) electrodes.

Electrode	**Rs, Ω**	**Rct, Ω**	**Cdl, F**	**W ohm $s^{-1/2}$**
PNIPAM-g-CNT	28.02	23.8	3.196e-7	53.73
PNIPAM-g-(Ru/CNT)	27.77	24.2	8.156e-4	342.0

The EIS tests were carried out in the frequency range between 0.1 Hz and 100 kHz. After fitting, the Nyquist plot shows the presence of a slash at low frequency and a very small semicircle at high frequency, as shown in Figure 4.25(a). The values Rs, Rct, Cdl, and W described the solution resistance, charge transfer resistance, double-layer capacitance, and ion diffusion rates, respectively. PNIPAM-g-(Ru/CNT) exhibited the lowest charge transfer and highest Cdl value according to the EIS data (Figure 4.25(a)).

5. CONCLUSION AND RECOMMENDATIONS

In conclusion, CNT electrode materials doped with metal catalysts were fabricated in this thesis. The electrode materials were coated with PAAc and PNIPAM hydrogels. Structural properties were analyzed using FTIR, XRD and Micro-Raman techniques. Surface properties were investigated by SEM analysis. Due to the insufficient capacitance values exhibited by carbon materials alone, doping with metals resulted in a significant increase in specific capacitance values. It is expected that commercially available supercapacitors should have high capacitance values and long term life. For this purpose, long cycle tests of all electrode materials were carried out. Another reason for using PAAc and PNIPAM materials in this thesis is the low cycle life of metals due to their redox behaviour. These hydrogels acted as adhesives during the coating of the active materials on the carbon felt electrode surface and provided interaction with the electrode surface. In addition, their hydrogel structure enabled the electrolyte ions to reach the active surfaces, so that the electrolyte ions could easily reach all parts of the coated surface.

The electrodes studied included PAAc, PAAc-g-CNT, PAAc-g-(Pt/CNT), PAAc-g-(Pd/CNT), PAAc-g-(Ru/CNT), PAAc-g-(Fe/CNT), PAAc-g-(Co/CNT), PAAc-g-(Ni/CNT), PAAc-g-(Mo/CNT), PAAc-g-(Ga/CNT), PAAc-g-(Bi/CNT), PNIPAM, PANIPAM-g-CNT, and PNIPAM-g-(Ru/CNT). Electrochemical characterizations were carried out using cyclic voltammetry (CV) at varying scan rates, galvanostatic charge-discharge (GCD) at different current densities and long-term cycle stability by CV and electrochemical impedance spectroscopy (EIS) measurements.

Amidst the tested electrodes, the PAAc-g-(Ru/CNT) electrode demonstrated excellent performance, surpassing both PAAc and CNT individually. This electrode, tested in a three-electrode setup with 0.5 M H_2SO_4 aqueous electrolyte, revealed a remarkable specific capacitance of 1294.5 F g^{-1} at a scan rate of 5 mV s^{-1}. Furthermore, the PAAc-g-(Ru/CNT) electrode exhibited consistent capacitance performance even after 1000 cycles, showcasing its long cycling life, strong electrochemical stability, and high capacitance retention of up to 97%, indicating its potential for supercapacitor applications.

The PAAc-g-(Ru/CNT) electrode outperformed the PNIPAM-g-(Ru/CNT) electrode in regard to specific capacitance and capacitance retention. PAAc-g-(Ru/CNT) exhibited a specific capacitance of 1294.5 F g^{-1} at a scan rate of 5 mV s^{-1} and retained 97.7% of its capacitance after 1000 cycles. The PNIPAM-g-(Ru/CNT) electrode had a specific capacitance of 346.0 F g^{-1} at 5.0 mA cm^{-2} and maintained 108.8% capacitance retention after 1000 cycles. The higher ionic conductivity of PAAc-based hydrogels, compared to PNIPAM-based hydrogels, allows for better ion transport within the electrode material. This is why PAAc-based hydrogels like PAAc-g-(Ru/CNT), are advantageous for supercapacitor applications. Ionic conductive hydrogel materials facilitate faster charge and discharge rates, leading to improved energy storage capabilities.

In addition, of the active metals supported on CNT, materials Ni, Pt, Co, gave the highest values, respectively. As a result of electrochemical investigations, specific capacitance values of 680.0 F g^{-1} were calculated for PAAc-g-(Ni/CNT) composite electrode, 286.75 F g^{-1} specific capacitance value for PAAc-g-(Pt/CNT), and 235.1 F g^{-1} specific capacitance value for PAAc-g-(Co/CNT). Furthermore, the long cycle lifetimes were 94.1%, 69.6 %, and 81.5%, respectively.

Overall, this thesis provides valuable knowledge on the fabrication of metal/carbon composites for high-performance supercapacitors. The findings offer new approaches for designing and optimizing supercapacitor electrodes, enabling the creation of more efficient and sustainable energy storage devices. By systematically exploring various electrode configurations and materials, including PAAc-g-(Ru/CNT), PAAc-g-(Ni/CNT), and PAAc-g-(Pt/CNT) this research contributes to the advancement of energy storage technologies and provides practical solutions for enhancing energy storage capabilities.

REFERENCES

Aftabuzzaman, M., Kim, C. K., Kowalewski, T., Matyjaszewski, K., & Kim, H. K. (2019). A facile route to well-dispersed Ru nanoparticles embedded in self-templated mesoporous carbons for high-performance supercapacitors. *J. Mater. Chem. A*, *7*(35), 20208–20222. https://doi.org/10.1039/C9TA06571G

Al-Gorair, A. S., Sayed, A., & Mahmoud, G. A. (2022). Engineered Superabsorbent Nanocomposite Reinforced with Cellulose Nanocrystals for Remediation of Basic Dyes: Isotherm, Kinetic, and Thermodynamic Studies. *Polymers*, *14*(3), 567. https://doi.org/10.3390/polym14030567

Ambade, R. B., & Patil, B. (2023). Chapter 20 - Conducting polymer-based nanocomposites as electrode materials for supercapacitors. In A. Khan, M. Nazim, & A. B. T.-A. in E. M. for C. E. C. and S. A. Asiri (Eds.), *Woodhead Publishing Series in Electronic and Optical Materials* (pp. 413–450). Woodhead Publishing. https://doi.org/https://doi.org/10.1016/B978-0-323-91206-8.00001-7

Aoki, K. J., Chen, J., Liu, Y., & Jia, B. (2020). Peak potential shift of fast cyclic voltammograms owing to capacitance of redox reactions. *Journal of Electroanalytical Chemistry*, *856*(November). https://doi.org/10.1016/j.jelechem.2019.113609

Arora, Y., Shah, A. P., Battu, S., Maliakkal, C. B., Haram, S., Bhattacharya, A., & Khushalani, D. (2016). Nanostructured MoS2/BiVO4 Composites for Energy Storage Applications. *Scientific Reports*, *6*(1), 36294. https://doi.org/10.1038/srep36294

Arvas, M. B., Gencten, M., & Sahin, Y. (2021). One-step synthesized N-doped graphene-based electrode materials for supercapacitor applications. *Ionics*, *27*(5), 2241–2256. https://doi.org/10.1007/s11581-021-03986-2

Arvas, M. B., Gürsu, H., Gencten, M., & Sahin, Y. (2021). Preparation of different heteroatom doped graphene oxide based electrodes by electrochemical method and their supercapacitor applications. *Journal of Energy Storage*, *35*, 102328. https://doi.org/10.1016/j.est.2021.102328

Baig, M. M., Gul, I. H., Baig, S. M., & Shahzad, F. (2021). The complementary advanced characterization and electrochemical techniques for electrode materials for supercapacitors. *Journal of Energy Storage*, *44*, 103370. https://doi.org/https://doi.org/10.1016/j.est.2021.103370

Banik, U., Malik, M. D. T. U., Rahat, S. M. S. M., & Mallik, A. K. (2022). Performance enhancement of ruthenium-based supercapacitors: A review. *Energy Storage*, *n/a*(n/a), e380. https://doi.org/https://doi.org/10.1002/est2.380

Baughman, R. H., Zakhidov, A. A., & de Heer, W. A. (2002). Carbon nanotubes--the route toward applications. *Science (New York, N.Y.)*, *297*(5582), 787–792. https://doi.org/10.1126/science.1060928

Bhat, M. Y., Hashmi, S. A., Khan, M., Choi, D., & Qurashi, A. (2023). Frontiers and recent developments on supercapacitor's materials, design, and applications: Transport and power system applications. *Journal of Energy Storage*, *58*, 106104. https://doi.org/https://doi.org/10.1016/j.est.2022.106104

Bhojane, P. (2022). Recent advances and fundamentals of Pseudocapacitors: Materials, mechanism, and its understanding. *Journal of Energy Storage*, *45*, 103654. https://doi.org/https://doi.org/10.1016/j.est.2021.103654

Chang, L., Xu, L., Liu, Y., & Qiu, D. (2021). Superabsorbent polymers used for agricultural water retention. *Polymer Testing*, *94*, 107021. https://doi.org/https://doi.org/10.1016/j.polymertesting.2020.107021

REFERENCES

Cheng, C., Xu, J., Gao, W., Jiang, S., & Guo, R. (2019). Preparation of flexible supercapacitor with RGO/Ni-MOF film on Ni-coated polyester fabric. *Electrochimica Acta*, *318*, 23–31. https://doi.org/https://doi.org/10.1016/j.electacta.2019.06.055

Choi, B., Ko, J., Kim, B., & Seo, M. (2022). Electrochemical Supercapacitors Based on Hydrous RuO2/ oxidized Multi-walled Carbon Nanotube Composites. *Journal of Nanotechnology and Nanomaterials*, *3*(2), 90–96. https://doi.org/10.33696/nanotechnol.3.035

Choudhary, R. B., Ansari, S., & Purty, B. (2020). Robust electrochemical performance of polypyrrole (PPy) and polyindole (PIn) based hybrid electrode materials for supercapacitor application: A review. *Journal of Energy Storage*, *29*, 101302. https://doi.org/https://doi.org/10.1016/j.est.2020.101302

Conzatti, G., Cavalie, S., Combes, C., Torrisani, J., Carrere, N., & Tourrette, A. (2017). PNIPAM grafted surfaces through ATRP and RAFT polymerization: Chemistry and bioadhesion. *Colloids and Surfaces B: Biointerfaces*, *151*, 143–155. https://doi.org/https://doi.org/10.1016/j.colsurfb.2016.12.007

Cui, K., Du, L., Du, W., Chen, W., Zhang, Y., Cui, L., & Wu, D. (2023). Structural engineering design of CoTe@NixSy core-shell nanowires supported by cobalt foams and functional application in aqueous/flexible hybrid supercapacitors. *Journal of Alloys and Compounds*, *955*, 170290. https://doi.org/https://doi.org/10.1016/j.jallcom.2023.170290

Delbari, S. A., Ghadimi, L. S., Hadi, R., Farhoudian, S., Nedaei, M., Babapoor, A., Sabahi Namini, A., Le, Q. Van, Shokouhimehr, M., Shahedi Asl, M., & Mohammadi, M. (2021). Transition metal oxide-based electrode materials for flexible supercapacitors: A review. *Journal of Alloys and Compounds*, *857*, 158281. https://doi.org/https://doi.org/10.1016/j.jallcom.2020.158281

Dong, W., Lin, T., Huang, J., Wang, Y., Zhang, Z., Wang, X., Yuan, X., Lin, J., Chen, I.-W., & Huang, F. (2020). Electrodes with Electrodeposited Water-excluding Polymer Coating Enable High-Voltage Aqueous Supercapacitors. *Research*, *2020*, 1–13. https://doi.org/10.34133/2020/4178179

Dong, W., Wang, Z., Zhang, Q., Ravi, M., Yu, M., Tan, Y., Liu, Y., Kong, L., Kang, L., & Ran, F. (2019). Polymer/block copolymer blending system as the compatible precursor system for fabrication of mesoporous carbon nanofibers for supercapacitors. *Journal of Power Sources*, *419*, 137–147. https://doi.org/https://doi.org/10.1016/j.jpowsour.2019.02.070

El Wanees, S. A., Abdallah, M., Al-Gorair, A. S., Tirkistani, F. A. A., Nooh, S., & Assi, R. (2021). Investigation of Anodic Behavior of Nickel in H2SO4 Solutions Using Galvanostatic Polarization Technique. I. Kinetics and Thermodynamic Approach. *International Journal of Electrochemical Science*, *16*(1), 1–18. https://doi.org/10.20964/2021.01.15

Elashnikov, R., Trelin, A., Tulupova, A., Miliutina, E., Zahorjanová, K., Ulbrich, P., Tomeček, D., Fitl, P., Švorčík, V., & Lyutakov, O. (2021). Switchable PNIPAm/PPyNT Hydrogel for Smart Supercapacitors: External Control of Capacitance for Pulsed Energy Generation or Prolongation of Discharge Time. *ACS Applied Materials & Interfaces*, *13*(40), 48030–48039. https://doi.org/10.1021/acsami.1c12228

REFERENCES

Feng, L., Yang, H., Dong, X., Lei, H., & Chen, D. (2018). pH-sensitive polymeric particles as smart carriers for rebar inhibitors delivery in alkaline condition. *Journal of Applied Polymer Science*, *135*(8), 45886. https://doi.org/https://doi.org/10.1002/app.45886

Forouzandeh, P., Kumaravel, V., & Pillai, S. C. (2020). Electrode Materials for Supercapacitors: A Review of Recent Advances. *Catalysts*, *10*(9). https://doi.org/10.3390/catal10090969

Gaikwad, N., Gadekar, P., Kandasubramanian, B., & Kaka, F. (2023). Advanced polymer-based materials and mesoscale models to enhance the performance of multifunctional supercapacitors. *Journal of Energy Storage*, *58*, 106337. https://doi.org/https://doi.org/10.1016/j.est.2022.106337

Gao, L., Chen, G., Zhang, L., Yan, B., & Yang, X. (2021). Engineering pseudocapacitive MnMoO4@C microrods for high energy sodium ion hybrid capacitors. *Electrochimica Acta*, *379*, 138185. https://doi.org/https://doi.org/10.1016/j.electacta.2021.138185

Grabowska, B., Bobrowski, A., Kaczmarska, K., Kurleto-Kozioł, Ż., & Szymański, Ł. (2016). Crosslink the Novel Group of Polymeric Binders BioCo by the UV-radiation. *Archives of Foundry Engineering*, *No 2*. https://doi.org/10.1515/afe-2016-0031

Guo, Y., Zhu, Z., Chen, Y., He, H., Li, X., Qin, T., & Wang, Y. (2020). High-performance supercapacitors of ruthenium-based nanohybrid compounds. *Journal of Alloys and Compounds*, *842*, 155798. https://doi.org/https://doi.org/10.1016/j.jallcom.2020.155798

He, F., Yang, N., Li, K., Wang, X., Cong, S., Zhang, L., Xiong, S., & Zhou, A. (2020). Hydrothermal synthesis of Ni-based metal organic frameworks/graphene oxide composites as supercapacitor electrode materials. *Journal of Materials Research*, *35*(11), 1439–1450. https://doi.org/10.1557/jmr.2020.93

Hu, Q., Yue, B., Shao, H., Yang, F., Wang, J., Wang, Y., & Liu, J. (2021). Facile syntheses of perovskite type LaMO3 (M=Fe, Co, Ni) nanofibers for high performance supercapacitor electrodes and lithium-ion battery anodes. *Journal of Alloys and Compounds*, *852*, 157002. https://doi.org/https://doi.org/10.1016/j.jallcom.2020.157002

Hu, X.-E., Shi, Y.-R., Zhu, X., Tian, K.-W., & Xu, X.-L. (2023). Temperature-responsive hydrogel for tumor embolization therapy. *Journal of Drug Delivery Science and Technology*, *80*, 104107. https://doi.org/https://doi.org/10.1016/j.jddst.2022.104107

Huang, Y., Li, H., Wang, Z., Zhu, M., Pei, Z., Xue, Q., Huang, Y., & Zhi, C. (2016). Nanostructured Polypyrrole as a flexible electrode material of supercapacitor. *Nano Energy*, *22*, 422–438. https://doi.org/https://doi.org/10.1016/j.nanoen.2016.02.047

Jiang, J., Bao, L., Qiang, Y., Xiong, Y., Chen, J., Guan, S., & Chen, J. (2015). Sol-gel process-derived rich nitrogen-doped porous carbon through KOH activation for supercapacitors. *Electrochimica Acta*, *158*, 229–236. https://doi.org/https://doi.org/10.1016/j.electacta.2015.01.144

Jiang, L., Chen, Y., Wang, Y., Lv, J., Dai, P., Zhang, J., Huang, Y., & Lv, W. (2022). Contributions of Various Cd(II) Adsorption Mechanisms by Phragmites australis - Activated Carbon Modified with Mannitol. *ACS Omega*, *7*. https://doi.org/10.1021/acsomega.2c00014

REFERENCES

Juodkazis, K., Juodkazytė, J., Šukienė, V., Grigucevičienė, A., & Selskis, A. (2008). On the charge storage mechanism at RuO2/0.5 M H2SO4 interface. *Journal of Solid State Electrochemistry*, *12*(11), 1399–1404. https://doi.org/10.1007/s10008-007-0476-0

Juodkazytė, J., Vilkauskaitė, R., Stalnionis, G., Šebeka, B., & Juodkazis, K. (2007). EQCM Study of Ru and RuO2 Surface Electrochemistry. *Electroanalysis*, *19*(10), 1093–1099. https://doi.org/https://doi.org/10.1002/elan.200703827

Kam, W., Liew, C.-W., Lim, J. Y., & Ramesh, S. (2014). Electrical, structural, and thermal studies of antimony trioxide-doped poly(acrylic acid)-based composite polymer electrolytes. *Ionics*, *20*(5), 665–674. https://doi.org/10.1007/s11581-013-1012-0

Kariper, İ. A., Korkmaz, S., Karaman, C., & Karaman, O. (2022). High energy supercapacitors based on functionalized carbon nanotubes: Effect of atomic oxygen doping via various radiation sources. *Fuel*, *324*, 124497. https://doi.org/https://doi.org/10.1016/j.fuel.2022.124497

Kausar, A. (2017). Overview on conducting polymer in energy storage and energy conversion system. *Journal of Macromolecular Science, Part A: Pure and Applied Chemistry*, *54*(9), 640–653. https://doi.org/10.1080/10601325.2017.1317210

Laschuk, N. O., Easton, E. B., & Zenkina, O. V. (2021). Reducing the resistance for the use of electrochemical impedance spectroscopy analysis in materials chemistry. *RSC Advances*, *11*(45), 27925–27936. https://doi.org/10.1039/d1ra03785d

Lekawa-Raus, A., Patmore, J., Kurzepa, L., Bulmer, J., & Koziol, K. (2014). Electrical Properties of Carbon Nanotube Based Fibers and Their Future Use in Electrical Wiring. *Advanced Functional Materials*, *24*(24), 3661–3682. https://doi.org/https://doi.org/10.1002/adfm.201303716

Li, G.-C., Liu, P.-F., Liu, R., Liu, M., Tao, K., Zhu, S.-R., Wu, M.-K., Yi, F.-Y., & Han, L. (2016). MOF-derived hierarchical double-shelled NiO/ZnO hollow spheres for high-performance supercapacitors. *Dalton Trans.*, *45*(34), 13311–13316. https://doi.org/10.1039/C6DT01791F

Li, J., Huang, X., Cui, L., Chen, N., & Qu, L. (2016). Preparation and supercapacitor performance of assembled graphene fiber and foam. *Progress in Natural Science: Materials International*, *26*(3), 212–220. https://doi.org/https://doi.org/10.1016/j.pnsc.2016.05.006

Li, J., Song, X., Zhang, W., Xu, H., Guo, T., Zhang, X., Gao, J., Pang, H., & Xue, H. (2020). Microporous Carbon Nanofibers Derived from Poly(acrylonitrile-co-acrylic acid) for High-Performance Supercapacitors. *Chemistry – A European Journal*, *26*(15), 3326–3334. https://doi.org/https://doi.org/10.1002/chem.201904563

Lichchhavi, Kumar, S., Srivastava, A. K., & Jha, S. K. (2023). Elucidation of intercalation-pseudocapacitor mechanism in Binder-free Bi2S3@Ni foam electrodes towards high-performance supercapattery. *Electrochimica Acta*, *456*, 142438. https://doi.org/https://doi.org/10.1016/j.electacta.2023.142438

Licht, F., Davis, M. A., & Andreas, H. A. (2020). Charge redistribution and electrode history impact galvanostatic charging/discharging and associated figures of merit. *Journal of Power Sources*, *446*, 227354. https://doi.org/https://doi.org/10.1016/j.jpowsour.2019.227354

REFERENCES

Liu, Q., Bai, Z., Fan, J., Sun, Z., Mi, H., Zhang, Q., & Qiu, J. (2018). A hydrogel-mediated scalable strategy toward core-shell polyaniline/poly(acrylic acid)-modified carbon nanotube hybrids as efficient electrodes for supercapacitor applications. *Applied Surface Science*, *436*, 189–197. https://doi.org/https://doi.org/10.1016/j.apsusc.2017.11.209

Liu, X., Zang, W., Guan, C., Zhang, L., Qian, Y., Elshahawy, A. M., Zhao, D., Pennycook, S. J., & Wang, J. (2018). Ni-Doped Cobalt–Cobalt Nitride Heterostructure Arrays for High-Power Supercapacitors. *ACS Energy Letters*, *3*(10), 2462–2469. https://doi.org/10.1021/acsenergylett.8b01393

Lokhande, C. D., Dubal, D. P., & Joo, O.-S. (2011). Metal oxide thin film based supercapacitors. *Current Applied Physics*, *11*(3), 255–270. https://doi.org/https://doi.org/10.1016/j.cap.2010.12.001

Low, W. H., Khiew, P. S., Lim, S. S., Siong, C. W., & Ezeigwe, E. R. (2019). Recent development of mixed transition metal oxide and graphene/mixed transition metal oxide based hybrid nanostructures for advanced supercapacitors. *Journal of Alloys and Compounds*, *775*, 1324–1356. https://doi.org/https://doi.org/10.1016/j.jallcom.2018.10.102

Lu, Z., Liu, X., Wang, T., Huang, X., Dou, J., Wu, D., Yu, J., Wu, S., & Chen, X. (2023). S/N-codoped carbon nanotubes and reduced graphene oxide aerogel based supercapacitors working in a wide temperature range. *Journal of Colloid and Interface Science*, *638*, 709–718. https://doi.org/https://doi.org/10.1016/j.jcis.2023.02.013

Munk, T., Baldursdottir, S., Hietala, S., Rades, T., Nuopponen, M., Kalliomäki, K., Tenhu, H., Rantanen, J., & Strachan, C. J. (2013). Investigation of the phase separation of PNIPAM using infrared spectroscopy together with multivariate data analysis. *Polymer*, *54*(26), 6947–6953. https://doi.org/https://doi.org/10.1016/j.polymer.2013.10.033

Mustaqeem, M., Naikoo, G. A., Rahimi, F., Pedram, M. Z., Pourfarzad, H., Hassan, I. U., Arshad, F., & Chen, Y.-F. (2022). Rational design of Cu based composite electrode materials for high-performance supercapacitors – A review. *Journal of Energy Storage*, *51*, 104330. https://doi.org/https://doi.org/10.1016/j.est.2022.104330

N, R. Y., Sharma, K., & Shafi, P. M. (2022). An overview, methods of synthesis and modification of carbon-based electrodes for supercapacitor. *Journal of Energy Storage*, *55*, 105727. https://doi.org/https://doi.org/10.1016/j.est.2022.105727

Nakayama, M., Tanaka, A., Sato, Y., Tonosaki, T., & Ogura, K. (2005). Electrodeposition of Manganese and Molybdenum Mixed Oxide Thin Films and Their Charge Storage Properties. *Langmuir*, *21*(13), 5907–5913. https://doi.org/10.1021/la050114u

Nie, C., Pan, L., Liu, Y., Li, H., Chen, T., Lu, T., & Sun, Z. (2012). Electrophoretic deposition of carbon nanotubes–polyacrylic acid composite film electrode for capacitive deionization. *Electrochimica Acta*, *66*, 106–109. https://doi.org/https://doi.org/10.1016/j.electacta.2012.01.064

Nishchith, B. S., Kalegowda, Y., Ashoka, S., Shreenivasa, L., Sriram, G., Kurkuri, M. D., Ajeya, K. V., & Jung, H.-Y. (2023). Electrochemical kinetic study and performance evaluation of surface-modified mesoporous sodium carbonophosphates nanostructures for pseudocapacitor applications. *Journal of Alloys and Compounds*, *939*, 168711. https://doi.org/https://doi.org/10.1016/j.jallcom.2023.168711

REFERENCES

Obeidat, A. M., & Rastogi, A. C. (2023). Co-electrodeposited poly (3, 4-ethylenedioxythiophene) (PEDOT)-multiwall carbon nanotubes (MWCNT) hybrid electrodes based solid-state supercapacitors using ionic liquid gel electrolyte for energy storage with pulsed power capabilities. *Journal of Energy Storage*, *67*, 107563. https://doi.org/https://doi.org/10.1016/j.est.2023.107563

Olabi, A. G., Abbas, Q., Al Makky, A., & Abdelkareem, M. A. (2022). Supercapacitors as next generation energy storage devices: Properties and applicationsOlabi, A. G., Abbas, Q., Al Makky, A., & Abdelkareem, M. A. (2022). Supercapacitors as next generation energy storage devices: Properties and applications. Energy, 248, . *Energy*, *248*, 123617. https://doi.org/https://doi.org/10.1016/j.energy.2022.123617

Pan, M., Yang, J., Liu, K., Yin, Z., Ma, T., Liu, S., Xu, L., & Wang, S. (2020). Noble Metal Nanostructured Materials for Chemical and Biosensing Systems. *Nanomaterials (Basel, Switzerland)*, *10*(2). https://doi.org/10.3390/nano10020209

Panasenko, I. V, Bulavskiy, M. O., Iurchenkova, A. A., Aguilar-Martinez, Y., Fedorov, F. S., Fedorovskaya, E. O., Mikladal, B., Kallio, T., & Nasibulin, A. G. (2022). Flexible supercapacitors based on free-standing polyaniline/single-walled carbon nanotube films. *Journal of Power Sources*, *541*, 231691. https://doi.org/https://doi.org/10.1016/j.jpowsour.2022.231691

Patil, D. S., Pawar, S. A., Devan, R. S., Gang, M. G., Ma, Y.-R., Kim, J. H., & Patil, P. S. (2013). Electrochemical supercapacitor electrode material based on polyacrylic acid/polypyrrole/silver composite. *Electrochimica Acta*, *105*, 569–577. https://doi.org/https://doi.org/10.1016/j.electacta.2013.05.022

Patil, D. S., Pawar, S. A., Devan, R. S., Mali, S. S., Gang, M. G., Ma, Y. R., Hong, C. K., Kim, J. H., & Patil, P. S. (2014). Polyaniline based electrodes for electrochemical supercapacitor: Synergistic effect of silver, activated carbon and polyaniline. *Journal of Electroanalytical Chemistry*, *724*, 21–28. https://doi.org/https://doi.org/10.1016/j.jelechem.2014.04.006

Pedro Aguiar dos Santos, J., Cesar Rufino, F., Yutaka Ota, J. I., Fernandes, R. C., Vicentini, R., Pagan, C. J. B., Morais Da Silva, L., & Zanin, H. (2023). Best practices for electrochemical characterization of supercapacitors. *Journal of Energy Chemistry*, *80*, 265–283. https://doi.org/https://doi.org/10.1016/j.jechem.2022.12.034

Raza, W., Ali, F., Raza, N., Luo, Y., Kim, K.-H., Yang, J., Kumar, S., Mehmood, A., & Kwon, E. E. (2018). Recent advancements in supercapacitor technology. *Nano Energy*, *52*, 441–473. https://doi.org/https://doi.org/10.1016/j.nanoen.2018.08.013

Real, S. G., Vilche, J. R., & Arvia, A. J. (1980). The characteristics of the potentiodynamic potential/current profiles obtained with the Ni/0.5N H2SO4 interface. A contribution to the mechanism of the electrode process. *Corrosion Science*, *20*(4), 563–586. https://doi.org/https://doi.org/10.1016/0010-938X(80)90072-4

Sahoo, B. B., Pandey, V. S., Dogonchi, A. S., Thatoi, D. N., Nayak, N., & Nayak, M. K. (2023). Synthesis, characterization and electrochemical aspects of graphene based advanced supercapacitor electrodes. *Fuel*, *345*, 128174. https://doi.org/https://doi.org/10.1016/j.fuel.2023.128174

Salanne, M., Rotenberg, B., Naoi, K., Kaneko, K., Taberna, P.-L., Grey, C. P., Dunn, B., & Simon, P. (2016). Efficient storage mechanisms for building better supercapacitors. *Nature Energy*, *1*(6), 16070. https://doi.org/10.1038/nenergy.2016.70

REFERENCES

Sánchez-Márquez, J. A., Fuentes-Ramírez, R., Cano-Rodríguez, I., Gamiño-Arroyo, Z., Rubio-Rosas, E., Kenny, J. M., & Rescignano, N. (2015). Membrane Made of Cellulose Acetate with Polyacrylic Acid Reinforced with Carbon Nanotubes and Its Applicability for Chromium Removal. *International Journal of Polymer Science, 2015*, 320631. https://doi.org/10.1155/2015/320631

Saravanan, T., Shanmugam, M., Anandan, P., Azhagurajan, M., Pazhanivel, K., Arivanandhan, M., Hayakawa, Y., & Jayavel, R. (2015). Facile synthesis of graphene-CeO2 nanocomposites with enhanced electrochemical properties for supercapacitors. *Dalton Trans.*, *44*(21), 9901–9908. https://doi.org/10.1039/C5DT01235J

Sato, N., & Okamoto, G. (1963). Anodic Passivation of Nickel in Sulfuric Acid Solutions. *Journal of The Electrochemical Society*, *110*(6), 605. https://doi.org/10.1149/1.2425838

Sayed, A., Hany, F., Abdel-Raouf, M. E.-S., & Mahmoud, G. A. (2022). Gamma irradiation synthesis of pectin- based biohydrogels for removal of lead cations from simulated solutions. *Journal of Polymer Research*, *29*(9), 372. https://doi.org/10.1007/s10965-022-03219-8

Shaikh, J. S., Pawar, R. C., Moholkar, A. V, Kim, J. H., & Patil, P. S. (2011). CuO–PAA hybrid films: Chemical synthesis and supercapacitor behavior. *Applied Surface Science*, *257*(9), 4389–4397. https://doi.org/https://doi.org/10.1016/j.apsusc.2010.12.069

Shaikh, J. S., Pawar, R. C., Tarwal, N. L., Patil, D. S., & Patil, P. S. (2011). Supercapacitor behavior of CuO–PAA hybrid films: Effect of PAA concentration. *Journal of Alloys and Compounds*, *509*(25), 7168–7174. https://doi.org/https://doi.org/10.1016/j.jallcom.2011.04.040

Sharma, A. K., Sharma, Y., & Duhan, S. (2015). Biocompatible Smart Matrices Based on Poly (3,4-ethylenedioxythiophene)-Poly (N-isopropylacrylamide) Composite. *International Journal of Polymeric Materials and Polymeric Biomaterials*, *64*(7), 333–337. https://doi.org/10.1080/00914037.2014.945204

Sharma, S., & Chand, P. (2023). Supercapacitor and electrochemical techniques: A brief review. *Results in Chemistry*, *5*, 100885. https://doi.org/https://doi.org/10.1016/j.rechem.2023.100885

Shin, S., & Shin, M. W. (2021). Nickel metal–organic framework (Ni-MOF) derived NiO/C@CNF composite for the application of high performance self-standing supercapacitor electrode. *Applied Surface Science*, *540*, 148295. https://doi.org/https://doi.org/10.1016/j.apsusc.2020.148295

Silverstein, R. M., & Bassler, G. C. (1962). Spectrometric identification of organic compounds. *Journal of Chemical Education*, *39*(11), 546. https://doi.org/10.1021/ed039p546

Sun, R., Zhang, X., Chen, Z., Ma, Y., & Ma, L. (2023). Application of long fibrous coconut silk-based porous carbon in flexible supercapacitor. *Journal of Energy Storage*, *66*, 107410. https://doi.org/https://doi.org/10.1016/j.est.2023.107410

Wang, C., Sun, P., Qu, G., Yin, J., & Xu, X. (2018). Nickel/cobalt based materials for supercapacitors. *Chinese Chemical Letters*, *29*(12), 1731–1740. https://doi.org/https://doi.org/10.1016/j.cclet.2018.12.005

REFERENCES

Wang, H., Hao, Q., Yang, X., Lu, L., & Wang, X. (2010). Effect of Graphene Oxide on the Properties of Its Composite with Polyaniline. *ACS Applied Materials & Interfaces*, *2*, 821–828. https://doi.org/10.1021/am900815k

Wang, H., Zhou, C., Zhu, H., Li, Y., Wang, S., & Shen, K. (2020). Hierarchical porous carbons from carboxylated coal-tar pitch functional poly(acrylic acid) hydrogel networks for supercapacitor electrodes. *RSC Adv.*, *10*(2), 1095–1103. https://doi.org/10.1039/C9RA09141F

Wang, L., Wu, J., & Fu, S. (2023). A mini review of recent progress in Mo-based electrode materials for supercapacitors. *Inorganic Chemistry Communications*, *148*, 110329. https://doi.org/https://doi.org/10.1016/j.inoche.2022.110329

Wang, Q., Chen, D., & Zhang, D. (2015). Electrospun porous CuCo2O4 nanowire network electrode for asymmetric supercapacitors. *RSC Adv.*, *5*(117), 96448–96454. https://doi.org/10.1039/C5RA21170K

Wang, X., Deng, C., Hong, X., Dong, W., & Liang, B. (2022). Controllable synthesis of NiCo2O4, NiCo2O4/graphene composite and their electrochemical application in supercapacitors. *Journal of Energy Storage*, *55*, 105837. https://doi.org/https://doi.org/10.1016/j.est.2022.105837

Wang, Y., Tang, S., Vongehr, S., Ali Syed, J., Wang, X., & Meng, X. (2016). High-Performance Flexible Solid-State Carbon Cloth Supercapacitors Based on Highly Processible N-Graphene Doped Polyacrylic Acid/Polyaniline Composites. *Scientific Reports*, *6*(April 2015), 1–10. https://doi.org/10.1038/srep12883

Wang, Y., Wang, X., Tang, S., Vongehr, S., Ali Syed, J., & Meng, X. (2015). Highly processible and electrochemically active graphene-doped polyacrylic acid/polyaniline allowing the preparation of defect-free thin films for solid-state supercapacitors. *RSC Adv.*, *5*(77), 62670–62677. https://doi.org/10.1039/C5RA05486A

Xing, X., Wang, X., Wang, W., Yang, C., & Wang, H. (2023). Hydrosoluble diacetone acrylamide as an electrolyte additive for high-capacity Zn-ion hybrid supercapacitors. *Colloids and Surfaces A: Physicochemical and Engineering Aspects*, 131602. https://doi.org/https://doi.org/10.1016/j.colsurfa.2023.131602

Yan, S., Qu, P., Wang, H., Tian, T., & Xiao, Z. (2008). Synthesis of Ru/multiwalled carbon nanotubes by microemulsion for electrochemical supercapacitor. *Materials Research Bulletin*, *43*(10), 2818–2824. https://doi.org/https://doi.org/10.1016/j.materresbull.2007.10.041

Yang, S., Li, J., Shao, D., Hu, J., & Wang, X. (2009). Adsorption of Ni(II) on oxidized multi-walled carbon nanotubes: Effect of contact time, pH, foreign ions and PAA. *Journal of Hazardous Materials*, *166*(1), 109–116. https://doi.org/https://doi.org/10.1016/j.jhazmat.2008.11.003

Yang, X., Sun, Z., Gao, J., Yang, C., & Tang, D. (2020). Plasma-initiated polymerization of N-isopropylacrylamide and functionalized with dopamine for the adhesion to Hela cells. *Polymer Bulletin*, *77*(2), 963–974. https://doi.org/10.1007/s00289-019-02784-1

Yaseen, M., Khattak, M. A. K., Humayun, M., Usman, M., Shah, S. S., Bibi, S., Hasnain, B. S. U., Ahmad, S. M., Khan, A., Shah, N., Tahir, A. A., & Ullah, H. (2021). A Review of Supercapacitors: Materials Design, Modification, and Applications. *Energies*, *14*(22). https://doi.org/10.3390/en14227779

REFERENCES

Yazar, S., Arvas, M. B., & Sahin, Y. (n.d.). An ultrahigh-energy density and wide potential window aqueous electrolyte supercapacitor built by polypyrrole/aniline 2-sulfonic acid modified carbon felt electrode. *International Journal of Energy Research*, *n/a*(n/a). https://doi.org/https://doi.org/10.1002/er.7706

Yazar, S., Arvas, M. B., & Sahin, Y. (2022). Hydrothermal Synthesis of Flexible Fe-Doped Polyaniline/Dye-Functionalized Carbon Felt Electrode for Supercapacitor Applications. *ChemistrySelect*, *7*(21). https://doi.org/10.1002/slct.202200016

Yazar, S., Arvas, M. B., Yilmaz, S. M., & Sahin, Y. (2022). Effects of pyridinic N of carboxylic acid on the polymerization of polyaniline and its supercapacitor performances. *Journal of Energy Storage*, *55*, 105740. https://doi.org/https://doi.org/10.1016/j.est.2022.105740

Yazar, S., & Atun, G. (n.d.). Electrochemical synthesis of tunable polypyrrole-based composites on carbon fabric for wide potential window aqueous supercapacitor. *International Journal of Energy Research*, *n/a*(n/a). https://doi.org/https://doi.org/10.1002/er.8168

Yazar, S., & Atun, G. (2022). Electrochemical synthesis of tunable polypyrrole-based composites on carbon fabric for wide potential window aqueous supercapacitor. *International Journal of Energy Research*, *May*, 1–16. https://doi.org/10.1002/er.8168

Yesuraj, J., Elumalai, V., Bhagavathiachari, M., Samuel, A. S., Elaiyappillai, E., & Johnson, P. M. (2017). A facile sonochemical assisted synthesis of α-MnMoO4/PANI nanocomposite electrode for supercapacitor applications. *Journal of Electroanalytical Chemistry*, *797*, 78–88. https://doi.org/https://doi.org/10.1016/j.jelechem.2017.05.019

Zhang, S.-W., Yin, B.-S., Liu, X.-X., Gu, D.-M., Gong, H., & Wang, Z.-B. (2019). A high energy density aqueous hybrid supercapacitor with widened potential window through multi approaches. *Nano Energy*, *59*, 41–49. https://doi.org/https://doi.org/10.1016/j.nanoen.2019.02.001

Zhao, R., Li, K., Liu, R., Sarfraz, M., Shakir, I., & Xu, Y. (2017). Reversible 3D Self-Assembly of Graphene Oxide and Stimuli-Responsive Polymers and Its Enabled High-Performance Graphene-Based Supercapacitors. *J. Mater. Chem. A*, *5*. https://doi.org/10.1039/C7TA05908F